Mathematical and Physical Modelling of Dynamic Electrical Impedance

GEORGIOS   GIANNOUKOS

TUT
PRESS

TALLINN UNIVERSITY OF TECHNOLOGY
Faculty of Information Technology
Thomas Johann Seebeck Department of Electronics

This dissertation was accepted for the defense of the degree of Doctor of Philosophy in Engineering on May 09, 2016.

Supervisor: Professor Mart Min, PhD,
Tallinn University of Technology,
Thomas Johann Seebeck Department of Electronics

Opponents: Professor Jari Hyttinen, PhD,
Tampere University of Technology,
Institute of Biosciences and Medical Technology

Professor Alvo Aabloo, PhD,
University of Tartu,
Institute of Technology

Defense of the thesis: July 05, 2016 in Tallinn, Estonia

Declaration:
Hereby I declare that this doctoral thesis, my original investigation and achievement, submitted for the doctoral degree at Tallinn University of Technology has not been submitted for any academic degree.

/Georgios Giannoukos/

Dünaamilise impedantsi matemaatiline ja füüsikaline modelleerimine

GEORGIOS GIANNOUKOS

To my wife Katie and my children Amy, Achilleas and Philippos,
whose love and support have made this possible

To the memory of my parents Ioannis and Evdoxia

CONTENTS

LISTS OF PUBLICATIONS

SELECTED PUBLICATIONS INCLUDED IN THE THESIS AND AUTHOR'S CONTRIBUTIONS

Paper I
Georgios Giannoukos, Mart Min, "Mathematical and physical modeling of the dynamic fluidic impedance of arteries using electrical impedance equivalents", Mathematical Methods in Applied Science, Volume 37, Issue 5, pp. 711-717, 2014, John Wiley and Sons, Ltd, Chichester, UK.
DOI: http://dx.doi.org/10.1002/mma.2829

The author developed a mathematical and physical model for calculating the fluidic impedance both of a healthy artery and of an artery with atherosclerosis using electrical impedance equivalents. The author prepared the publication of the paper.

Paper II
Georgios Giannoukos, Mart Min "Using Neural Networks to Model Self-immune Disease in Terms of the Alterations of the Dynamic Electrical Impedance", Numerical Analysis and Applied Mathematics (ICNAAM 2014): International Conference of Numerical Analysis and Applied Mathematics, 22–28 September 2014, Rhodes, Greece, volume 1648, pp.850001.1-850001.4, American Institute of Physics (AIP) Conference Proceedings, AIP Publishing, Melville, NY, USA.
DOI: http://dx.doi.org/10.1063/1.4913056

The author presents a mathematical and physical model to simulate the immune system and the interactions between T-cells and B-cells using artificial neural networks. Immune diseases can affect the bioimpedance of the immune system and can cause changes between the interactions of the cells. The author prepared the publication of the paper and presented this paper at the conference.

Paper III
Georgios Giannoukos, Mart Min, "Mathematical and Physical Modelling of the Dynamic Electrical Impedance of a Neuron" International Journal of Circuits, Systems and Signal Processing, Volume 6, Issue 5, 2012, pp. 359-366, ISSN: 1998-4464, North Atlantic University Union (NAUN), Salem, Oregon, USA.
URL:http://www.naun.org/multimedia/NAUN/circuitssystemssignal/16587.pdf

The author developed a mathematical and physical model of a neuron using an RLC circuit or operational amplifier circuits in order to calculate the electrical impedance of a healthy neuron and one affected by Parkinson's disease. The author prepared the publication of the paper.

Paper IV

The author presents a mathematical and physical model in order to calculate the electrical impedance of a parallel RC circuit using a balanced Wien bridge oscillator. The model can be used as an electrical equivalent of a tooth or a neuron. The author prepared the publication of the paper.

FULL LIST OF AUTHOR'S PUBLICATIONS RELATED TO THE THESIS

1. **Georgios Giannoukos**, "Mathematical and Physical modelling of the dynamic electrical impedance both of a healthy neuron and one affected by Parkinson's disease", 5th WSEAS International Conference on Biomedical Electronics and Biomedical Informatics, BEBI 12, Istanbul, Turkey, August 21-23, 2012, Proceedings, pp.79-84, World Scientific and Engineering Academy and Society (WSEAS) Press.

2. **Georgios Giannoukos**, "Mathematical and physical modelling of atherosclerosis in terms of the alterations of the dynamic electrical impedance of the arteries" Numerical Analysis and Applied Mathematics (ICNAAM 2012): International Conference of Numerical Analysis and Applied Mathematics, 19–25 September 2012, Kos, Greece, volume 1479, pp.2174-2177, American Institute of Physics (AIP) Conference Proceedings, AIP Publishing, Melville, NY, USA.
DOI: http://dx.doi.org/10.1063/1.4756623

3. **Georgios Giannoukos**, Mart Min, "Mathematical and Physical Modelling of the Dynamic Electrical Impedance of a Neuron" International Journal of Circuits, Systems and Signal Processing, Volume 6, Issue 5, 2012, pp. 359-366, ISSN: 1998-4464, North Atlantic University Union (NAUN), Salem, Oregon, USA.
URL:http://www.naun.org/multimedia/NAUN/circuitssystemssignal/16587.

4. **Georgios Giannoukos**, Mart Min, "Mathematical and physical modeling of the dynamic fluidic impedance of arteries using electrical impedance equivalents" Mathematical Methods in Applied Science, Volume 37, Issue 5, pp. 711-717, 2014, John Wiley and Sons Ltd, Chichester, UK.
DOI: http://dx.doi.org/10.1002/mma.2829

5. **Georgios Giannoukos**, Mart Min, "Modelling of Dynamic Electrical Bioimpedance and Measurements Safety", 2nd American Applied Sciences Research Institute (AASRI) Conference on Computational Intelligence and Bioinformatics (CIB 2013), December 27-28, 2013, Jeju Island, Korea. AASRI Procedia, volume 6, pp. 12-18, 2014, ELSEVIER.
DOI: http://dx.doi.org/10.1016/j.aasri.2014.05.003

6. **Georgios Giannoukos**, Mart Min, "Mathematical and Physical modelling of the dynamic electrical biompedance" International Journal of Circuits, Systems and Signal Processing, Volume 8, 2014, pp. 600-606, ISSN: 1998-4464, North Atlantic University Union(NAUN), Salem, Oregon, USA..
URL:http://www.naun.org/main//NAUN/circuitssystemssignal/2014/a542005-049.pdf

7. **Georgios Giannoukos**, Mart Min "Mathematical and physical modelling of the dynamic electrical impedance of a tooth" Numerical Analysis and Applied Mathematics (ICNAAM 2014): International Conference of Numerical Analysis and Applied Mathematics, 22–28 September 2014, Rhodes, Greece, volume 1648, pp.850002.1-850002.4, American Institute of Physics (AIP) Conference Proceedings, AIP Publishing, Melville, NY, USA.
   DOI: http://dx.doi.org/10.1063/1.4913057

8. **Georgios Giannoukos**, Mart Min "Using Neural Networks to Model Self-immune Disease in Terms of the Alterations of the Dynamic Electrical Impedance" Numerical Analysis and Applied Mathematics (ICNAAM 2014): International Conference of Numerical Analysis and Applied Mathematics, 22–28 September 2014, Rhodes, Greece, volume 1648, pp.850001.1-850001.4, American Institute of Physics (AIP) Conference Proceedings, AIP Publishing, Melville, NY, USA.
   DOI: http://dx.doi.org/10.1063/1.4913056

9. **Georgios Giannoukos**, Mart Min "Dynamic Electrical Impedance Measurement Methods" International Conference on Engineering Technology, Engineering Education and Engineering Management ETEEEM 2014, 15-16 November, Guangzhou, China. Engineering Technology, Engineering Education and Engineering Management Proceedings, June 16, 2015, pp. 379-383, ISBN: 9781138027800, CRC Press, Taylor & Francis Group.
   URL: https://www.crcpress.com/product/isbn/9781138027800

10. **Georgios Giannoukos**, Mart Min "Mathematical modelling of the dynamic electrical impedance of a parallel RC circuit using a Wien bridge oscillator" Journal of Computational Methods in Sciences and Engineering JCMSE, ISSN print1472-7978, ISSN online 1875-8983, Volume 15, Issue 2, 2015 pp.287-293, IOS Press, Amsterdam, The Netherlands.
    DOI: http://dx.doi.org/10.3233/JCM-150543

11. **Georgios Giannoukos**, Mart Min "Application of Artificial Neural Networks to model the interaction between T-cells and B-cells and their equivalent impedance of the linearized model" Journal of Computational Methods in Sciences and Engineering JCMSE, ISSN print1472-7978, ISSN online 1875-8983, Volume 15, Issue 2, 2015, pp.295-302, IOS Press, Amsterdam, The Netherlands.
    DOI: http://dx.doi.org/10.3233/JCM-150544

ACRONYMS, ABBREVIATIONS, DESIGNATIONS

A/D	Analogue to Digital
ASVD	Arteriosclerotic Vascular Disease
CEN	European Committee for Standardization
CENELEC	European Committee for Electrotechnical Standardization
CPE	Constant Phase Element
DUT	Device Under Test
ECG	Electrocardiography
EF	Electric field
ICU	Intensive Care Unit
IEC	International Electrotechnical Commission
ISO	International Organization for Standardization
MD	Measuring Device
PELV	Protected Extra Low Voltage
SELV	Safety Extra Low Voltage
UV	Ultra Violet
OpAmp	Operational Amplifier
R	Electrical resistance
C	Electrical capacitance
L	Electrical inductance

LIST OF FIGURES

LIST OF TABLES

CHAPTER 1

INTRODUCTION

Electrical impedance has been used for characterization of different objects for several decades. The most known fields of successful implementations are electrochemistry and material science, but also in biology and biotechnology. Food technology and especially medicine are the most interesting application fields for electrical bioimpedance [1] nowadays. At the same time, the creation of new methods and devices for impedance measurement are required, for example, wearable and implantable devices for medical monitoring and diagnosing and microfluidic devices for detection and identification of biological objects like living cells, cell cultures and different pathogens.

The creation and implementation of bioimpedance based methods is a highly multidisciplinary field of science and technology, which requires the collaboration of experts in physics, chemistry, biology and medicine together with specialists and scientists from electrical and electronic engineering and information technology. Collaboration of the above mentioned professionals from such different fields requires common understanding of problems and a common language for their communication. It is expected that mathematical modelling on the bases of such physical models as electrical equivalent circuits can serve as common tools for that. Measurement of impedance is mostly time dependent (time-variant or non-stationary dynamic systems). Therefore, the time domain approach is used together with the frequency domain analysis.

The implementation of bioimpedance based methods for monitoring and diagnosing in medicine has been one of the main research fields of Thomas Johann Seebeck Department of Electronics at Tallinn University of Technology for more than 20 years already. The present thesis work was carried out within the framework of the institutional research funded project IUT19-11 (2014-2019) "Impedance spectroscopy based identification and control of objects: signals, algorithms, energy efficient solutions". The ongoing research at the Department is also supported by Horizon2020-WIDESPREAD-2014-2-668995-ERA Chair project Cognitive Electronics (2015-2019), which endeavours to spread excellence and greater participation in the European Research Area (ERA). Therefore neural networks have also been underlined in the thesis as artificial intelligence tools for achieving cognition ability.

The results of the thesis will be used by the consortium of Horizon 2020 flagship project FLAG-ERA JTC 2016 CONVERGENCE (proposal) - Energy Efficient Convergent Wearables for Healthcare and Lifestyle Applications (2016-2019). The consortium connects 15 European universities (leaders are EPF Lausanne and ETH Zürich) and several companies to offer unique

solutions for new generations of continuous healthcare and environmental monitoring and for development of smart apparel with embedded autonomous sensing. Such wearable systems enable personalized assistance for promoting a healthier lifestyle and improving preventive healthcare. The role of Tallinn University of Technology is to develop electrical bioimpedance based sensing methods for cardiovascular monitoring and to implement these methods together with European end users' networks in healthcare.

This thesis presents the methods of mathematical and physical modelling of the dynamic electrical bioimpedance of such biological objects in medicine as neuron, thymus and tooth, as well as the dynamic fluidic impedance of arteries using their electrical impedance equivalents. These models were developed theoretically and evaluated with the use of electronic simulation software and it is hoped that they will be the basis for future experimental work. Safety of electrical bioimpedance measurements of patients is considered as a pertaining specific requirement for human experiments. Artificial neural networks have been discussed in the thesis as the tools for the diagnostic decision making in medicine on the bases of bioimpedance measurement results. Methods of electrical bioimpedance measurements and the subsequent safety of these methods in human experiments are of utmost importance.

1.1 Motivation

Rapid advances in technology as well as the fact that a large proportion of the population in the developed world lead a fast pace of life has been partly responsible for the sedentary lifestyle which many people have today. One possible consequence of this has been an increase in disorders such as Parkinson's disease [2], cardiovascular problems (cause about 50% of deaths in developed countries [3]) and autoimmune diseases [4].

Parkinson's disease occurs when nerve cells or neurons that control movement become impaired and may die. Healthy neurons usually produce an important brain chemical called dopamine [5]. However, when the neurons die or become impaired, they produce less dopamine, a shortage of which causes mobility problems to sufferers of the disease. Over 4 million people worldwide are affected by the disease [6]. The fact that the human life span has increased in recent years means a larger number of people are likely to be afflicted by this disease. It would be both useful and practical to develop an equivalent electrical circuit which simulates and predicts the behaviour of a healthy neuron and one affected by Parkinson's disease. Hypothetically, this model could be used to test the effects of different treatments on neurons.

Atherosclerosis is a common cardiovascular condition which leads to the hardening of arteries [7]. It affects the inner lining of an artery and typically deposits of plaque narrow the diameter of the artery as the artery wall itself thickens impeding blood flow and restricting oxygen delivery. High blood

pressure and diseases as diabetes or just normal aging can cause atherosclerosis. For this reason it would be beneficial to simulate the fluidic bioimpedance of an artery by developing equivalent electrical circuits. Theoretically, this model could be used to compare a healthy artery with one with atherosclerosis.

The immune system's T-cells develop in a gland called the thymus but if these cells fail to recognize just one of the body's myriad of proteins as its own, then autoimmunity, when the body no longer recognizes its own cells and attacks itself, results [8]. The complex process of the development of B-cells in the bone marrow is a delicate balance between cell proliferation and apoptotic selection. If this balance is disturbed it causes an autoimmune reaction. With the use of artificial neural networks we can simulate the interaction between these cells and in theory we can better understand autoimmune diseases.

1.2 Problem formulation

For a better understanding of the physiological processes in biological systems, it is necessary to model the electric bioimpedance of these systems. The development of mathematical and physical models based on RLC electrical components and active operational amplifier (OpAmp) circuits is of interest. For example, such models enable the calculation of the electrical bioimpedance of both a healthy neuron and one affected by Parkinson's disease.

It would also be helpful to develop such electrical and mathematical models with the intention of calculating both the electrical impedance of an equivalent circuit and the fluidic impedance as of a healthy artery, as well as of one affected by atherosclerosis.

In addition, with the use of artificial neural networks, which are very important tools in the field of artificial intelligence, we can develop a mathematical model to simulate the interaction between neural T-cells and B-cells in brain. This has been of particular interest in recent years as analogies between the brain and the immune system have been exploited to build artificial immune systems and immune algorithms with applications in computer science.

1.3 Contributions

The main contributions of this thesis towards the study of the aforementioned diseases and conditions are summarized as follows:

(a) Electrical models based on RLC and OpAmp circuits were developed. With the aid of these (changing the values of their components), opened an ability to calculate the bioimpedance of a healthy neuron and of another one affected by Parkinson's disease.

(b) Similarly, electrical models which were based on RLC and RL components and OpAmp circuits were developed to calculate both the electrical impedance of the equivalent circuit and the fluidic impedance of a healthy artery or another one affected by atherosclerosis.

(c) Third, a detailed mathematical and physical model for simulating the immune system was also developed. The model uses neural networks of three neuron module to simulate the interaction between T-cells and B-cells taking into account that the biompedance is represented by the transfer functions from antigens to immune responses. This model also compares the dynamic behaviour of the cells of immune system, particularly the immune memories and the bifurcations from normal to abnormal behaviour.

(d) Finally, a detailed mathematical and physical model for calculating the bioimpedance of a tooth was developed on the bases of a parallel RC equivalent circuit. The model helps to examine the root canal of a diseased tooth.

1.4 Thesis structure
The thesis contains 4 chapters and 1 appendix with 5 sub-sections.

Chapter 1 introduces and describes the essence and role of the electrical impedance based approach in different fields of science and technology, concentrating the main attention onto implementation of electrical bioimpedance base methods in medical diagnostics.

Chapter 2 provides background information related to this work. It describes dielectric material properties and their relative complex permittivity as well as its dependence on frequency. The expression of complex permittivity for different approaches such as Debye, Cole-Cole, Cole-Davidson and Havriliak-Negami are discussed. In addition, the dielectric polarization is studied, the dielectric measurements are analysed, and both serial and parallel RC equivalent circuits are compared. Subsequently, a study of the dielectric response in time domain as the reaction to stepwise excitation is analysed.

Chapter 3 describes the electrical impedance of biological specimens. Different equivalent circuits of tissues are studied, e.g. such as the Fricke-Morse model and the Debye model. Frequency dispersion, which defines the frequency dependence of the conductivity and the permittivity of a tissue, is presented. In addition, the two electrode and the four electrode methods for measuring impedance are analysed.

The final chapter, Chapter 4, represents different mathematical and physical methods for analytical modelling of dynamic electrical bioimpedance. It begins with the mathematical and physical modelling of the dynamic electrical impedance of a neuron based on RLC and operational amplifier circuits and with the modelling of the dynamic fluidic impedance of arteries using electrical impedance equivalents such as RLC, RL and operational amplifier circuits. Subsequently, a mathematical and physical modelling of immune disease in terms of the alterations of the dynamic electrical impedance of thymus and bone marrow based on artificial neural networks and in non-linear components is studied, as well as mathematical and physical RC circuit based modelling of a tooth.

The Appendix gives the facts, aspects and results, which support the scientific part of the thesis and consists of the following 5 sub-sections.

A-I presents the copies of selected research papers relevant to the thesis.

A-II gives the programming codes developed.

A-III describes the mathematical calculations with RC circuit.

A-IV presents and compares the methods of impedance measurement.

A-V considers the basics of electrical safety and analyses measurement safety.

CHAPTER 2

DIELECTRIC MATERIALS AND MEASUREMENTS

This chapter gives a brief overview of dielectric properties, relative complex permittivity and its dependence on frequency [9]. The significance of different approaches to complex permittivity is also discussed. The different mechanisms of polarization are then presented. Dielectric measurements are given and a comparison of RC serial and parallel equivalent circuits is made and the way in which the impedance of these circuits is affected by frequency is illustrated in the respective diagrams. The way in which dielectric properties change with time and frequency are also discussed.

2.1 Dielectric Materials

When an electric field (EF) can be maintained with zero or almost zero power losses in a material, then it is characterised as a dielectric or electrical insulator. In fact, the dielectric is not an ideal insulator, because a number of electrons can pass through the material. Because of the processes of changing the polarity in the material, part of the electrical energy is lost as heat. Dielectric material is one that has the ability to store energy when an external EF is applied. When a constant voltage is applied across the parallel plates of a capacitor with a dielectric between them, then more energy is stored. This means that the dielectric increases the ability of energy storage in the capacitor, eliminating some of the charges of the electrodes that would help in increasing the EF strength between the plates. The measured capacity with dielectric depends on the electrical loads of the material and is related to the dielectric constant. The following equation applies

$$C = \varepsilon_r^{'} C_O \Rightarrow \varepsilon_r^{'} = \frac{C}{C_O} , \qquad (2.1)$$

where C and C_o are the capacities with a dielectric and vacuum, respectively, and $\varepsilon_r{'}$ is the relative dielectric permittivity of the material. Dielectric materials used in the manufacture of capacitors, are the most suitable for preventing the creation of electrical currents through their mass while at the same time maintaining the voltage in the different parts of the electrical devices.

The relative dielectric constant of an insulating material should be close to 1 while for a dielectric it can generally be up to 10. The terms dielectric and insulator are often used almost synonymously, but with the former we focus on the physical properties of the material while with the latter its use in practical applications.

2.2 Dielectric sizes
2.2.1 Force between charges
The electric force between the charges in a material is given by the following formula (Coulomb's law) [1]

$$F = \frac{1}{4\pi\varepsilon_o}\frac{Q_1Q_2}{r^2}$$ (2.2)

where ε_o = $8.854.10^{-12}$ F/m is the <u>electric permittivity of free space</u>. If material is inserted between the charges, power is reduced according to the formula

$$F = \frac{1}{4\pi\varepsilon}\frac{Q_1Q_2}{r^2}$$ (2.3)

where ε is the <u>absolute permittivity</u> of the medium, which is given as $\varepsilon = \varepsilon_r \cdot \varepsilon_o$, and ε_r is the relative permittivity of the medium. The dimensions of ε and ε_o are F/m in SI, but ε_r is a dimensionless number greater or equal to 1 in the case of the vacuum.

The capacitance of a capacitor consisting of two parallel plates is given by the equation

$$C = \frac{\varepsilon_o A}{d}$$ (2.4)

where A is the area of each plate and d is the distance between them.

The presence of a dielectric material between the plates reduces the electrical field between the plates due to the existence of a polarized field in the opposite direction within the material in which case the above equation becomes

$$C = \frac{\varepsilon A}{d} \Rightarrow C = \frac{\varepsilon_r \varepsilon_o A}{d} \text{ or } C = \varepsilon_r C_0.$$ (2.5)

For an ideal dielectric material ε is a real number but in practice for any dielectric material there is also an imaginary component that is associated with the dielectric loss because of the poor conductivity of the material which is why ε is called absolute complex permittivity which is also denoted by ε * and describes the total interaction of the dielectric materials with the variable electrical field. In this case the following equation is used

$$\varepsilon = \varepsilon' - j\varepsilon''.$$ (2.6)

2.2.2 Relative complex permittivity (ε_r)
In practice the <u>relative complex permittivity</u> is used instead of the absolute complex permittivity because it is dimensionless and takes simple numerical values. It is equal to the absolute complex permittivity divided by the electrical permittivity of free space, as given in equation (2.7) on the next page [1]:

$$\varepsilon_r = \frac{\varepsilon}{\varepsilon_o} = \left(\frac{\varepsilon'}{\varepsilon_o}\right) - j\left(\frac{\varepsilon''}{\varepsilon_o}\right) = \varepsilon_r' - j\varepsilon_r'' \qquad (2.7)$$

where $\varepsilon_o = 8.854 \cdot 10^{-12}$ F/m is the <u>electrical permittivity of free space</u>.

The component ε' in eq. (2.7) is the real part of the relative complex permittivity which is related to the stored energy within the medium, and ε_r'' is the imaginary part of the relative complex permittivity which is related to the dissipation (or loss) of energy within the medium.

The ε_r' is an indication of how much energy can be stored in the material by the applied EF and is called relative permittivity. For the vacuum $\varepsilon_r' = 1$ while for gaseous dielectric materials $\varepsilon_r' \approx 1$, but for most liquid and solid insulators: $1 \leq \varepsilon_r' \leq 10$. For semiconductors it is usually $10 \leq \varepsilon_r' \leq 20$ and for metals $\varepsilon_r' \to \infty$ because there are no dielectrics. The ε_r'' is related to the loss of energy in the medium and is an indication of how polar loose the material is to the external imposed EF. Loose material in a frequency occurs when the polarization mechanism of the material is able to follow the EF changes applied to the material. The ε_r'' is always a positive quantity much smaller than the ε_r'.

Another symbol for ε_r is the ε_r^* or k_r^*, in which case $k_r^* = k' - jk''$, where k′= ε_r' and k′′= ε_r''.

2.2.3 Alternative approach of the relative complex permittivity

When alternating voltage is applied to an ideal capacitor with a dielectric material but without losses, then the current in the circuit charges and discharges the capacitor every period (I_{charge}). This current has a phase difference of 90^0 to the voltage and is equal to

$$I = I_{charge} = Vj\omega C \Rightarrow I = Vj\omega C_0 \varepsilon_r' . \qquad (2.8)$$

If the same voltage is applied to real capacitor containing a dielectric, the total current will be a sum of two currents. Apart from the charging current I_{charge}, there is a current loss I_{loss}, which is related to the energy loss in the material and therefore has the same phase as the voltage. The losses are modeled as a conductance (G) connected in parallel with the capacitance $C = \varepsilon_r' C_0$ of the capacitor. The parallel CG equivalent circuit is shown in Fig. 2.1.
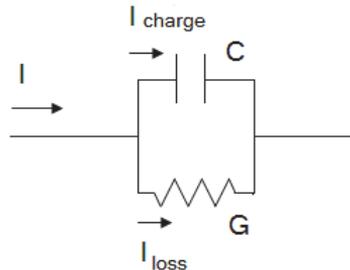
Fig.2.1 Parallel equivalent circuit capacity-conductivity

The total current I is a sum:

$$I = I_{charge} + I_{loss} = V(j\omega C + G) \Rightarrow I = V(j\omega C_0 \varepsilon_r' + G) \Rightarrow$$

$$I = Vj\omega C_O \left(\varepsilon_r' - j\frac{G}{\omega C_0} \right), \tag{2.9}$$

having $\varepsilon_r'' = \dfrac{G}{\omega C_0}$ and $\varepsilon_r = \varepsilon_r' - j\varepsilon_r''$. So the equation (2.9) becomes

$$I = Vj\omega C_O \varepsilon_r. \tag{2.10}$$

This equation has the same form as eq. (2.8), but the real relative permittivity ε_r' has been replaced by the relative complex permittivity ε_r. The complex capacitance $C^* = \varepsilon_r C_0$ can also be defined in the same way and includes both the actual capacity and losses due to the conductivity of the dielectric material.
The complex dielectric permittivity ε_r consists of the real part (ε_r'), which is related to the storage of electrical charges in an ideal capacitor and an imaginary part (ε_r'') which is related to the losses of electrical charges through the conductance (G) of the tested dielectric material.

2.2.4 Loss tangent
When the relative complex dielectric permittivity ε_r is designed in vector format then the real and imaginary component of the equivalent circuit must have a phase difference of 90º. The vector sum forms the angle δ with the real axis ε_r' (Fig.2.2).The tangent of this angle tanδ is an important factor in characterizing dielectrics and is called tangent losses.
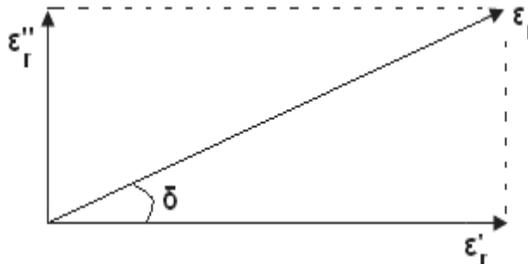
Fig.2.2 Vector diagram of the relative complex dielectric permittivity

The currents charges and losses are proportional to the energy stored in the capacitance and the energy released in the form of heat, respectively. The expected levels of relaxation of any material are derived from the ratio of emitted and stored energy in a period of time.

For each cycle the following applies

$$\tan \delta = \frac{\varepsilon_r{''}}{\varepsilon_r{'}} = \frac{I_{loss}}{I_{charge}} \ .$$

(2.11)

For good insulating materials, the vector ε_r approaches that of $\varepsilon_r{'}$, while $\tan\delta \rightarrow 0$. So when the measure of vector error ε_{error} of the metering device is greater than $\varepsilon_r{''}$ of the material, the total measured δ_{error} angle can be negative (Fig.2.3).
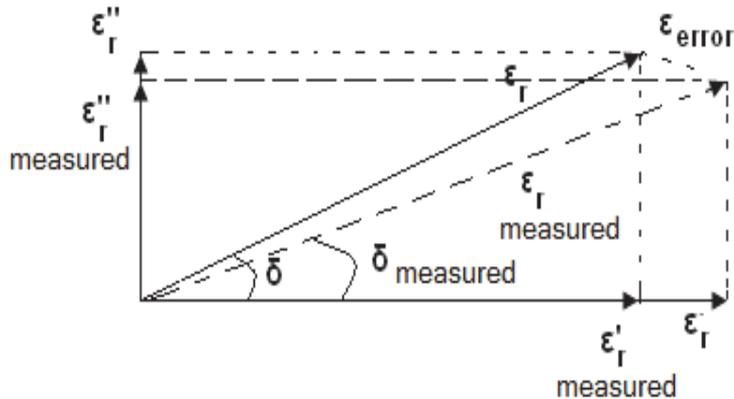
Fig.2.3 Vector diagram of measurement of the relative complex dielectric permittivity taking into account the vector error

To calculate the $\tan\delta$ a reduction of the measurement error is necessary. The accurate measurement of the current loss (I_{loss}) is normally difficult because this current is very small ($I_{loss} \rightarrow 0$) which is why the geometry of the measuring electrode must be suitable so it can amplify the signal of I_{loss}, in order to be recorded by a high precision LCR bridge in a wide range of frequencies. This is achieved by increasing the surface area of the capacitor plates.

2.2.5 Dependence of dielectric permittivity on frequency
The dependence of the frequency of dielectric permittivity is associated with the mechanisms of polarization which take place in each frequency range (Fig.2.4).
At low frequencies all mechanisms are present. Increasing the frequency and reaching the microwave region (105-1010 Hz), the permanent dipoles, due to inertia, can monitor changes in the field and align with it. The polarization orientation stops and the dielectric permittivity declines. Also some energy no longer goes to the circuit but is absorbed by the material indicating the existence of losses. The curve $\varepsilon{''}$ in this region takes the form of a resonance curve.
At higher frequencies in the infrared the mechanism of ionic polarization stops while in the UV the mechanism of electronic polarization stops.
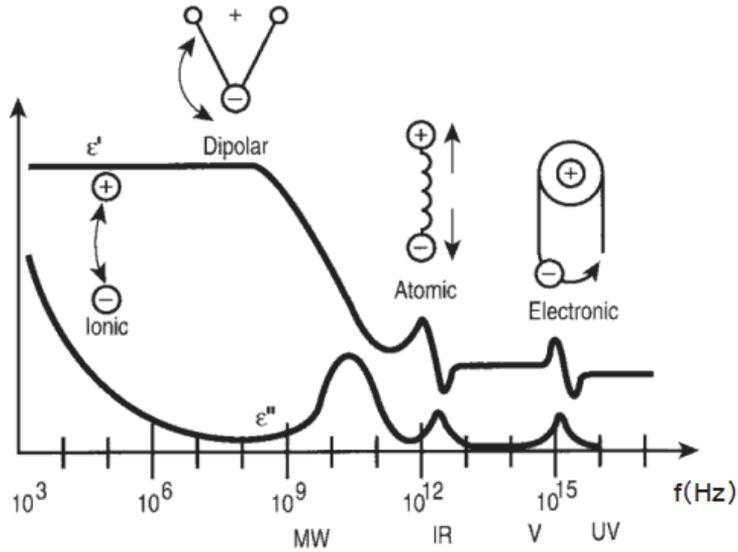
Fig.2.4 Variations of the real part ε' and imaginary part ε'' of the dielectric permittivity
ε versus frequency f [10]

The real part of dielectric permittivity ε' varies between a maximum value ε_s, corresponding to static fields or very low frequencies and a minimum value ε_∞, corresponding to very high frequencies. The imaginary part ε'' is related to losses and has a maximum at the resonance frequency. The ε' and ε'' are given by Debye's equations [11]

$$\varepsilon' = \varepsilon_\infty + \frac{\varepsilon_s - \varepsilon_\infty}{1 + \omega^2 \tau^2}, \ \varepsilon'' = \omega\tau\frac{\varepsilon_s - \varepsilon_\infty}{1 + \omega^2 \tau^2} \ , \tag{2.12}$$

where τ is the relaxation time of the material.

From the above equations we get the following relationship (2.13):

$$\varepsilon - \varepsilon_\infty = \varepsilon'\varepsilon_\infty - j\ \varepsilon'' = \frac{\varepsilon_s - \varepsilon_\infty}{1 + \omega^2 \tau^2} - j\omega\ \tau\frac{\varepsilon_s - \varepsilon_\infty}{1 + \omega^2 \tau^2} \ \Rightarrow$$

$$\left(\varepsilon' - \varepsilon_\infty\right)^2 + \varepsilon''^2 = \left(\varepsilon' - \varepsilon_\infty\right)\left(\varepsilon_s - \varepsilon_\infty\right) \Rightarrow$$

$$\varepsilon'^2 + \varepsilon''^2 = \varepsilon'\left(\varepsilon_s - \varepsilon_\infty\right) - \varepsilon_s\varepsilon_\infty \ . \tag{2.13}$$

The above equation (2.13) represents a circle in the diagram, which has its center at the point $(\varepsilon_s + \varepsilon_\infty)/2$ on the axis ε', see Fig.2.5 on the next page. This diagram is a graph called Cole-Cole plot (Fig.2.5).

34
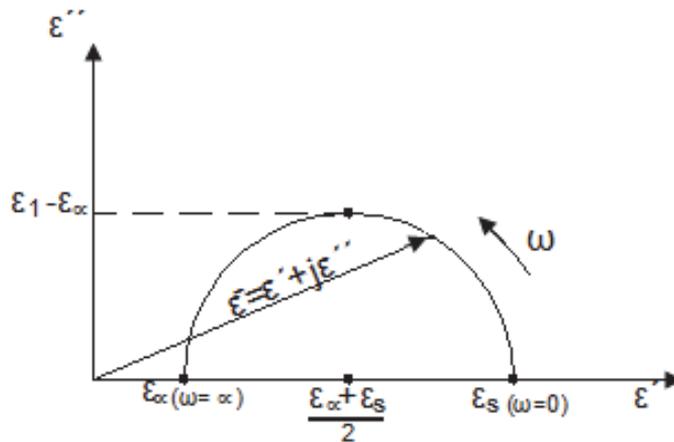
Fig.2.5 Cole-Cole graph of the complex permittivity ε [10]

A dielectric material subjected to a field can be visualized at any frequency from an equivalent circuit of a capacitance and a resistance in series or parallel. For materials that exhibit dielectric losses the parallel equivalent is usually considered more suitable.
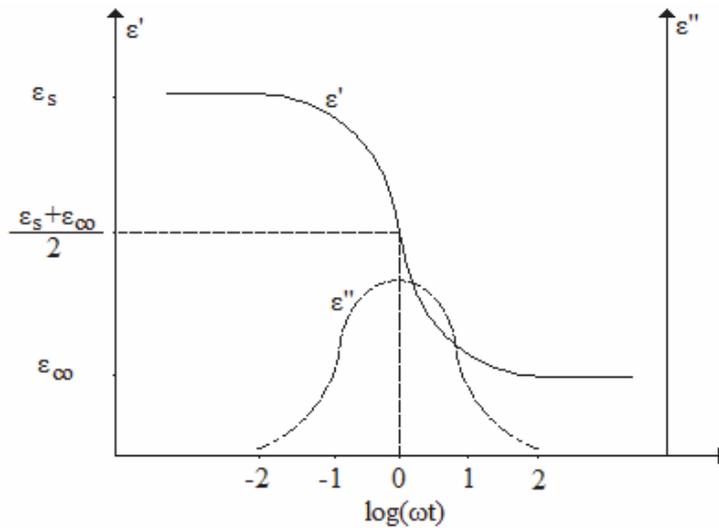
Fig.2.6 Real part ε'and imaginary part ε'' of the dielectric permittivity ε for a Debye mechanism [10]

As shown in the Fig. 2.6, in a frequency range around the value $\omega = 1 / \tau$ we observe a peak in ε'', which is because in this region energy losses are maximized due to the frequencies ω and $1/\tau$ being comparable. The maximum peak located at the frequency $\omega_{max} = 1/\tau$. (2.14)

We also see a step in ε because in much smaller frequencies than ω_{max} the dipoles have time to follow the changes in the field whereas at much higher frequencies they don't thus they are not involved in the polarization which is why at low frequencies $\varepsilon' = \varepsilon_s$ and at high frequencies $\varepsilon' = \varepsilon_\infty$.

Debye's dispersion equations describe a relaxation process which is characterised by a single relaxation time and each relaxation process is described separately. The experimental results are consistent with the theoretical in the case of polar liquids. However, when studying systems in condensed matter, due to interactions between atoms and molecules, several relaxation times appear and the experimental data deviates from Debye's theory. For a description of the experimental data different theories are used such as the Cole-Cole, Cole-Davidson and Havriliak-Negami because they take into account different types of distribution of relaxation times [12]. The expression of the complex permittivity for each approach (theory Debye [11], Cole-Cole [13], Cole-Davidson [14], Havriliak-Negami [15]) is given by the relations (2.15-2.17) below:

Debye: $\varepsilon = \varepsilon_\infty + \dfrac{(\varepsilon_s - \varepsilon_\infty)(1 - j\omega\tau)}{1 + \omega^2\tau^2}$, (2.15)

Cole-Cole: $\varepsilon = \varepsilon_\infty + \dfrac{(\varepsilon_s - \varepsilon_\infty)}{1 + (j\omega\tau)^{1-\alpha}}$, $\quad 0 \le \alpha \le 1$, (2.16)

where α is a parameter and the distribution of relaxation times is symmetrical around τ (if α = 0, then it gives the Debye equation (2.15)). Next, the relation of

Cole-Davidson: $\varepsilon = \varepsilon_\infty + \dfrac{(\varepsilon_s - \varepsilon_\infty)}{(1 + j\omega\tau)^{\beta}}$, $\quad 0 \le \beta \le 1$, (2.17)

in which the distribution of relaxation times is not symmetrical and β is a parameter, which determines the shape of function. If β = 1, then it gives the Debye equation.

And last, the relation of Havriliak-Negami [16], [17], [18]:

$\varepsilon = \varepsilon_\infty + \dfrac{(\varepsilon_s - \varepsilon_\infty)}{[1 + (j\omega\tau)^{1-\alpha}]^{\beta}}$, in which $0 \le \alpha \le 1$ and $0 \le (1-\alpha)\beta \le 1$. (2.18)

The equation (2.18) gives the Cole-Cole relation, if β = 1, the Cole-Davidson relation, if α = 0, and the Debye relation, if β = 1 and α = 0 [19].

2.3 Dielectric polarization

There are different mechanisms of polarization, the main ones being: electronic (Fig.2.7), ionic (Fig.2.8), bipolar, and atomic [20].

• The Electronic polarization effect on each atom or molecule as the center of mass of the electron cloud that surrounds the atom will shift because of the EF. This effect is extremely fast, as the electrons are very light, and can be observed by optical frequencies.

36

No Field, (E = o)   Applied Field, (E ≠ o)
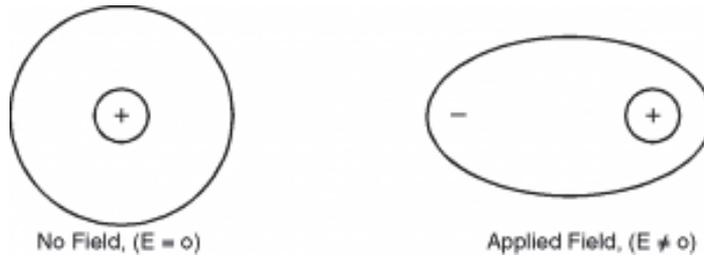
Fig.2.7 Electronic polarization in the electric field E [21]

• Atomic or ionic polarization refers to materials whose molecules form ions. When an EF is applied then cations and anions become displaced in opposite directions. Apart from electric polarization elastic displacements of the electrical charges (nuclei and electrons) will also occur. This means that these types of molecules are polar compounds that can be polarized up to infrared frequencies.
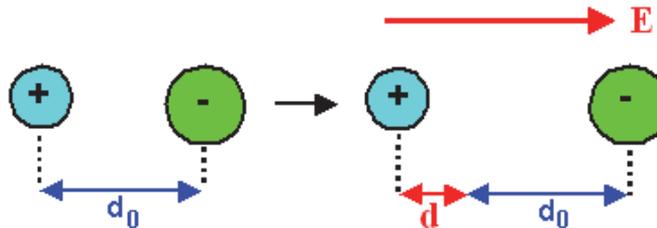
Fig.2.8 Ionic polarization [21]

• Bipolar polarization refers to materials that contain molecules with permanent dipole moments. Under the influence of EF, the dipoles are oriented in the direction of the EF.

In conclusion, the dielectric polarization is the result of the relative displacement of positive and negative charges in a material. During this process the EF is not able to force the charge to escape from the material which would cause electrical conductivity. Each of the dielectric polarization mechanisms is associated with a characteristic resonance frequency (sharp increase of dielectric permittivity at a given frequency) and relaxation frequency (gradual decrease in dielectric permittivity with increasing frequency). As the frequency increases, the slower dielectric polarization mechanisms are eliminated, leaving only the fastest to contribute to the phenomena of energy storage ($\varepsilon_r{'}$). Similarly, the rate of loss ($\varepsilon_r{''}$) is incremented at each critical frequency. The resonance is usually associated with electronic polarization.

2.4 Parallel plates with a dielectric

The most common dielectric characterization device is a capacitor with parallel plates between which the dielectric material under study is located.

The capacity of a pair of parallel charged plates is increased by introducing a dielectric material. The capacitance is inversely proportional to the electric field, while the presence of the dielectric reduces the field between the plates due to the existence of a field with opposite direction within the material because of the polarization of the material (Fig.2.9).

The capacity of a pair of parallel charged plates increases when a dielectric material is introduced. It is known that the dielectric is characterised by the dielectric permittivity ε_r and the capacity is multiplied by this factor. Overview of the capacity is

$$C = \frac{\varepsilon_r \cdot \varepsilon_o \cdot A}{d},$$ (2.19)

but if there is air between the plates then $C = \frac{\varepsilon_o \cdot A}{d}$. (2.20)
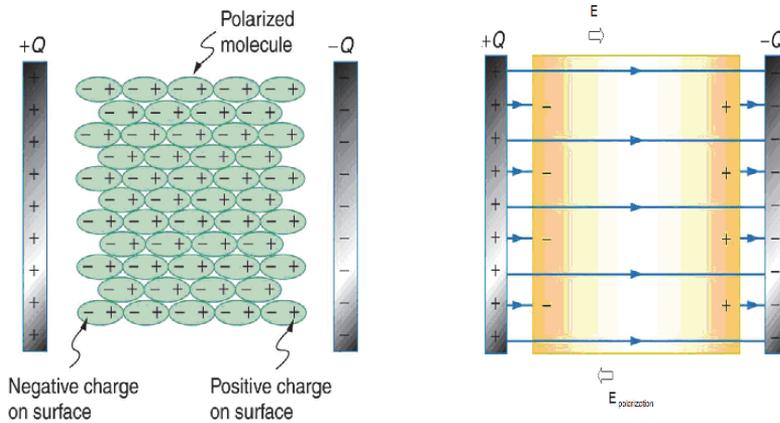
Fig.2.9 Parallel plates charged: polarized molecules (left) and electric field (right) [22]

When there is air or other dielectric material between the plates, the electric field E is expressed as

$$E = \frac{\sigma}{\varepsilon} = \frac{V}{d}, \quad \text{and}$$ (2.21)

$$E_{effective} = E - E_{polarization} = \frac{\sigma}{\varepsilon_r \cdot \varepsilon_o},$$ (2.22)

where V is the applied voltage and d the distance between the plates and σ is the surface charge density in each plate. The relative dielectric permittivity ε_r shows the amount of reduction of the active field in relation to the initial field. This reduction of the field results in the ability for more energy to be stored in the capacitor having the same voltage between the plates.

Along with energy storage, non-ideal capacitor is characterised by power consumption (losses). In the dielectric we have two types of losses:

i) Ohmic losses: there is a difference between the volume resistance (R_V) and surface resistance (R_S). The total resistance is

$$R_{total} = \frac{R_V \cdot R_S}{R_V + R_S}. \tag{2.23}$$

The ohmic losses are greater when the temperature of the insulator is increased.

ii) Dielectric losses: They are the result of a change of polarity of the dielectric due to changing the direction of the field in each period. This change causes oscillations that produce heat due to friction so part of the electrical energy turns to heat. The extent of loss expresses as

$$P = V_{rms}{}^2 2\pi f C \tan \delta, \tag{2.24}$$

where tanδ is the loss factor and is a measure of dielectric losses depending on the frequency.

2.5 Comparison of serial and parallel equivalent circuit

The electrical equivalent circuit, which is used to simulate a parallel plate capacitor may consist of a resistor and an ideal capacitor connected either in series or parallel (Fig.2.10).
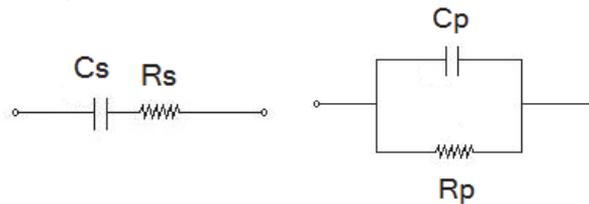
Fig.2.10 Series (left) and parallel (right) electrical RC circuits

The vector diagrams of voltages and currents for the two equivalent circuits in Fig. 2.10 are respectively given in Fig.2.11:
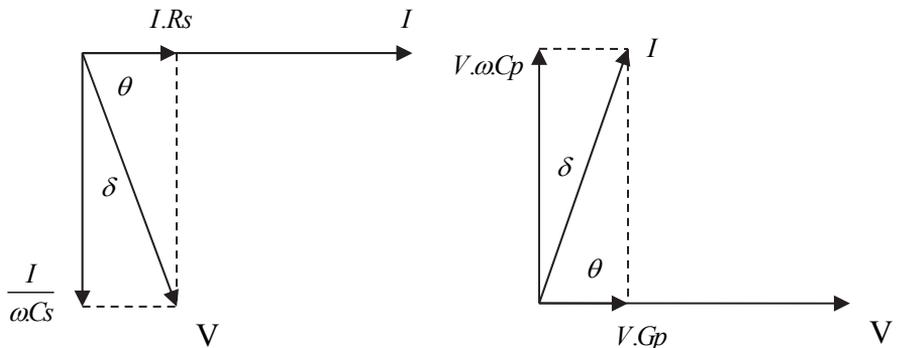
Fig.2.11 Vector diagrams of voltages and currents of series (left) and parallel (right) electrical circuits
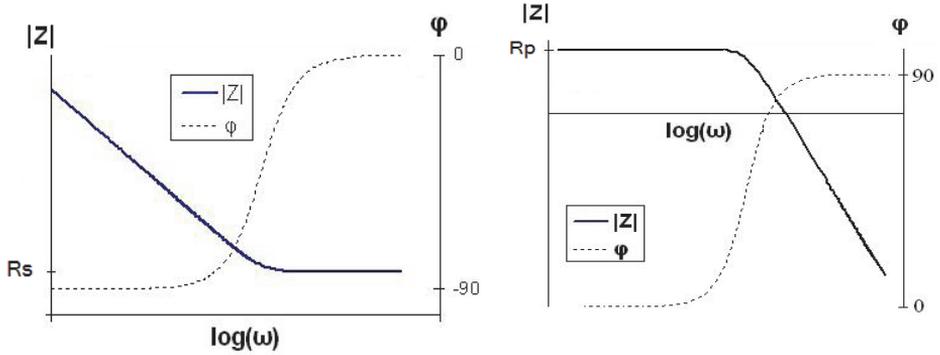
Fig.2.12 Frequency responses (Bode diagrams) of the series (left) and the parallel (right) electrical circuits

These two circuits describe the same system which is why the result concerning the relation between voltage and current must be the same. In this case the angles θ, δ in both diagrams and the complex impedance must be the same.
Subsequently, the necessary definitions are given to determine the analytical equations which connect the elements of the serial equivalent circuit with the complex dielectric permittivity and the loss tangent obtained from the parallel equivalent circuit.

The loss tangent from the parallel circuit is

$$\tan \delta = \frac{1}{\omega C_p R_p} = \frac{\varepsilon_r''}{\varepsilon_r'} \tag{2.25}$$

and from the series circuit the loss tangent is

$$\tan \delta = \omega R_s C_s . \tag{2.26}$$

The complex impedance of the parallel circuit is

$$Z_p = \frac{1}{\dfrac{1}{R_p} + j\omega R_p} \tag{2.27}$$

and from the series circuit it is

$$Z_s = R_s + \frac{1}{j\omega C_s} . \tag{2.28}$$

Given that $Z_p = Z_s$ means the real parts must be equal as must the imaginary parts, and by solving the equation system we get

$$C_P = \frac{C_S}{1 + \tan^2 \delta} \Rightarrow C_P = \frac{1}{1 + \omega^2 R_S^2 C_S^2} . \tag{2.29}$$

The ratio of resistors is:

$$\frac{R_P}{R_S} = \frac{1 + \tan^2 \delta}{\tan^2 \delta} = 1 + \frac{1}{\tan^2 \delta} \; . \tag{2.30}$$

So the real and the imaginary parts of dielectric permittivity are

$$\varepsilon_r{'} = \frac{C_P}{C_O} \Rightarrow \varepsilon_r{'} = \frac{C_S}{C_O \cdot \left(1 + \omega^2 R_S{}^2 C_S{}^2\right)} \quad , \tag{2.31}$$

$$\varepsilon_r{''} = \varepsilon_r{'} \tan \delta = \varepsilon_r{'} \omega R_S C_S = \frac{\omega R_S C_S{}^2}{C_O \left(1 + \omega^2 R_S{}^2 C_S{}^2\right)}$$

but $\varepsilon_r = \varepsilon_r{'} - j\varepsilon_r{''}$. $\tag{2.32}$

Finally, the complex permittivity is

$$\varepsilon_r = \frac{C_S}{C_O \left(1 + \omega^2 R_S{}^2 C_S{}^2\right)} - j \frac{\omega R_S C_S{}^2}{C_O \left(1 + \omega^2 R_S{}^2 C_S{}^2\right)} \; . \tag{2.33}$$

The last equation describes the complex dielectric permittivity with the help a serial equivalent circuit. In practice, the result which is obtained for the material under test does not depend on which equivalent circuit was used. The parallel circuit is more commonly used because the calculation of $\varepsilon_r{'}$ and $\varepsilon_r{''}$ is simpler.

2.6 Dielectric spectroscopy

In the above analysis we assumed that the electrical field applied to the dielectric is a sinusoidal waveform with stable frequency. Dielectric spectroscopy studies the change in dielectric properties of the material with time and frequency. Inside in an isotropic and homogeneous dielectric the polarization density vector P and the intensity E of the EF have the same direction and are linked as in the following equation [23, 24]:

$$P = \chi \varepsilon_O E \; , \tag{2.34}$$

where χ is the electrical susceptibility of the material. The χ indicates the degree of all kinds of polarizing of a dielectric and is dimensionless (for the vacuum it is equal to zero). The ε_0 = 8.85419·10^{-12} A·s/V·m is the dielectric constant of the vacuum. The electric displacement D is determined by the overall positive or negative electric charge per unit area induced in the corresponding electrode. The electrical charge of two electrodes is the origin of all the electrical field lines. In the area between the electrodes without a dielectric, the electrical displacement is parallel to the electric field E and is connected to it by the equation D = ε_0 E. When there is an isotropic dielectric between the electrodes, then the electrical displacement increases by the polarization density P and the equation becomes D=ε_0E+P [25, 26]. This happens, because in each of electrode part of the charge creates the electric field E, while the remaining

charge compensates polarization charges of the dielectric. Considering the above equations, we get

$$D = \varepsilon_O E + \chi \varepsilon_O E = (1 + \chi)\varepsilon_O E \ . \tag{2.35}$$

Thus the electrical displacement D is proportional to E, and for isotropic dielectric materials, the vectors P and D are parallel to E. The proportionality factor $(1 + \chi)\varepsilon_0$ is the dielectric permittivity ε of the material, and $1 + \chi$ is the relative dielectric permittivity ε_r. In this case the use of complex equations is not necessary.

2.6.1 Dielectric Response - Spectroscopy in time domain

When the electrical field is time varying, E (t), then the D in the vacuum immediately follows changes in the field $D(t) = \varepsilon_0 E(t)$. The charge density at electrodes is determined by the displacement current, which is derived from the voltage source and equals to dQ/dt, where Q is the total charge on each electrode.

When the vacuum is replaced by an isotropic dielectric material, then the electric displacement D is

$$D(t) = \varepsilon_o E(t) + P(t). \tag{2.36}$$

The time dependence of P(t) is not the same as E(t), because the polarization of the dielectric is not directly related to the applied field but has a time delay, which is different for the various types of polarization. To find the relationship between the field and the polarization, we will try to determine a time-varying function of the electrical susceptibility $\chi = \chi(t)$, and hence the relative dielectric permittivity $\varepsilon_r = 1 + \chi(t)$ applies to the equations:

$$P(t) = \chi(t)\varepsilon_O E(t) \tag{2.37}$$

and

$$D(t) = (1 + \chi(t))\ \varepsilon_o\ E(t). \tag{2.38}$$

2.6.2 Response to stepwise excitation

It is assumed that a temporal changing EF is applied: that is $E(t) = E_0 u(t - t_0)$, where $u(t - t_0)$ is the step function of the temporal change. Initially the field is zero and at t_0 the applied EF has a constant value E_0, which is maintained for $t > t_0$ (Fig.2.13).
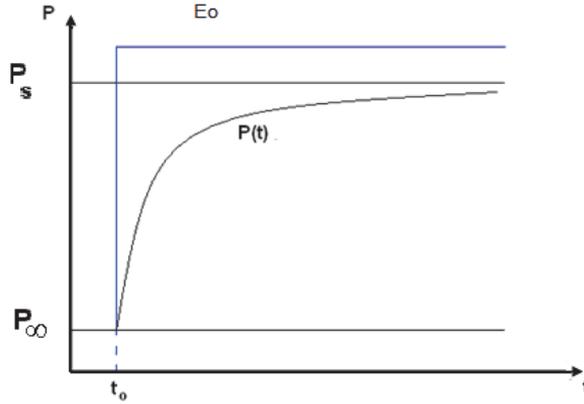
Fig.2.13 Temporal variation of the dielectric polarization P(t) as a result of stepping electric field

In this case the polarization $P(t)$ of dielectric is associated with the time-dependent susceptibility of $\chi(t)$ according to the equation

$$\frac{P(t)}{E_o} = \varepsilon_o \chi(t) u(t - t_0).$$ (2.39)

That is, the time-dependence of the polarization follows that of susceptibility $\chi(t)$, which is a characteristic function of the material, and the magnitude of the polarization is proportional to the applied field.

The function of polarization and susceptibility is generally distinguished into three time domains. In principle, there are very fast processes of polarization (mainly electronic) that can be considered to be affected in a very short time close to zero. Simultaneously with the application of the field, there is an instantaneous polarization $P(t = t_0)$, denoted P_∞ because it is performed at very high speed. This part of the polarization function cannot be recorded with the usual measuring equipment. After a long period of time, the polarization eventually becomes constant and takes the value P_s. Considering these two extreme values, the polarization can be given by the equation

$$P(t) = P_\infty + (P_S - P_\infty) g(t - t_o)$$ (2.40)

where g(t) is a dimensionless, monotonically increasing function (characteristic of the material), which determines the way the polarization goes from the baseline value P_∞ to the final value P_s.

Using the indices s and ∞ for the respective values of χ, the polarization can be written as follows:

$$P(t) = \varepsilon_o \left[\chi_\infty + (\chi_S - \chi_\infty) g(t - t_o) \right] E_o \Rightarrow P(t) = \varepsilon_o \chi(t) E_o$$ (2.41)

where

$$\chi(t) = \chi_\infty + (\chi_S - \chi_\infty) g(t - t_o).$$ (2.42)

43

If $1+\chi_s = \varepsilon_s \Rightarrow \chi_s = \varepsilon_s - 1$, and $1+\chi_\infty = \varepsilon_\infty \Rightarrow \chi_\infty = \varepsilon_\infty - 1$, $\qquad$ (2.43)

then the above equations become as

$$P(t) = \varepsilon_o \left[(\varepsilon_\infty - 1) + (\varepsilon_S - \varepsilon_\infty) g(t - t_o) \right] E_o, \qquad (2.44)$$

and

$$\chi(t) = (\varepsilon_\infty - 1) + (\varepsilon_S - \varepsilon_\infty) \cdot g(t - t_o). \qquad (2.45)$$

According to equation $D = (1+\chi)\varepsilon_0 E$, we obtain

$$D(t) = \varepsilon_o \left[\varepsilon_\infty + (\varepsilon_S - \varepsilon_\infty) g(t - t_o) \right] E_o, \qquad (2.46)$$

in which

$$\varepsilon(t) = 1 + \chi(t) = \varepsilon_\infty + (\varepsilon_S - \varepsilon_\infty) g(t - t_o) \qquad (2.47)$$

is the time depending relative permittivity of the dielectric material. All of the above are valid only for the simple case of stepping.

2.7 Summary
The goal of this chapter was to give an analytical overview of the characteristics of dielectrics and how frequency affects relative complex permittivity, and to present different approaches to and equations for relative complex permittivity such as that of Debye, Cole-Cole, Cole-Davidson and Havriliak-Negami. In addition, the three mechanisms of polarization, namely electronic, atomic and bipolar, are presented. The most common dielectric characterization device, a capacitor with parallel plates, between which the dielectric material under study is located, is also discussed. Ohmic and dielectric losses of a non-ideal capacitor were accounted for. Furthermore, we studied the equivalent circuits of a non-ideal parallel plate capacitor, those being a resistor and an ideal capacitor connected either in series or parallel. Finally, dielectric responses to both time domain and to stepwise excitation are given.

CHAPTER 3

ELECTRICAL BIOIMPEDANCE AND METHODS OF MEASUREMENT

A description of electrical bioimpedance as well as the Fricke-Morse model and the Debye model of different equivalent circuits of a tissue are given in this chapter. Next frequency dispersion is discussed. Lastly, the two methods of measuring bioimpedance are given.

3.1 Electrical bioimpedance

Electrical bioimpedance describes how a living organism responds to an externally applied electrical current [1]. It can be defined as the impedance of biological specimens. It is a measure of the difficulty of the flow of electrical current through the tissues. A biological tissue can be modeled from a structural viewpoint as the grouping of a number of elements called cells, which are immersed in an ionic medium (Na^+, K^+, Ca^{2+}, Cl^-) called extracellular fluid. This fluid contains also proteins and can be divided into plasma and interstitial fluid. We can consider any biological tissue as an electrolyte because of the ions it contains. Inside the cell membrane there is also a fluid (cytosol or intracellular fluid) and ion concentration in the intracellular environment, which is where the body's metabolic processes take place. It also contains the nucleus of the cell and numerous organelles (Fig.3.1).
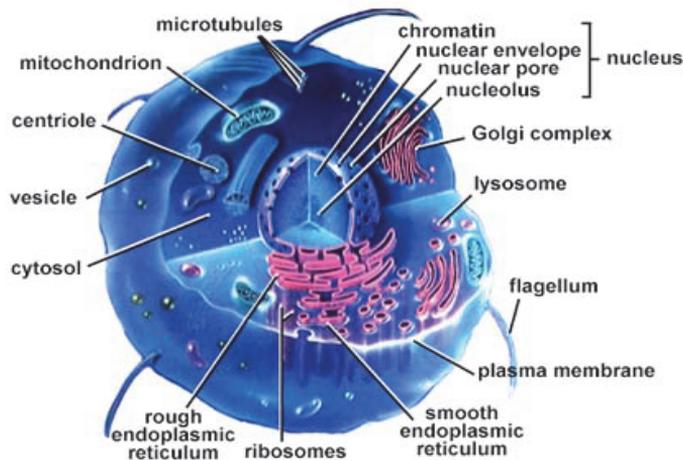
Fig.3.1 Cell contents [27]

The cell membrane consists of proteins and phospholipids forming a bilayer lipid membrane (Fig.3.2). Each monolayer has very small electrical conductance (10^{-6} A/V) and for that reason we can consider it as a dielectric material. Also there are ion gates in the membrane, which control the ion conductance (which is the inverse of the resistance).

For these reasons we can model the cell membrane as a two plated capacitor connected to a resistor in parallel ($C_m R_m$). The intracellular medium of the cell also behaves as a resistor (R_i).

Taking into account the ions in the extracellular fluid, we can add another resistor (R_e) to represent the extracellular fluid to the equivalent circuit [28], given in Fig.3.3.
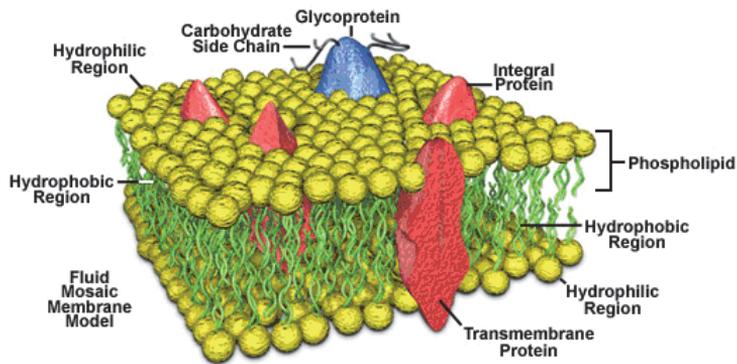
Fig.3.2 Plasma membrane structural components [29]
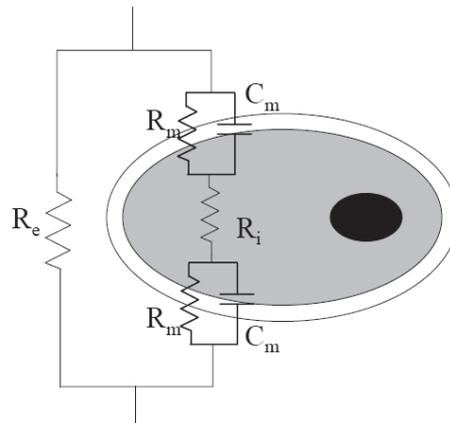
Fig.3.3 Equivalent electrical circuit of a cell and tissue [28]

By simplifying the above circuit taking into account that the two R_m resistors are connected in series and also the capacitors C_m, then the circuit becomes to a configuration sown in Fig.3.4.
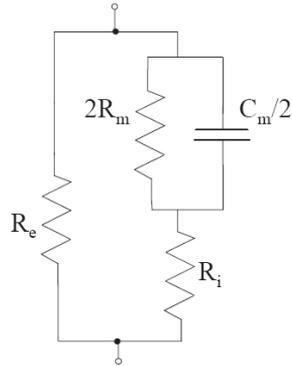
Fig.3.4 Simplified equivalent electrical circuit of a tissue

As aforementioned, the conductance of the membrane is very low in which case R_m takes a very high value. So the above circuit is further simplified (this is the Fricke-Morse model [30], see Fig.3.5):
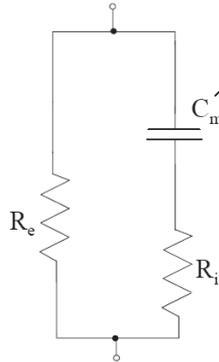
Fig.3.5 Fricke-Morse model

The impedance of the above circuit is equal to

$$Z = \frac{R_e\left(1 + jR_iC\omega\right)}{1 + jC\omega(R_i + R_e)}.$$

(3.1)

At low frequencies most of the current flows around the cell and only a little goes through the cell the membrane impedance is very high (Fig.3.6). If in eq. (3.1) the frequency $\omega \to 0$, then $Z = R_e$ due to that fact.
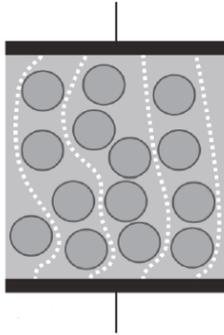
Fig.3.6 Passage of low frequency currents currents through a cell suspension or tissue
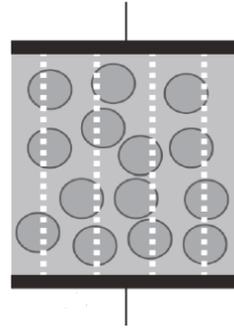
Fig.3.7 Passage of high frequency through a cell suspension or tissue

At high frequencies the current flows through both the extracellular and intracellular fluid because the membrane capacitance doesn't act as an impediment (Fig.3.7). When $\omega \to \infty$, then

$$Z_C = \frac{1}{jC\omega} \to 0 \text{ . Thus } R_e \text{ // } R_i \text{, and } Z = \frac{R_e R_i}{R_e + R_i} \text{ .}$$ (3.2)
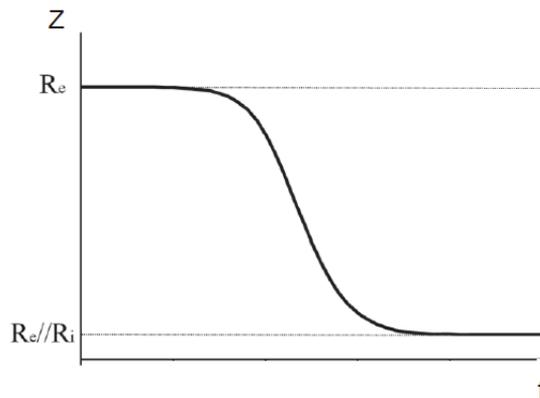
Fig.3.8 Impedance vs frequency in a tissue

3.2 Dispersion

The conductivity and the permittivity of tissue are frequency dependent. This phenomenon is called dispersion [1, 31, 32, 33] of which there are four types: α, β, δ and γ (Fig.3.9) in different frequency ranges.
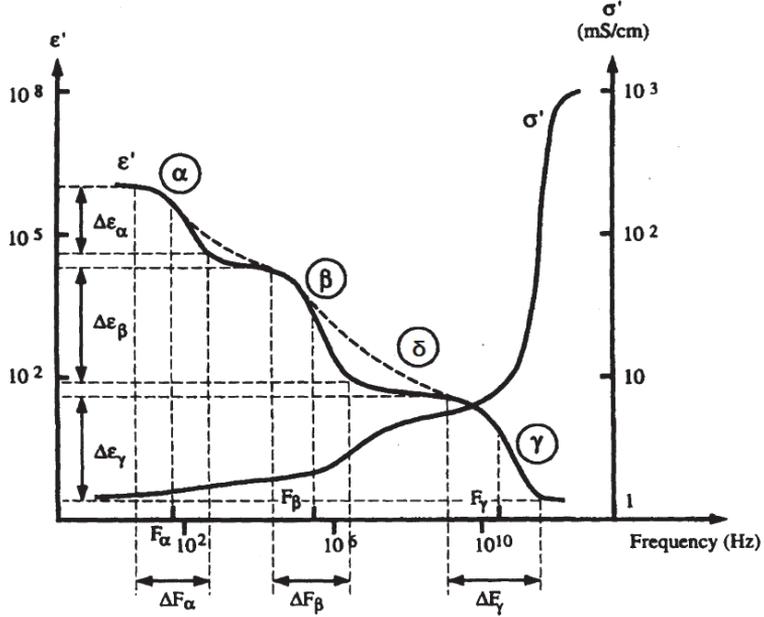
Fig.3.9 Frequency dispersions of the tissue permittivity [32]

The Fricke-Morse model is not very accurate, so the Cole impedance model was proposed for tissue. The Cole empirical equation [1] is expressed by the following equation

$$Z = R_\infty + \frac{R_0 - R_\infty}{1 + (j\omega\tau)^\alpha} , \tag{3.3}$$

where Z is the complex impedance, R_0 is the resistance at zero frequency, R_∞ is the resistance when $f \to \infty$ (only resistive parts), ω is the angular frequency, τ is the characteristic relaxation time constant and α is an introduced parameter with values between 0 and 1. For example, if $\alpha = 1$, we obtain Fricke-Morse model.

In the Fricke-Morse model we substitute the capacitance (Debye model in Fig.3.10, next page) with the Constant Phase Element (CPE) [34], which is described as an imperfect capacitor. The impedance of the CPE is

$$Z_{CPE} = \frac{1}{(j\omega C)^a} . \tag{3.4}$$

When α = 1 in (3.4), then the CPE behaves as an ideal capacitor C.
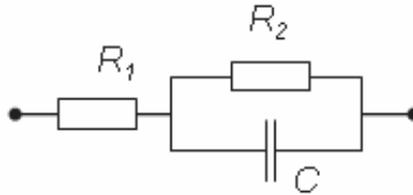
Fig.3.10 Debye model for tissues

By applying the Cole equation to this model we obtain:

$R_0 = R_1 + R_2$, $R_\infty = R_1$ and $\tau = R_2C$. (3.5)

3.3 Electrode Impedance and measuring methods

The interface between the body and the measuring device is where the bio-potential electrodes are located. Most electrodes are made from noble metals or stainless steel. These electrodes are called blocking electrodes because the current flowing into the body is the result of the ions but in the measuring device is the result of the electrons. So, there is no electronic exchange between electrodes and the tissue, which means direct current can't flow from the electrodes to the body or vice-versa. It is only possible for alternating current to flow through the body. Chemical reactions between the electrode and the electrolyte create a potential difference between them which is called half-cell potential. The equivalent circuit for a bio-potential electrode is shown in the following figure Fig.3.11, acquired from [35]:
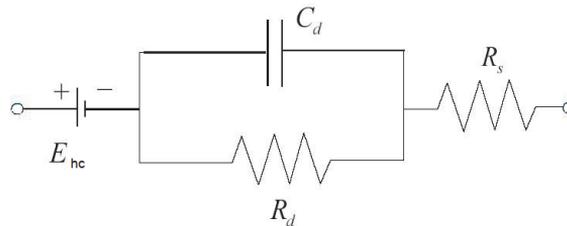
Fig.3.11 Equivalent circuit of a bio-potential electrode [35]

In the circuit, there is the half-cell potential E_{hc}, whereas R_d and C_d are the resistance and the capacitance of the electrode-electrolyte interface and R_s is the resistance of the electrolyte.

There are two common measurement methods in electrical bioimpedance, the two electrode or bipolar method and the four electrode or tetrapolar method [36].

3.3.1 Two electrode or bipolar method

An electrical current is injected into the body using two electrodes. In this configuration there are three impedances in series: the tissue impedance and the two electrode-electrolyte impedances (Fig.3.12). The voltmeter, which is connected to the tissue with the help of the same electrodes, as shown in the next Fig. 3.12, measures a voltage containing all the voltages of the three impedances, so the measured impedance is

$$Z_{measured} = \frac{V_{measured}}{I_{measured}} = Z_{e1} + Z_{e2} + Z_x. \tag{3.6}$$
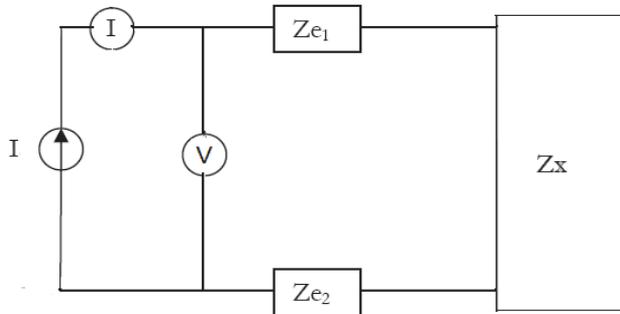
Fig.3.12 Two electrode or bipolar measurement method

3.3.2 Four electrode or tetrapolar method

With this method, the current is injected into the tissue through two electrodes, and with the use of another two electrodes we can measure the voltage [37], see Fig.3.13. With this method, the influence of the impedance of electrode-electrolyte is canceled. The measured impedance is

$$Z_{measured} = \frac{V_{measured}}{I_{measured}} = Z_x. \tag{3.7}$$
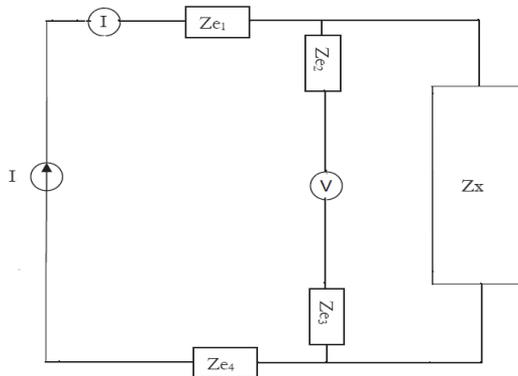
Fig.3.13 Four electrode or tetrapolar measurement method

3.4 Summary

In chapter 3 we analytically looked at the electrical bioimpedance which describes how tissue responds to an external electrical current. Electrical circuits equivalent to tissue are studied, namely those of the Fricke-Morse model and the Debye model. The four types of dispersion, which show the dependence of conductivity and the permittivity of tissue on frequency, are also analysed. Finally, the two electrode or bipolar and the four electrode or tetrapolar methods are given for impedance measurements. The latter method is preferred owing to the fact that the impedance of the electrode-electrolyte interface is canceled.

CHAPTER 4

MATHEMATICAL AND PHYSICAL MODELLING OF DYNAMIC ELECTRICAL BIOIMPEDANCE

In this chapter we develop different mathematical and physical models simulating dynamic electrical bioimpedance. The first model, based on RLC and operational amplifier circuits, represents the dynamic electrical impedance of a neuron. Next, using electrical impedance equivalents based on RLC, RL and operational amplifier circuits, a mathematical and physical modelling of the dynamic fluidic impedance of arteries is analysed. Then a mathematical and physical modelling of immune disease in terms of the alterations of the dynamic electrical impedance of thymus and bone marrow based on artificial neural networks and in non-linear components is studied. Finally, a mathematical and physical modelling of a tooth based on a RC circuit is developed.

4.1 Dynamic electrical impedance of a neuron

The basic structural and functional unit of the nervous system is the nerve cell or neuron [38, 39]. The nerve cells produce electrical signals transmitted from one part of the cell to another, while generating biochemical substances (acetylcholine - Ach) in order to communicate with other cells. A neuron consists of the cell body, the axon and the dendrites (Fig. 4.1). The neurons exchange information through a synapse (Fig. 4.2).
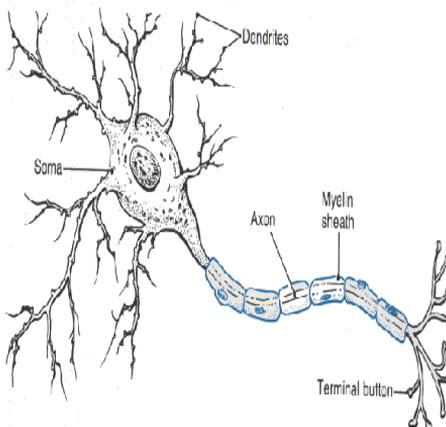
Fig.4.1 The structure of a neuron [40]   *Fig.4.2 Synapse between two neurons [41]*
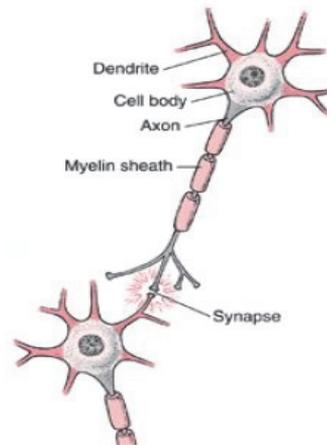
One of the functions of synapses is to determine the conduction of electrical impulses in one direction only. Therefore we can say that the synapses function as a transistor that allows the passage of electrical current in one direction [38] (Fig.4.3).
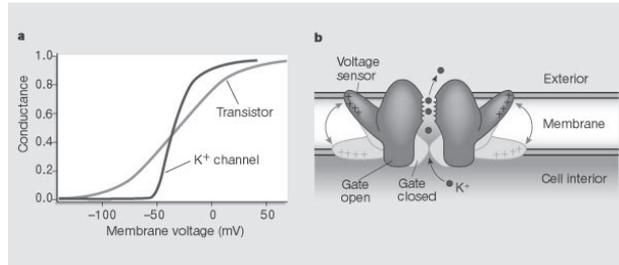
Fig.4.3 Comparison between a transistor and a neuron conductance vs membrane voltage diagram [38]

Along the surface of each neuron, potential electrical difference is due to the presence of excess negative charges on the inside and excess positive charges on the outer membrane which is why the neuron is polarized. The interior of the cell is typically 60-90 mV more negative than the outside. This potential difference is called the resting potential of the neuron (Fig.4.4 and Fig.4.5). When the neuron is stimulated an immediate change in the resting potential occurs. The change in the potential difference is called action potential (Fig.4.6) and is transmitted along the axis.
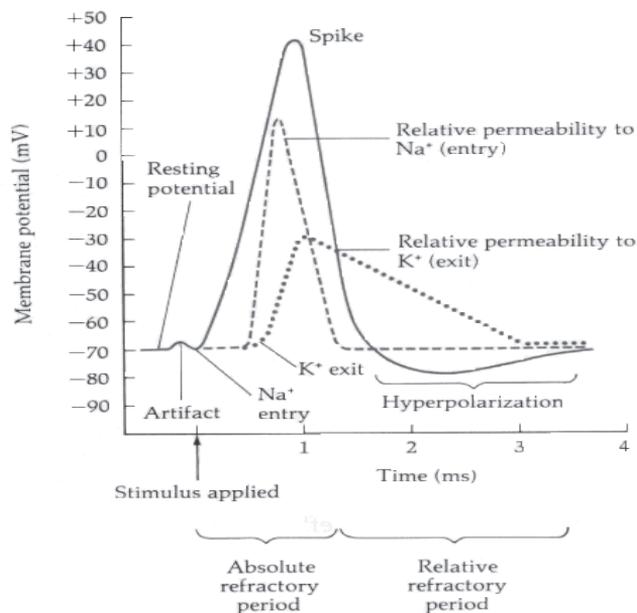
Fig.4.4 Membrane potential vs time [42]

Fig.4.5 Resting potential of a neuron

Fig.4.6 Active response of a neuron to current injection [43]

The developed models were based on RLC and Operational Amplifier circuits [44]. By changing the values of the components, we can calculate the bioimpedance of a healthy neuron or one affected by Parkinson's disease. With the use of the appropriate computational software, namely Maxima [45] and Maple [46, 47], the relevant equations of the models can be solved analytically. The next step is to use electronic simulation software in order to evaluate the performance of the models. Lastly, we check the biompedance of neurons which have undergone medical treatment, using the above models.
We assume the following RLC circuit (Fig.4.7):
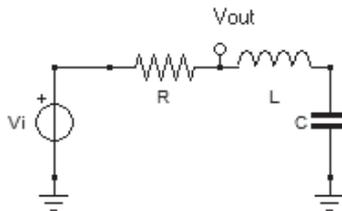
Fig.4.7 Electrical RLC equivalent circuit of a neuron

The differential equation in terms of the charge for the RLC circuit in Fig. 4.7 is the following [48], see eq. (4.1) below:

$$L\left(\frac{d^2}{dt^2}q(t)\right)+R\left(\frac{d}{dt}q(t)\right)+\frac{q(t)}{C}=0. \tag{4.1}$$

Next assume that we have a RLC circuit with time depending resistance R (t). So the differential equation (4.1) above is expressed as

$$L\left(\frac{d^2}{dt^2}q(t)\right)+R(t)\left(\frac{d}{dt}q(t)\right)+\frac{q(t)}{C}=0. \tag{4.2}$$

If the R (t) decreases exponentially, then $R(t)=Re^{-\frac{t}{\tau}}$, and eq. (4.2) becomes

$$L\left(\frac{d^2}{dt^2}q(t)\right)+Re^{-\frac{t}{\tau}}\left(\frac{d}{dt}q(t)\right)+\frac{q(t)}{C}=0. \tag{4.3}$$

The transfer function of the circuit is

$$\frac{V_{out}(s)}{V_i(s)}=\frac{1+CLs^2}{1+(CR)s+(CL)s^2}, \tag{4.4}$$

The transfer function (4.4) has a damping factor
$$\alpha=\frac{R}{2L}, \tag{4.5}$$

a resonant frequency
$$\omega_0=\frac{1}{\sqrt{LC}}, \tag{4.6}$$

and a quality factor
$$Q=\frac{\omega_0}{2\alpha} \tag{4.7}$$
or
$$Q=\frac{1}{R}\sqrt{\frac{L}{C}}. \tag{4.8}$$
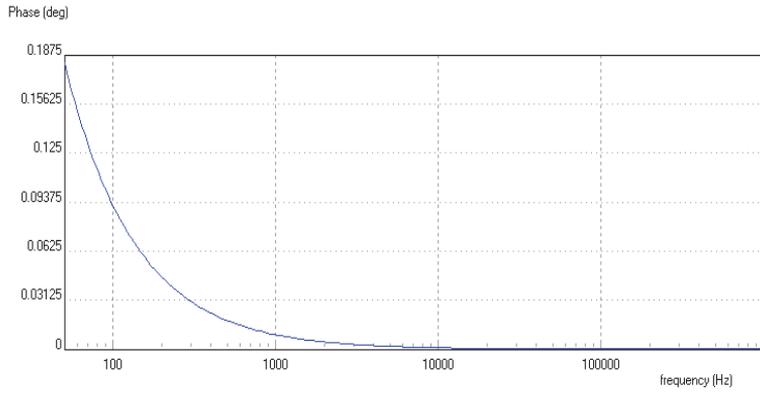
Fig.4.8 Phase shift vs frequency of the RLC circuit
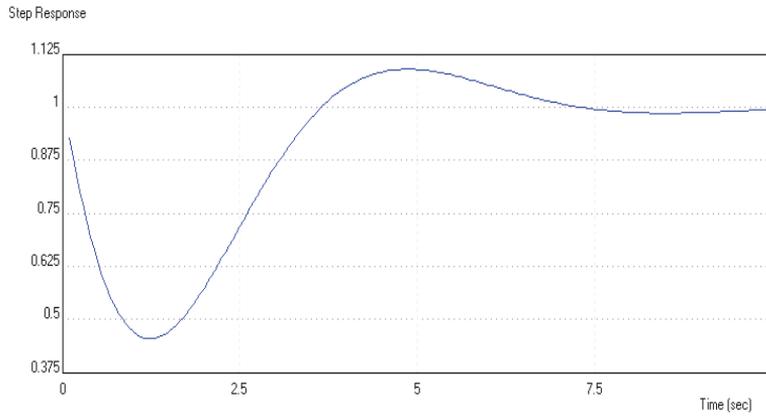
Fig.4.9 Step response of the RLC circuit
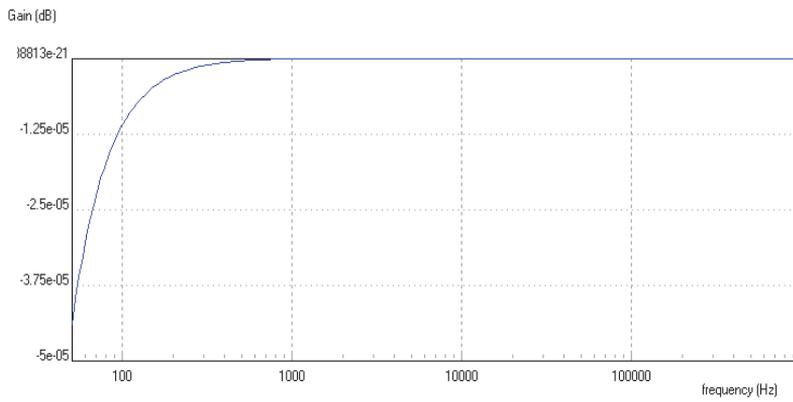
Fig.4.10 Gain vs frequency

57
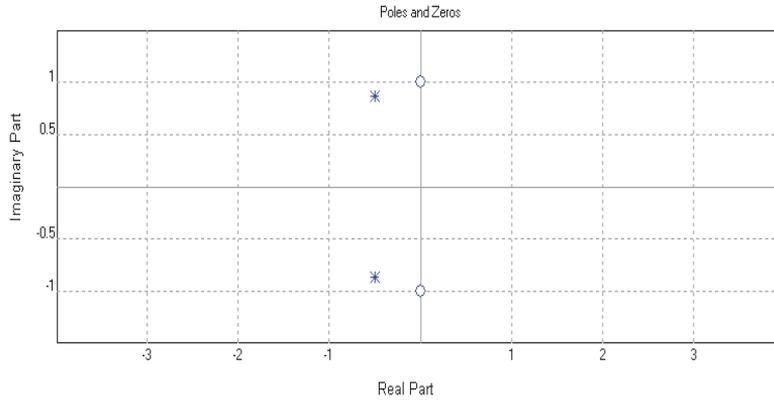
Fig.4.11 Pole-zero placement plot
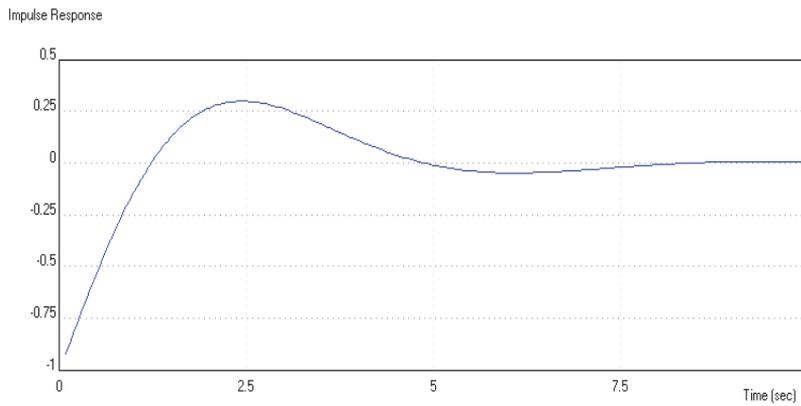
Fig.4.12 Impulse response

Instead of a typical RLC circuit we can use the following circuits [44] which behave in a manner very similar to an RLC circuit taking into account that bio inductors do not exist so in this case L in a similar differential equation is replaced with a combination of resistances and capacitors [49], see Fig.4.13.
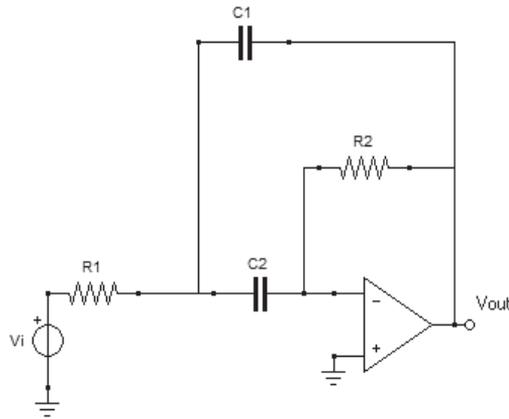
Fig.4.13 An active circuit, which behaves similarly to the RLC circuit given in Fig. 4.7

The impedance model of the above given circuit (Fig. 4.13) is shown in the next figure (Fig. 4.14).
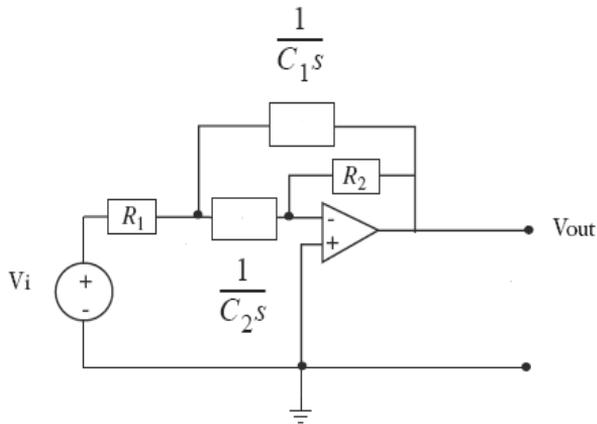
Fig.4.14 Impedance model of the circuit in fig.4.13

The transfer function of this circuit in Fig. 4.13 is the following:

$$\frac{V_{out}(s)}{V_i(s)} = \frac{-C_2 R_2 s}{1 + (C_1 R_1 + C_2 R_1)s + (C_1 C_2 R_1 R_2)s^2}. \tag{4.9}$$

The inverse Laplace function of eq. (4.9) gives eq. (4.10) in the time domain:

$$\frac{V_{out}(t)}{V_i(t)} = e^{-\frac{1}{2}\frac{(C_1+C_2)t}{C_1C_2R_2}} \left(-\frac{1}{C_1R_1}\left(\cosh\left(\frac{t\sqrt{R_1\left(R_1C_1^2 + 2C_1C_2R_1 + R_1C_2^2 - 4C_1C_2C_1\right)}}{2C_1C_2R_1R_2} \right) \right) + \right.$$

$$\left. \left(\sinh\left(\frac{t\sqrt{R_1\left(R_1C_1^2 + 2C_1C_2R_1 + R_1C_2^2 - 4C_1C_2R_2\right)}}{2C_1C_2R_1R_2} \right) \right)(C_1+C_2) \right) \Bigg/$$

$$\left(\sqrt{R_1\left(R_1C_1^2 + 2C_1C_2R_1 + R_1C_2^2 - 4C_1C_2R_2\right)}C_1 \right) \right)$$

(4.10)

The time domain response (4.10) has a damping factor

$$\alpha = \frac{C_1 + C_2}{2C_1C_2R_2},$$

(4.11)

a resonant frequency

$$\omega_0 = \frac{1}{\sqrt{C_1C_2R_1R_2}} ,$$

(4.12)

and a quality factor

$$Q = \frac{\sqrt{C_1C_2R_1R_2}}{C_1R_1 + C_2R_1}.$$

(4.13)
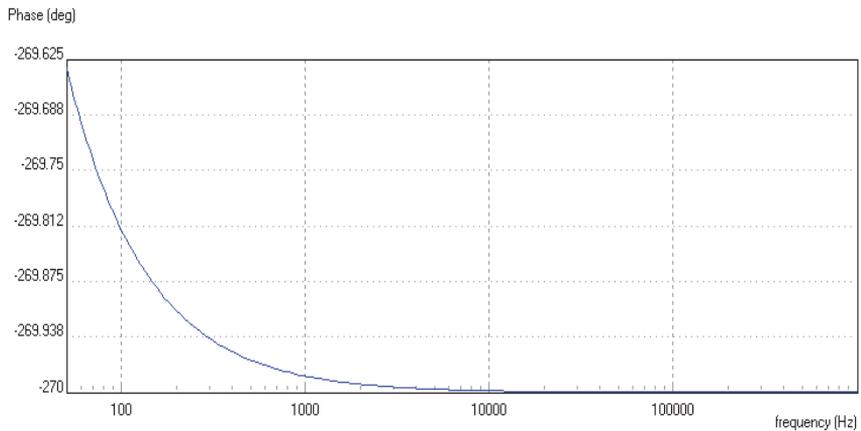
Fig.4.15 Phase vs frequency of the circuit in fig.4.13
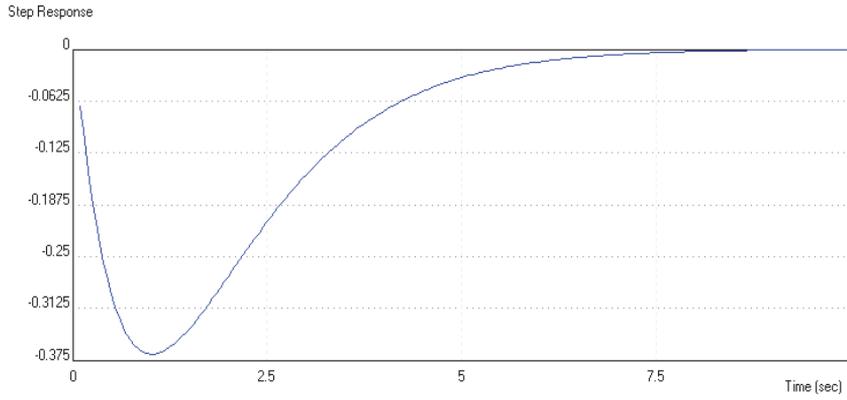
Fig4.16 Step response of the circuit in fig.4.13
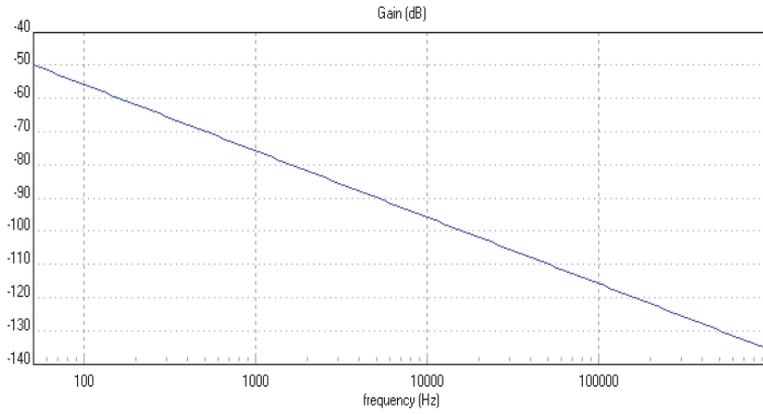
Fig.4.17 Gain vs frequency
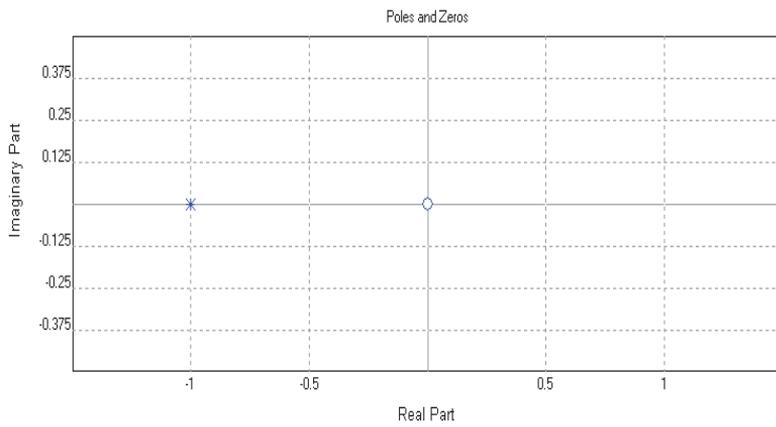
Fig.4.18 Pole-zero plot
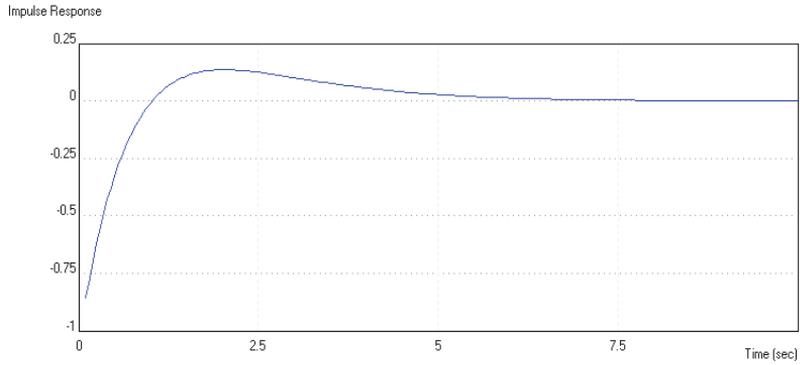
Fig.4.19 Impulse response

Another similar circuit is the following in Fig.4.20.
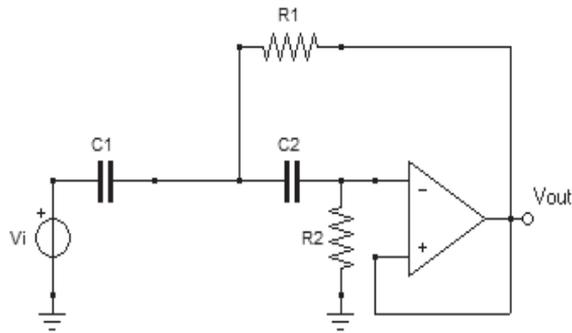
Fig.4.20 Circuit which behave similar to an RLC circuit

The impedance model of the above circuit is shown in the next figure (Fig.4.21).
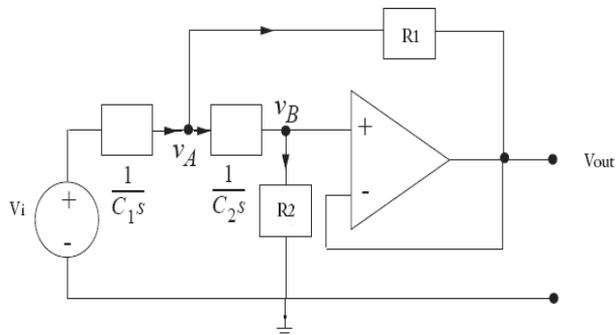
Fig.4.21 Impedance model of the circuit in fig.4.20

The transfer function of this circuit is

$$\frac{V_{out}(s)}{V_i(s)} = \frac{C_1 C_2 R_1 R_2 s^2}{1 + (C_1 R_1 + C_2 R_1)s + C_1 C_2 R_1 R_2 s^2} .$$ (4.14)

The inverse Laplace function of eq. (4.14) describing the circuit in Fig. 4.20 in the time domain is given below.

$$\frac{V_{out}(t)}{V_i(t)} = Dirac(t) +$$

$$\left(\left(-2C_1 C_2 R_2 + C_2^2 R_1 + C_1^2 R_1 + 2C_1 C_2 R_1 \right) \sinh\left(\frac{t\sqrt{R_1\left(R_1 C_1^2 + 2C_1 C_2 R_1 + R_1 C_2^2 - 4C_1 C_2 R_2 \right)}}{2C_1 C_2 R_1 R_2} \right) \right) e^{\frac{1}{2}\frac{(C_1+C_2)t}{C_1 C_2 R_2}} \Bigg/$$

$$\left(C_1 C_2 R_2 \sqrt{R_1\left(R_1 C_1^2 + 2C_1 C_2 R_1 + R_1 C_2^2 - 4C_1 C_2 R_2 \right)} \right) - \frac{1}{C_1 C_2 R_2}$$

$$\left((C_1 + C_2) \left(\cosh\left(\frac{t\sqrt{R_1\left(R_1 C_1^2 + 2C_1 C_2 R_1 + R_1 C_2^2 - 4C_1 C_2 R_2 \right)}}{2C_1 C_2 R_1 R_2} \right) \right) e^{\frac{1}{2}\frac{(C_1+C_2)t}{C_1 C_2 R_2}} \right)$$

(4.15)

The time domain response above has a damping factor

$$\alpha = \frac{C_1 + C_2}{2C_1 C_2 R_2},$$ (4.16)

a resonant frequency

$$\omega_0 = \frac{1}{\sqrt{C_1 C_2 R_1 R_2}} ,$$ (4.17)

and a quality factor

$$Q = \frac{\sqrt{C_1 C_2 R_1 R_2}}{C_1 R_1 + C_2 R_1} .$$ (4.18)
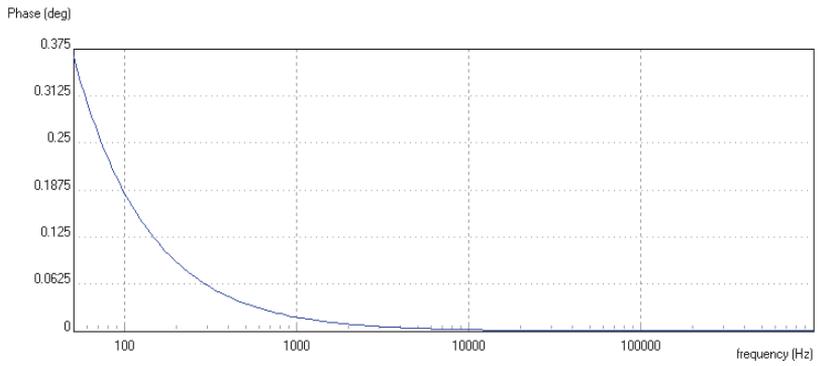
Fig.4.22 Phase vs frequency of the circuit in fig.4.20
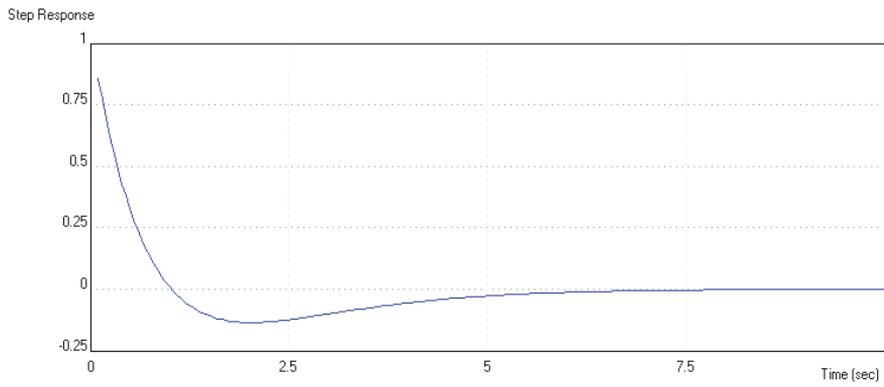
Fig.4.23 Step response of the circuit in fig.4.20
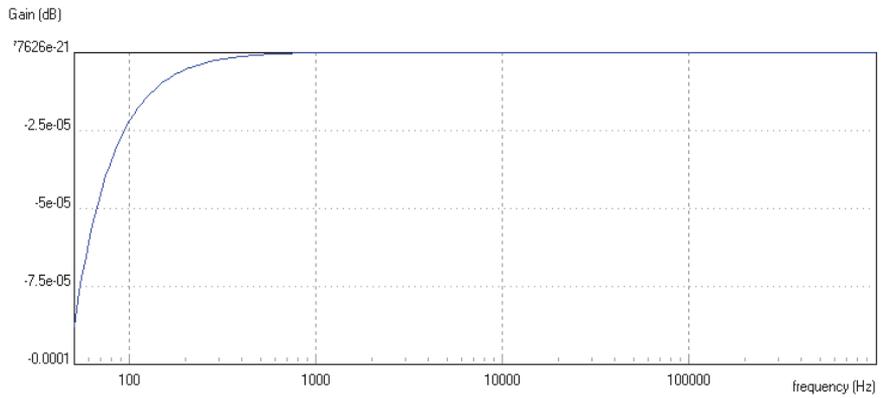
Fig.4.24 Gain vs frequency
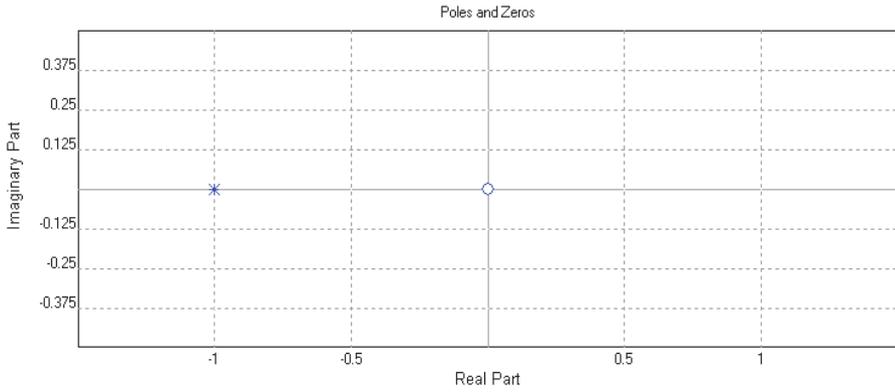
Fig.4.25 Pole-zero plot
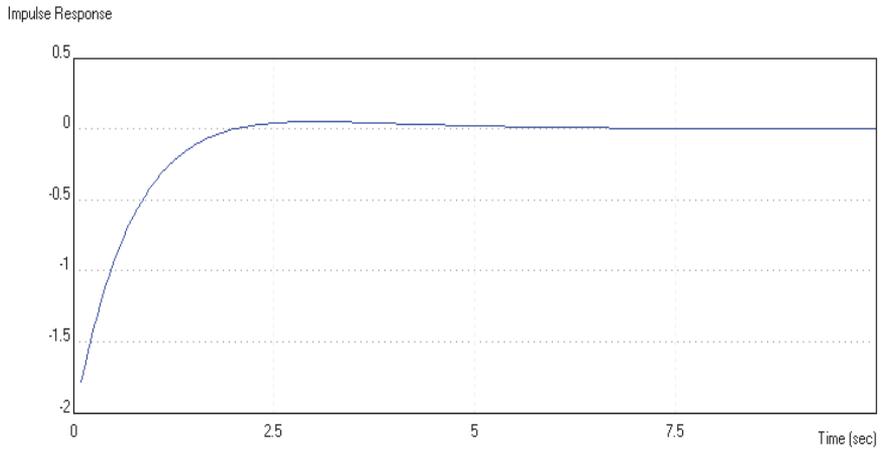
Fig.4.26 Impulse response

The solution to eq. (4.1) is as follows:

$$q(t) = {\_C_1}e^{-\frac{1}{2}\left(\frac{CR-\sqrt{C^2R^2-4CL}}{CL}\right)t} + {\_C_2}e^{-\frac{1}{2}\left(\frac{CR+\sqrt{C^2R^2-4CL}}{CL}\right)t}.$$ (4.19)

The condition for no oscillation, which a healthy neuron satisfies but a defective neuron doesn't, is as follows:

$$0 \le C^2R^2 - 4CL,$$ (4.20)

which is frequently expressed as

$$2\sqrt{\frac{L}{C}} \leq R \qquad (4.21)$$

For the initial conditions $q(0) = 0$ and $i(0) = 0$, we choose $\_C_1 = 1$ and $\_C_2 = -1$, and eq. (4.19) is turned to (4.22) now:

$$q(t) = e^{-\frac{1}{2}\left(\frac{CR-\sqrt{C^2R^2-4CL}}{CL}\right)t} - e^{-\frac{1}{2}\left(\frac{CR+\sqrt{C^2R^2-4CL}}{CL}\right)t}. \qquad (4.22)$$

Experimental results show that a neuron's response time is 10^{-4} s and according to eq. (4.19), the effective time is R/2L and according to eq. (4.21), it is possible to find appropriate values for the parameters L and C, the above give the following values: $L = 10^{-3}$ H and $C = 10^{-6}$ F [50].

With the above values eq. (4.22) becomes

$$q(t) = e^{-5.10^8\left(\frac{1}{10^6}R - \sqrt{\frac{1}{10^{12}}R^2 - \frac{1}{25.10^7}}\right)t} - e^{-5.10^8\left(\frac{1}{10^6}R + \sqrt{\frac{1}{10^{12}}R^2 - \frac{1}{25.10^7}}\right)t}$$

$$(4.23)$$

and eq. (4.21) gives the following result as $R \geq 63.24\ \Omega$. $\qquad (4.24)$

With the value of R = 70 Ω, eq. (4.23) becomes

$$q(t) = e^{-2.10^4 t} - e^{-5.10^4 t}. \qquad (4.25)$$

According to eq. (4.25), graph q = f(t) is drawn as follows (Fig. 4.27).
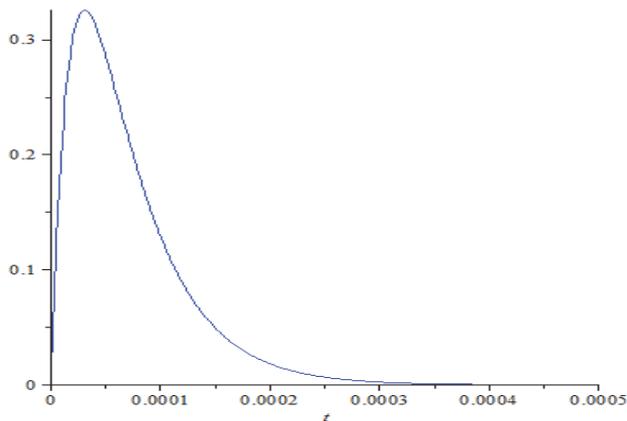
Fig.4.27 Charge vs time

66

If the resistance R is very low, close to zero, then eq. (4.23) becomes

$$q(t) = e^{31622.7766\,jt} - e^{-31622.7766\,jt}. \tag{4.26}$$

According to eq. (4.23), the following graph q = f(t), given that the charge q is in Coulombs, and time t is in seconds, can be drawn as a sine wave in Fig.4.28.
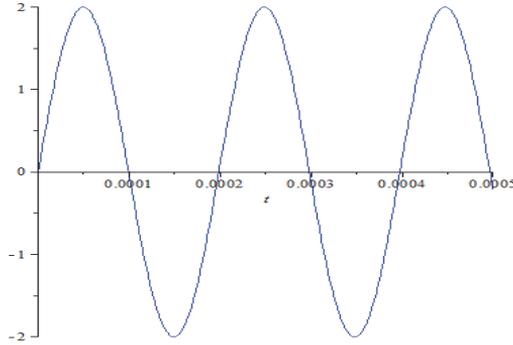
Fig.4.28 Charge vs time

As we can see when resistance is high (R = 70 Ω) there is no oscillation (no shaking) but when resistance is low (close to zero) there is oscillation (shaking). Thus, it appears that this behavior which is similar to the symptoms of Parkinson's disease is caused by decreasing resistance in the neuron. The solution to differential equations (4.2) and (4.3) expresses in terms of Bessel functions [51] in a very complicated form which is given in Appendix A-III on p.149.
Assume a neuron affected by Parkinson's disease, considering that the disease takes approximately 5 years (60 months) to develop and taking into account that the effective time is R/2L according to eq. (4.22), it is possible to find appropriate values for the parameters L and C. The above give the following values: L = 10 H and C =20 F. Also as we calculated before, values for R for the affected neuron should be under 63 Ω approximately. We can choose any value below that, so we choose R = 10 Ω (any value in R under 63 Ω will give similar results). The fact that the disease causes total degeneration within 10 years (120 months) after its first appearance and the life span of a person affected by Parkinson's disease after that is approximately 15 years (180 months) should be taken into account. Considering all the above as well as the fact that, hypothetically, the time required for the neuron to lose its resistance is approximately 15 months, τ = 15 months, so now eq. (4.3) becomes

$$10\left(\frac{d^2}{dt^2}q(t)\right) + 10e^{-\frac{1}{15}t}\left(\frac{d}{dt}q(t)\right) + \frac{1}{20}q(t) = 0. \tag{4.27}$$

67

According to eq. (4.27) the following graphs q = f(t) in Fig.4.29 and I = f(q) in Fig.4.30 have been drawn, given that q is in C, current I is in A and t is in months.
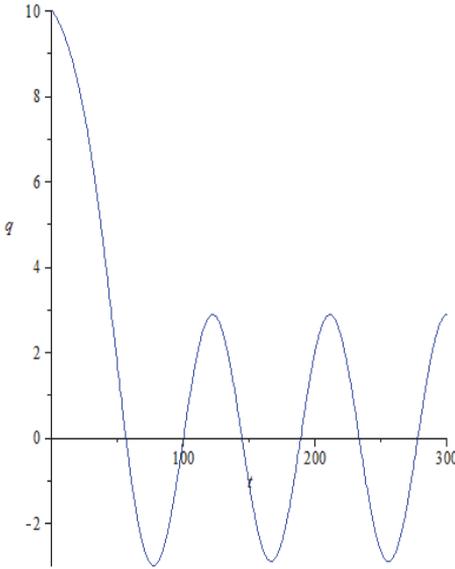
Fig.4.29 Charge vs time   Fig.4.30 Current vs charge
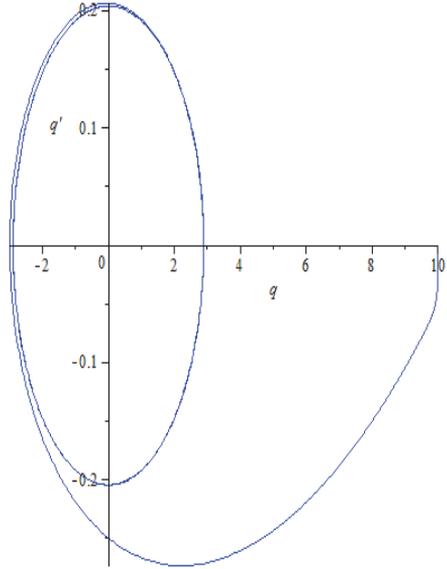
4.2 Dynamic fluidic impedance of arteries using electrical impedance equivalents

In this work a detailed mathematical and physical model for calculating the bioimpedance of an artery is developed. Initially the model calculates the biompedance of a healthy artery and then it compares this with the alteration in the bioimpedance of an artery with atherosclerosis [52].

Arteries are elastic blood vessels which carry oxygenated blood away from the heart, except the pulmonary artery which carries deoxygenated blood [53]. The structure of an artery wall consists of three layers (Fig.4.31):

a. Tunica Adventitia – this is the outer covering of the walls of the arteries. It is very strong and it is composed of connective tissues, collagen and also elastic fibres which can stretch to stop overexpansion because of the pressure of the blood. b. Tunica Media – this is the middle layer of the walls of arteries. It consists of smooth muscle and elastic fibres. c. Tunica Intima – this is the inner layer of the walls of arteries. It consists of an elastic membrane and smooth endothelial cells. The blood flows in the lumen which is the hollow centre of this layer.
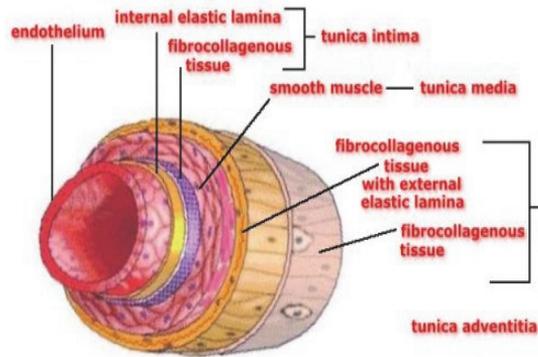
Fig.4.31 Structure of an artery [54]

Atherosclerosis (ASVD) occurs when the artery wall becomes thicker and hardens because of fatty material (such as cholesterol) build up on the artery wall. These hard formations are called atheromatous plaques (Fig.4.32). Atheromatous plaques consist of the atheroma which is a soft yellow material at the center of the plaque, cholesterol crystals and calcium deposition. The result is that the artery hardens and narrows which limits the normal flow of the blood (Fig.4.33).
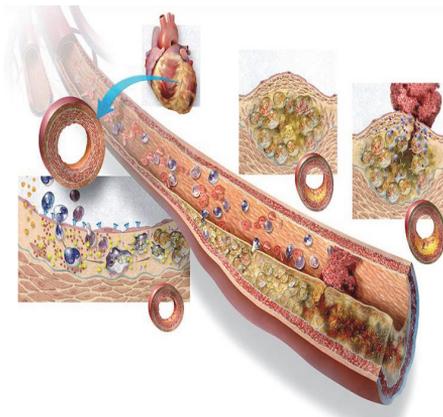
Fig.4.32 Atheromatous plaques [55]
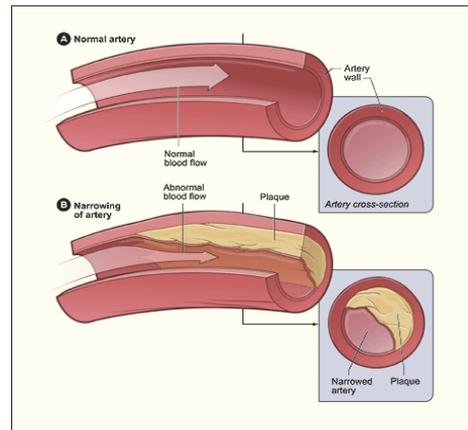
Fig.4.33 Narrowing of artery [56]

The developed models were based on RLC, RL and Operational Amplifier circuits [44]. By changing the values of the components, we can calculate the bioimpedance of a healthy artery or one affected by atherosclerosis. With the use of the appropriate computational software, namely Maxima [45] and Maple [46], the relevant equations of the models can be solved analytically. The next step is to use electronic simulation software in order to evaluate the

performance of the models. The Navier-Stokes equation for the incompressible flow of Newtonian fluids is

$$\rho\left(\frac{\partial \upsilon}{\partial t}+\upsilon.\nabla\,\upsilon\right)=-\nabla p+\eta\nabla^2\upsilon+F$$

(4.28)

where υ is flow velocity, ρ is fluid density, p is pressure, F are forces (such as gravity or centrifugal force) per unit volume, η dynamic viscosity, ∇ is the del operator and ∇^2 is the vector Laplacian. The derivative $\dfrac{\partial \upsilon}{\partial t}$ is unsteady acceleration, $\upsilon.\nabla\upsilon$ is convective acceleration, $-\nabla p$ is the pressure gradient and $\eta\nabla^2\upsilon$ is viscosity. The parameters η dynamic viscosity and ρ fluid density are space and time independent.
Considering that an artery is cylindrical we can study the Poiseuille flow in the artery [57]. Because of the cylindrical symmetry of the artery and assuming that the blood flow is axisymmetric in one dimension through a rigid artery which means the pressure inside the artery will be assumed to be independent of the radial coordinate then the Navier-Stokes equation becomes

$$\rho\partial_t\upsilon_x(r,t)-\eta[\partial_r^2+\frac{1}{r}\partial_r]\upsilon_x(r,t)=-\partial_r p(r,t)\ .$$

(4.29)

The boundary and initial conditions for $\upsilon_\chi(r,t)$ are

$$\upsilon_x(a,t)=0,\ \partial_x\upsilon_x(0,t)=0,\ \upsilon_x(r,0)=\frac{\Delta p}{4\eta\ell}(a^2-r^2),\ \upsilon_x(r,\infty)=0$$

(4.30)

where Δp is the change in pressure between the inlet and the outlet of the artery and ℓ is the length of the artery taking into account that the blood stops flowing in the end.

The no-slip condition $\upsilon_x(a,t)=0,$ refers to the assumption that concerns the fluid-solid interface or blood-vessel wall interface. No-slip boundary condition refers to the condition when the flow velocity at the tube wall is the same as the wall velocity, such that there is no "jump" or a step change in velocity to cause discontinuity. The general assumption is that the fluid in contact with the wall does not move at all (Fig.4.34).
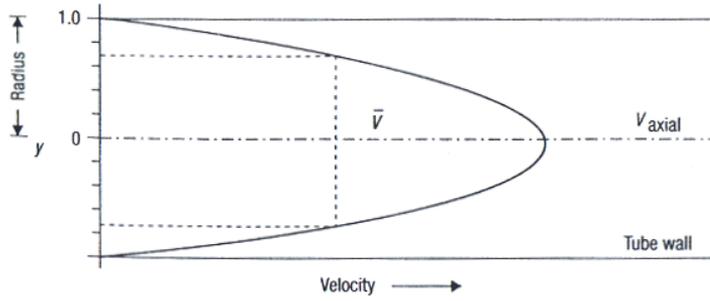
Fig.4.34 Blood flow in an artery

In the event that a Poiseuille flow starts in a circular channel the Navier-Stokes equation becomes an inhomogeneous, linear partial differential equation. In this case the pressure gradient is

$$-\partial_r p(r,t) = \frac{p(0,t) - p(\ell,t)}{\ell} = \frac{\Delta p}{\ell} \tag{4.31}$$

where $p(0,t)$ and $p(\ell,t)$ are the pressure at the inlet and the outlet of the artery respectively.
Therefore eq. (4.29) becomes

$$\rho \partial_t \upsilon_x(r,t) - \eta [\partial_r^2 + \frac{1}{r} \partial_r] \upsilon_x(r,t) = \frac{\Delta p}{\ell}. \tag{4.32}$$

The equation which gives the final result for the velocity field $\upsilon_\chi(r,t)$ of a stopping Poiseuille flow in the form of a Fourier-Bessel eigen-function expansion is the following [58]:

$$\upsilon_x(r,t) = \frac{a^2 \Delta p}{4\eta \ell} \sum_{n=1}^{\infty} \frac{8}{\gamma_n^3 J_1(\gamma_n)} J_0(\gamma_n \frac{r}{a}) \exp(-\gamma_n^2 \frac{v}{a^2} t) \tag{4.33}$$

where the values of γ_n are the roots of the Bessel function.

Considering that the dynamic viscosity of blood (in 37^0 C) is approx. $\eta = 3.10^{-3}$ Pas and the density of the blood is approx. $\rho = 1060$ Kg/m^3, we can calculate the kinematic viscosity of the blood. So, $v = \eta/\rho = 2.83 \ 10^{-6}$ m^2/s.
The time scale can be calculated with the following equation:

$$t_{acc} = \frac{1}{\gamma_1^2} \frac{a^2}{v} = \frac{1}{\gamma_1^2} T_0 \tag{4.34}$$

where t_{acc} is the time scale, α the radius of the artery, v the kinematic viscocity of the blood and T_0 is the momentum diffusion time.

71

Taking into account that the smallest Bessel function root is $\gamma_1 = 2.405$, according to eq. (4.34), the time scale of blood in an artery with the radius $\alpha = 1$ cm $= 10^{-2}$ m is calculated to be $t_{acc} = 6.1$ s and for an artery with atherosclerosis with radius $\alpha = 1$ mm $= 10^{-3}$ m is calculated to be $t_{acc} = 0.061$ s.

With the initial conditions

$$\upsilon_x(a,t) = 0, \ \partial_x \upsilon_x(0,t) = 0, \ \upsilon_x(r,0) = 0, \ \upsilon_x(r,\infty) = \upsilon_\infty, \tag{4.35}$$

eq. (4.33) becomes

$$\upsilon_x(r,t) = \frac{a^2 \Delta p}{4\eta\ell}[1 - \frac{r^2}{a^2} - \sum_{n=1}^{\infty} \frac{8}{\gamma_n^3 J_1(\gamma_n)} J_0(\gamma_n \frac{r}{a}) \exp(-\gamma_n^2 \frac{v}{a^2} t)]. \tag{4.36}$$

The volumetric flow rate Q for the elliptic channel (when an artery takes on an elliptic shape) can be calculated with the following equation [58]:

$$Q = \int_C dy dz \upsilon_x(y,z) = ab \int_0^{2\pi} d\phi \int_0^1 d\rho \rho \upsilon_x(\rho,\phi) = \frac{\pi}{4} \frac{1}{\eta\ell} \frac{a^3 b^3}{a^2 + b^2} \Delta p. \tag{4.37}$$

In the case of a circular channel using $\alpha = b$, eq. (4.37) becomes

$$Q = \frac{\pi a^4}{8\eta\ell} \Delta p. \tag{4.38}$$

To calculate the volumetric flow rate Q for a randomly deformed artery, the following equation can be applied:

$$Q = \frac{1}{\gamma} \frac{\Delta p}{2\eta\ell} \frac{A^3}{P^2} \tag{4.39}$$

where A is the cross sectional area and P the perimeter.

When $A = \pi a^2$ and $P = 2\pi a$ eq. (4.39) is reduced to eq. (4.38).

If $\bar{q}(s)$ is the Laplace transform of Q(t) and $\bar{p}(s)$ is the Laplace transform of p(t), then

$$\bar{q}(s) = \frac{\pi \bar{p}(s)}{s}(1 - \frac{2J_1(i\sqrt{s})}{i\sqrt{s}J_0(i\sqrt{s})}) \tag{4.40}$$

where

$$\bar{q}(s) = \bar{p}(s)K(s), \quad K(s) = \frac{\pi}{s}(1 - \frac{2J_1(i\sqrt{s})}{i\sqrt{s}J_0(i\sqrt{s})}) \tag{4.41}$$

and where K(s) is the hydrodynamic admittance and J_0 and J_1 are the Bessel functions of order 0 and 1 respectively, given that the Bessel function can be expressed as a series of gamma functions then eq. (4.41) can be expressed as follows:

$$K(s) = \frac{\pi}{s}\left(1 - \frac{2J_1\left(i\sqrt{s}\right)}{i\sqrt{s}J_0\left(i\sqrt{s}\right)}\right) = \frac{\pi}{s}\left(1 - \left[1 + \frac{\left(i\sqrt{s}\right)^2}{8} + \frac{\left(i\sqrt{s}\right)^4}{48} + \frac{11\left(i\sqrt{s}\right)^6}{3072} + ...\right]\right)$$

$$= \frac{\pi}{s}\left(\frac{s}{8} + \frac{s^2}{48} - \frac{11s^3}{3072} + O(s^4)\right) = \frac{\pi}{8} - \frac{\pi s}{48} + \frac{11\pi s^2}{3072} + O(s^3),$$

$$= \frac{\pi}{8} - \frac{\pi s}{48} + \frac{11\pi s^2}{3072} + O(s^3), \qquad (4.42)$$

so the result is

$$K(s) = \frac{\pi}{8} - \frac{\pi s}{48} + \frac{11\pi s^2}{3072}. \qquad (4.43)$$

Considering that the impedance is

$$H(s) = \frac{1}{K(s)}, \qquad (4.44)$$

the eq. (4.44) with the help of eq. (4.43) becomes

$$H(s) = \frac{1}{\dfrac{\pi}{8} - \dfrac{\pi s}{48} + \dfrac{11\pi s^2}{3072}}. \qquad (4.45)$$

If we compare the above impedance with the impedance of an RLC circuit in series

$$H(s) = \frac{1}{Ls^2 + Rs + \dfrac{1}{C}} \qquad (4.46)$$

where L is the inductance, R the resistor and C the capacitance, we get the values

$$L = \frac{11\pi}{3072}H, \ C = \frac{8}{\pi}F, \ \text{and} \ R = -\frac{\pi}{48}\Omega.$$

Taking into account the negative resistance we calculated above, we need to replace the resistance R in the RLC circuit in series with the following operational amplifier (Fig.4.35), which has an effective negative resistance R_{eff} [44]:

$$R_{eff} = -\frac{R_2 R_1}{R_3}. \qquad (4.47)$$

73
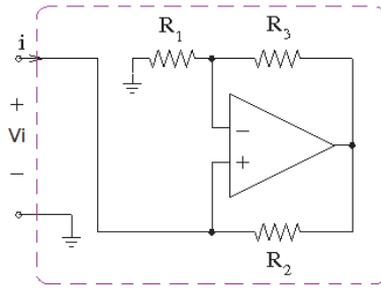
Fig.4.35 Operational amplifier with negative resistance R_{eff}

The new circuit is following (Fig.4.36):
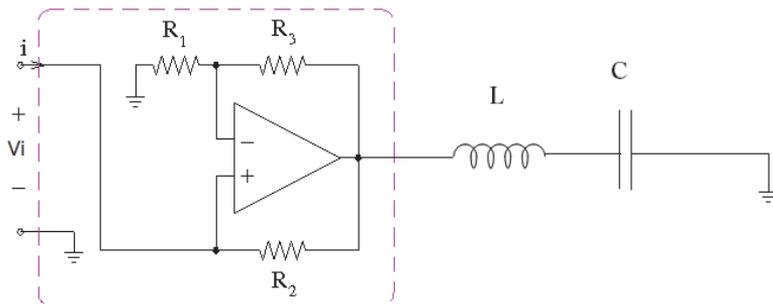
Fig.4.36 Equivalent circuit model of an artery

Figure 4.36 shows an equivalent circuit model of an artery with an arbitrary pressure gradient (pressure gradient with any temporal variation). Choosing the output V_{out} as given in Fig.4.37, we get the transfer function (4.48):

$$\frac{V_o(s)}{V_i(s)} = \frac{R_2 R_3 + R_1 R_2}{R_1 R_2 + CLR_1 R_2 s^2}. \tag{4.48}$$
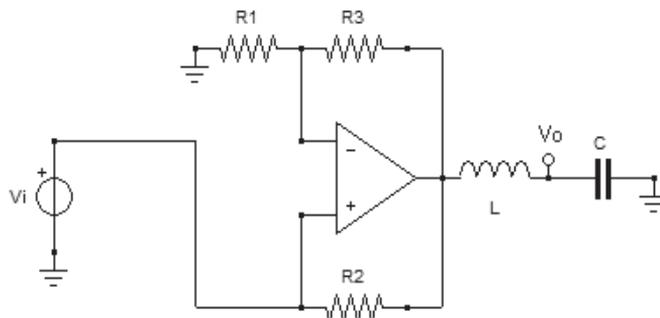
Fig.4.37 Equivalent circuit model of an artery

The inverse Laplace function of eq. (4.48) in time domain is following:

$$\frac{V_o(t)}{V_i(t)} = -\frac{(R_3 + R_1)\sinh\left(\dfrac{t}{\sqrt{-CL}}\right)}{R_1\sqrt{-CL}}. \tag{4.49}$$

Putting the values for R, L and C which we calculated before, eq. (4.49) becomes

$$\frac{V_o(t)}{V_i(t)} = \frac{2}{11}\sinh\left(-\frac{1}{11}\sqrt{-11}\sqrt{384}\ t\right)\sqrt{-11}\sqrt{384}. \tag{4.50}$$

With the help of the above equation we can draw the sine wave plot of $\dfrac{V_o(s)}{V_i(s)}$ versus time (Fig.4.38).
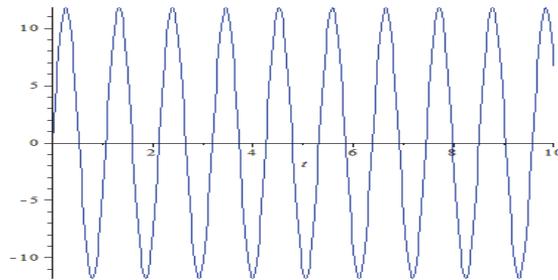
Fig.4.38 Function $\dfrac{V_o(s)}{V_i(s)}$ *vs time*

The step response (Fig. 4.39) and the impulse response (Fig. 4.40) plot of the circuit are shown below.
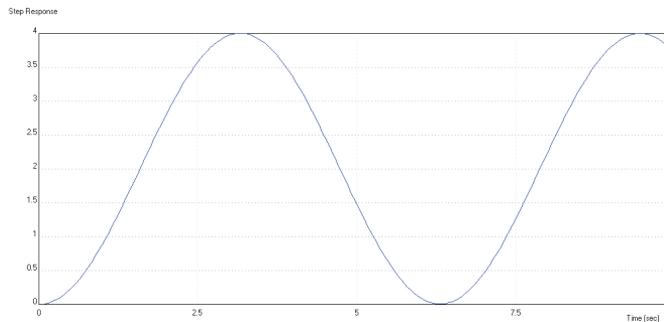
Fig.4.39 Step-response plot of the circuit in fig.4.37

75
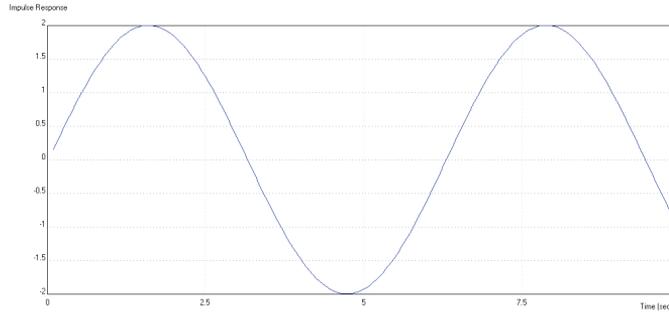
Fig.4.40 Impulse response plot of the circuit in fig.4.37

The following equation [58] derives from eq. (4.41):

$$Q(t) = \frac{\pi}{8} p(t) - 4\pi \sum_{n=1}^{\infty} \frac{1}{\gamma_n^4} \int_0^t e^{-\gamma_n^2(t-\tilde{t})} p'(\tilde{t}) d\tilde{t}. \tag{4.51}$$

The terms in the summation of eq. (4.51) are decreasing exponentials, so when the time tends to infinity then only the first term contributes to the sum, so eq. (4.51) becomes eq. (4.52) given below

$$t_{acc} \frac{dq}{dt} + q = \frac{\pi a^4}{8\eta\ell} p . \tag{4.52}$$

The eq. (4.52) is similar to an equation of an RL circuit in series. The following circuit (Fig.4.41) is equivalent to an artery in the case where the pressure gradient is fixed (constant pressure gradient) and it represents normal operation of the artery.
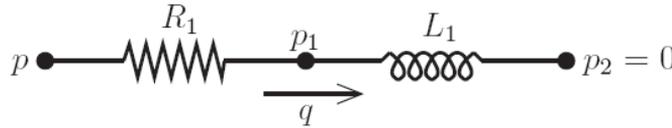
Fig.4.41 Equivalent circuit model of an artery at fixed pressure gradient

The differential equation for the above circuit is

$$\frac{L_1}{R_1} \frac{dq}{dt} + q = \frac{1}{R_1} p . \tag{4.53}$$

Comparing eq. (4.52) and eq. (4.53) we obtain

$$R_1 = \frac{8\eta\ell}{\pi a^4} \quad \text{and} \quad L_1 = t_{acc} \frac{8\eta\ell}{\pi a^4} = \frac{8\eta\ell}{\gamma_1^2 \nu \pi a^2}. \tag{4.54}$$

The transfer function of the above circuit is

$$\frac{V_o(s)}{V_i(s)} = \frac{L_1 s}{R_1 + L_1 s}. \tag{4.55}$$

The step response (Fig.4.42) and the impulse response (Fig.4.43) plots are given below.
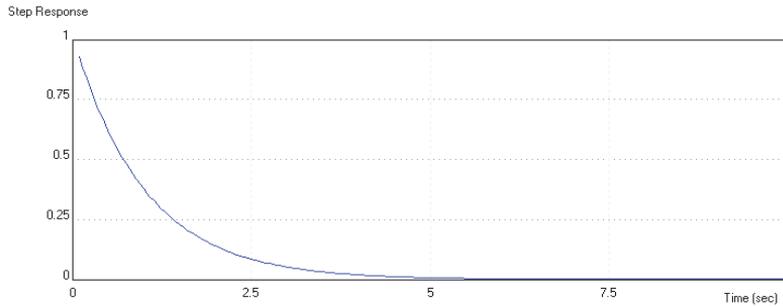
Fig.4.42 Step response plot of the circuit in fig.4.41
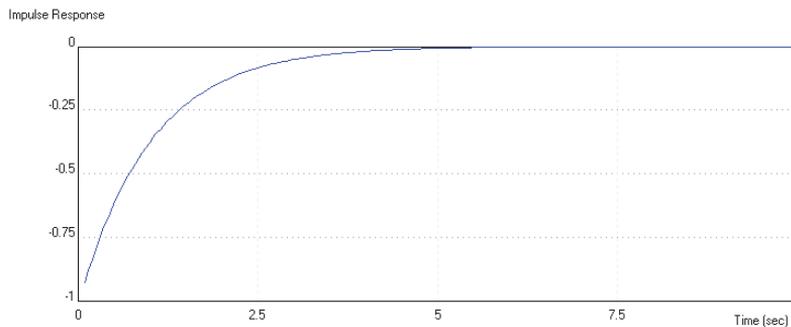
Fig.4.43 Impulse response plot of the circuit in fig.4.41

4.3 Immune disease in terms of the alterations of the dynamic electrical impedance

In this work a detailed mathematical and physical model for simulating the immune system is developed. The neural networks [59, 60] are very important tools in the field of artificial intelligence. Recently the analogies between the brain and the immune system [61] were exploited to build artificial immune systems and immune algorithms [62, 63, 64] with applications in computer science. The model uses neural networks of two and three neuron module to simulate the interactions between T-cells and B-cells taking into account that the biompedance is represented by the transfer functions from antigens to immune responses. Also this model compares the dynamical behaviour of the cells of the immune system, particularly the immune memories and the bifurcations from a normal behaviour to an abnormal behaviour.

Lymphocyte is a type of white blood cell. The most abundant lymphocytes are the B lymphocytes (B-cells) and the T lymphocytes (T-cells). The B-cells are produced in the bone marrow, which is a tissue inside the bones. Also the

precursors of T-cells produced in the bone marrow and after they mature in the thymus.

Thymus is a glad of the immune system. It is located in the chest, between the breast bone and the heart (Fig.4.44). It has two lobes, the left and the right. Each lobe is composed of a number of lobules together. Each lobule consists of the outer cortex and the inner medulla. The cortex has a very large number of developing T-cells and a smaller number of associated epithelial cells. T-cells migrate to the medulla in order to mature and to learn how to recognize self from non self so that inappropriate immune responses are prevented.

Immune diseases are caused of different reasons such as lack of enough T-cells production because of improper development of the thymus gland or an excessive immune response or even an autoimmune attack.
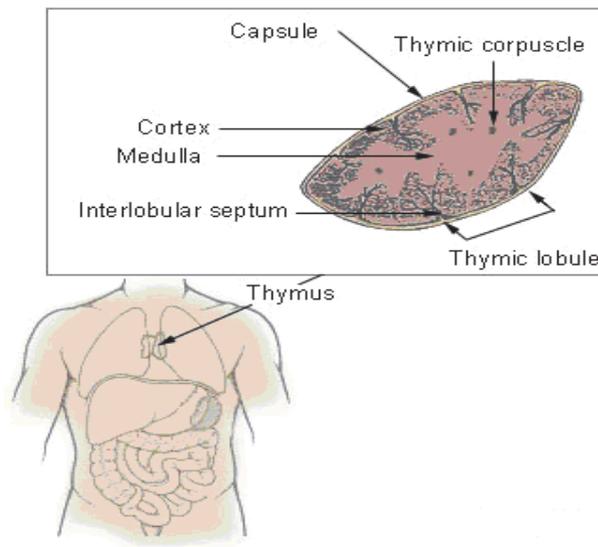
Fig.4.44 Thymus [65]

The developed models are based on neural network of two and three neuron module which they can be constructed by non linear circuits. By changing the values of the synaptic weights and the activation functions, we can simulate the dynamical behaviour of the cells when the immune system is working without a problem and when is affected by a disease. With the use of the appropriate computational software, namely Maxima [45] and Maple [46], the relevant equations of the models can be solved analytically.

The next figure (Fig.4.45) [60] represents a T-cell or a B-cell either of which can be simulated using a non linear component.
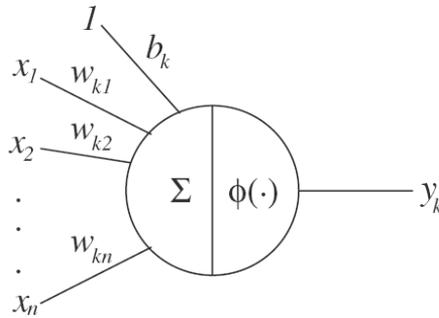
Fig.4.45 T-cell or B-cell [60]

In fig. 4.45, x_1, x_2 to x_n is the set of input signals, y_k is the output signal, and w_{k1}, w_{k2m} ... to w_{kn} are the synaptic weight between the cells, φ is the activation functions and b_k is the bias. In electrical terms x_1, x_2, to x_n are the input voltages, y_k is the output voltage, w_{k1}, w_{k2},..,w_{kn} are the mutual inductances, φ is the threshold of a nonlinear component and b_k is the noise margin.

The activation potential and the output are given by the following equations respectively:

$$\upsilon_k = w_k x + b_k, \; y_k = \phi(\upsilon_k). \tag{4.56}$$

The next two figures represent different immune networks.

Figure 4.46 shows a feedforward single-layer network and figure 4.47 is a feedforward neural network with one hidden layer. Inputs (x) represent the antigens and outputs (y) represent the lymphocytes (T-cells or B-cells) and the antibodies. The impedance of these networks is the transference functions from antigens to immune responses (antibodies and lymphocytes). Electrically that could be a circuit with non-linear components.
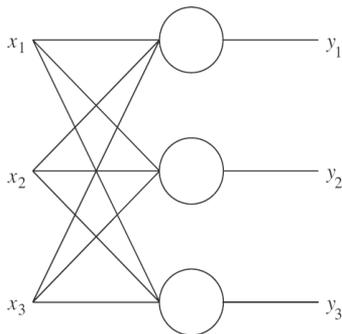
Fig.4.46 A feedforward single-layer network
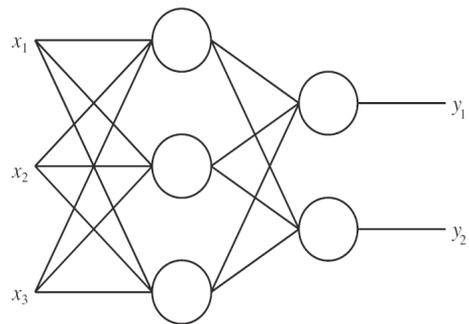
Fig.4.47 A feedforward neural network with one hidden layer

The following Figure 4.48 represents a recurrent Hopfield neural network with feedback. It is a network, whose purpose is to recognise self-antigens in such a way that the immune system does not attack the cells of the body.
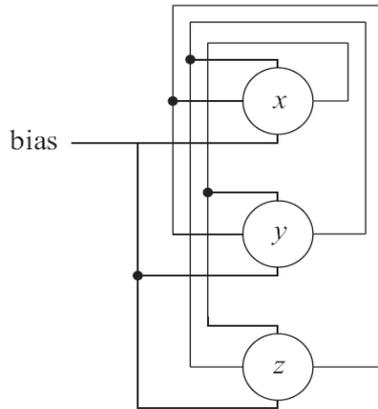
Fig.4.48 Hopfield neural network
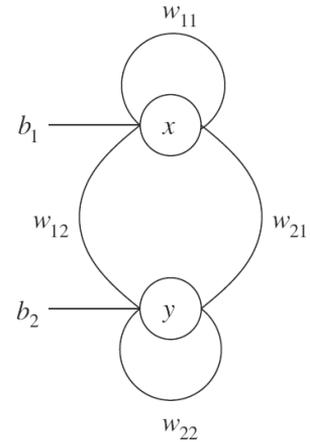
Fig.4.49 Two neuron network

Figure 4.49 and 4.50 show a two-neuron and a three-neuron module respectively. It also shows the interactions between the cells which can be either an activation interaction or inhibition interaction.
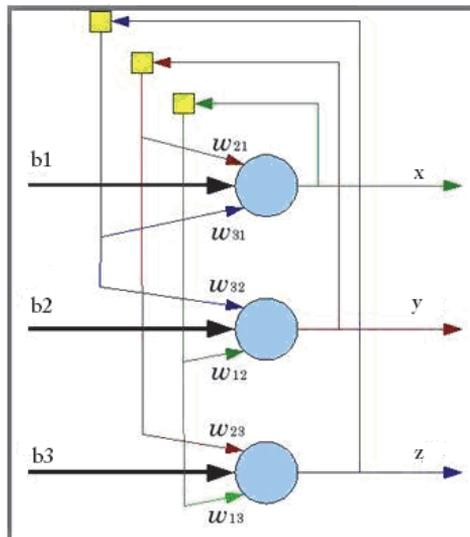
Fig.4.50 Three neuron network

For the two-cell module we can calculate the following:

$$x_{n+1} = b_1 + \frac{w_{1,1}}{1+e^{-x_n}} + \frac{w_{1,2}}{1+e^{-y_n}} \tag{4.57}$$

$$y_{n+1} = b_2 + \frac{w_{2,1}}{1+e^{-x_n}} + \frac{w_{2,2}}{1+e^{-y_n}} \tag{4.58}$$

where x's and y's are the output voltages (in mV), b's are the external voltages (in mV) and w's are inductances and mutual inductances (in mH) of the cells. Pasemann and Stollenwerk [60] considered the model with the following parameter values:

$$b_1 = -2, \ b_2 = 3, \ w_{1,1} = -20, \ w_{1,2} = 6, \ w_{2,1} = -6, \ w_{2,2} = 0. \tag{4.59}$$

Eq. (4.57) and eq. (4.58) become

$$x_{n+1} = -2 - \frac{20}{1+e^{-x_n}} + \frac{6}{1+e^{-y_n}} , \ y_{n+1} = 3 - \frac{6}{1+e^{-x_n}}. \tag{4.60}$$

When $x_{n+1}=x_n$ and $y_{n+1}=y_n$ (equilibrium point) then eq. (4.60) become

$$x = -2 - \frac{20}{1+e^{-x}} + \frac{6}{1+e^{-y}} , \ y = 3 - \frac{6}{1+e^{-x}}. \tag{4.61}$$

The solution is following:

$$x = -1.28037, \ y=1.69508. \tag{4.62}$$

If eq. (4.61) is written as a vector with the right hand sides, then we get:

$$\left[-2 - \frac{20}{1+e^{-x}} + \frac{6}{1+e^{-y}} , 3 - \frac{6}{1+e^{-x}} \right]. \tag{4.63}$$

Using the Jacobian of eq. (4.63), see Appendix A-III, and taking into account eq. (4.62), we get:

$$\begin{bmatrix} -\dfrac{20e^{1.28037}}{\left(1+e^{1.28037}\right)^2} & \dfrac{6e^{-1.69508}}{\left(1+e^{-1.69508}\right)^2} \\[4ex] -\dfrac{6e^{1.28037}}{\left(1+e^{1.28037}\right)^2} & 0 \end{bmatrix}$$

(4.64)

In the case of a MOSFET (non-linear component) the derivative of the voltage (output) respect to the current (input) is the equivalent resistance. In this case eq. (4.64) is the equivalent impedance for the linearized model.

The eigenvalues (in sec^{-1}) of the impedance matrix of eq. (4.64) are

$$[-3.14872, \; -0.25499].$$

(4.65)

Because of at least one of the absolute values in the eq. (4.65) is greater than 1, according to the stability theorem for discrete systems represented by difference equations. The system is unstable.

Subsequent equations are the same with the higher memory states. Eq. (4.66) represents the equation that determines the equilibrium point of the order of 2 (excited memory state) being in eq. (4.62) the fundamental memory state:

$$\left[x_{n+2} = -2 - \frac{20}{1+e^{-x_{n+1}}} + \frac{6}{1+e^{-y_{n+1}}}, y_{n+2} = 3 - \frac{6}{1+e^{-x_{n+1}}} \right]$$

(4.66)

In this case the solution and the eigenvalues are (Appendix A-III):

$$x = -1.28037, \; y = 1.69508$$

(4.67)

and

$$[-3.14872, \; -0.25499].$$

(4.68)

Using the appropriate programs (program 1 and program 2 in Appendix A-II), we get Figures 4.51 and 4.52, respectively.
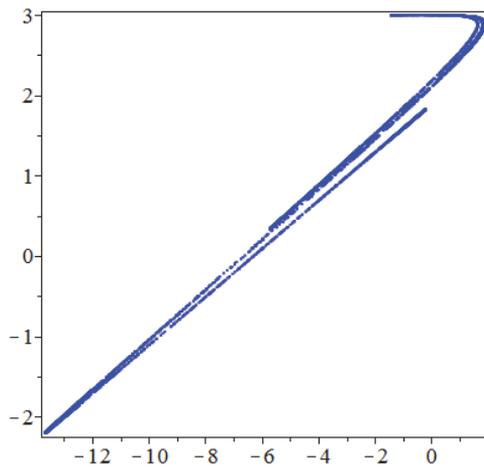
Fig.4.51 Chaotic attractor for a minimal chaotic neuron module where the output voltage is represented on the horizontal axis for one of the cells and the vertical axis for the other cell

Figures 4.51 and 4.52 show the dynamical behaviour of the cells of the immune system, particularly the immune memories and the bifurcations from a normal behaviour (Figure 4.51) to an abnormal behaviour (Figure 4.52).

The horizontal axis shows the voltage gradient (in mV) between the inside and outside of a cell, and the vertical axis shows the voltage of another cell in a system of two with feedback.
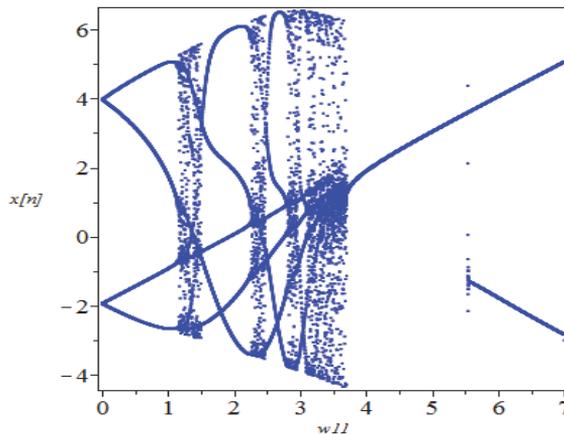
Fig.4.52 Bifurcation diagram for a bi-stable neuron module which displays quasiperiodic and bi-stable behaviours. The horizontal axis shows the voltage gradient between the inside and outside of a cell, and the vertical axis shows the voltage of another cell in a system of two with feedback.

83

Figure 4.52 shows how the state of a cell changes when the connectivity between the cells is altered. If the connectivity between the cells is altered the memories are lost and the immune system will attack the body and create self-immune disease.

With the use of another program (program 3 in Appendix A-II) we get a numerical solution for a system of two normal cells and the equivalent Figure 4.53 which represents a stable immune memory and a normal immune system. The immune system keeps the memory of the self-antigens and the immune system does not attack the body.
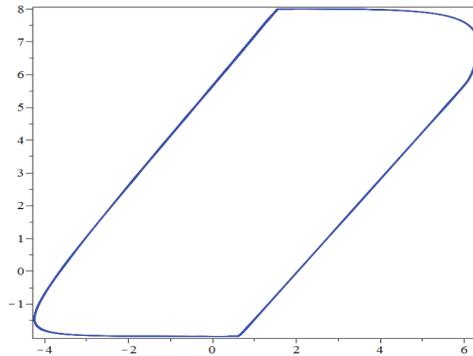
Fig.4.53 System of two normal cells where the output voltage is represented on the horizontal axis for one of the cells and the vertical axis is for the other cell

For a three cell module, taking into account that the state at time n+1 is determined by the state at time n, means that we must use difference equations. Then the dynamic equations are

$$x_{n+1} = b_1 + \frac{w_{1,1}}{1+e^{-x_n}} + \frac{w_{1,2}}{1+e^{-y_n}} + \frac{w_{1,3}}{1+e^{-z_n}} \qquad (4.69)$$

$$y_{n+1} = b_2 + \frac{w_{2,1}}{1+e^{-x_n}} + \frac{w_{2,2}}{1+e^{-y_n}} + \frac{w_{2,3}}{1+e^{-z_n}} \qquad (4.70)$$

$$z_{n+1} = b_3 + \frac{w_{3,1}}{1+e^{-x_n}} + \frac{w_{3,2}}{1+e^{-y_n}} + \frac{w_{3,3}}{1+e^{-z_n}} \qquad (4.71)$$

where x's, y's, z's are the output voltages (in mV), b's are the external voltages (in mV) and w's are the inductances and mutual inductances (in mH) of the cells. The values are as follows:

$b_1 = -2, \ b_2 = 3, \ b_3 = 1, \ w_{1,1} = -20, \ w_{1,2} = 6, \ w_{1,3} = 5, \ w_{2,1} = -6, \ w_{2,2} = 0, \ w_{2,3} = 0, \ w_{3,1} = 0,$

$w_{3,2} = 0, \ w_{3,3} = -10.$

$$(4.72)$$

Eq. (4.69), eq. (4.70) and eq. (4.71) become

$$x_{n+1} = -2 - \frac{20}{1+e^{-x_n}} + \frac{6}{1+e^{-y_n}} + \frac{5}{1+e^{-z_n}},$$

$$y_{n+1} = 3 - \frac{6}{1+e^{-x_n}}, z_{n+1} = 1 - \frac{10}{1+e^{-z_n}}$$

(4.73)

When $x_{n+1} = x_n$, $y_{n+1} = y_n$ and $z_{n+1} = z_n$ (equilibrium point), then eq. (4.73) becomes as follows

$$x = -2 - \frac{20}{1+e^{-x}} + \frac{6}{1+e^{-y}} + \frac{5}{1+e^{-z}},$$

$$y = 3 - \frac{6}{1+e^{-x}}, z = 1 - \frac{10}{1+e^{-z}}$$

(4.74)

The solution is (see Appendix A-III):

$$x = -1.07704, y = 1.47561, z = -1.24159.$$

(4.75)

If eq. (4.74) is written as a vector with the right hand sides, then it becomes

$$\left[-2 - \frac{20}{1+e^{-x}} + \frac{6}{1+e^{-y}} + \frac{5}{1+e^{-z}}, 3 - \frac{6}{1+e^{-x}}, 1 - \frac{10}{1+e^{-z}} \right].$$

(4.76)

Taking into account eq. (4.76) and using the Jacobian of eq. (4.76) (Appendix A-III) we get the following eigenvalues (in sec^{-1}) of the impedance matrix:

$$[-3.49461, \ -0.29569, \ -1.73911].$$

(4.77)

Because of at least one of the absolute values in the eq. (4.77) is greater than 1, the system is unstable according to the stability theorem for discrete systems represented by difference equations.

Subsequent equations are the same with the higher memory states. Eq. (4.78) represents the equation that determines the equilibrium point of order of 2 (excited memory state) being the fundamental memory state.

$$\left[x_{n+2} = -2 - \frac{20}{1+e^{-x_{n+1}}} + \frac{6}{1+e^{-y_{n+1}}} + \frac{5}{1+e^{-z_{n+1}}}, y_{n+2} = 3 - \frac{6}{1+e^{-x_{n+1}}}, z_{n+2} = 1 - \frac{10}{1+e^{-z_{n+1}}} \right]$$

(4.78)

In this case the solution and the eigenvalues are given in Appendix A-III.

The results are following:

$$x = -14.18518, \ y = -2.37301, \ z = 0.98117.$$

(4.79)

The eigenvalues (in sec^{-1}) of the impedance matrix are given below:

[$-0.000006 + 0.001392$ j, $-0.000006 - 0.001392$ j, -1.983156].   (4.80)

The equilibrium point of eq. (4.78) represents the memory of one self-antigen, given that such memory is unstable the immune systems is not able to remember such states and the immune system generates antibodies against the self-antigen and the self-immune disease is developed.

Using the appropriate program (program 4 in Appendix A-II) we get the figures 4.54, 4.55, 4.56 and 4.57. Figures 4.55 – 4.57 show that the values on the vertical axis fluctuate which means that the cell system is unstable.
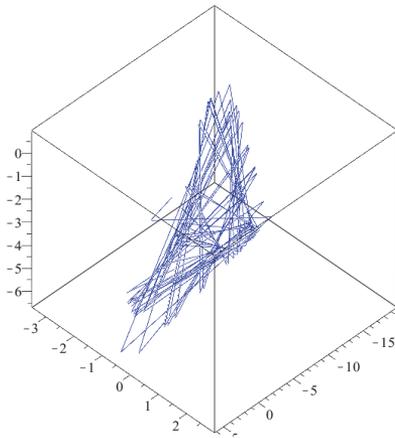
Fig.4.54 *Chaotic attractor where the output voltage for each of the three cells is represented on each axis respectively*
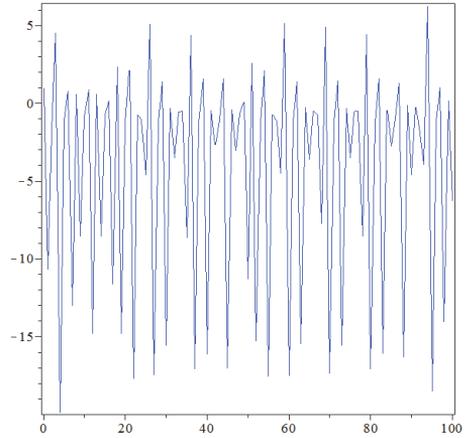
Fig.4.55 *Cell state x vs time where the vertical axis represents the output voltage of cell x and on the horizontal axis is time*
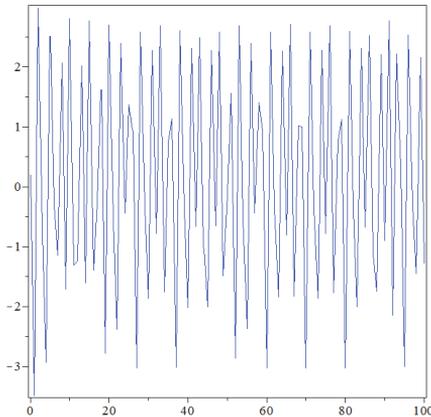
Fig.4.56 *Cell state y vs time where the vertical axis represents the output voltage of cell y and on the horizontal axis is time*
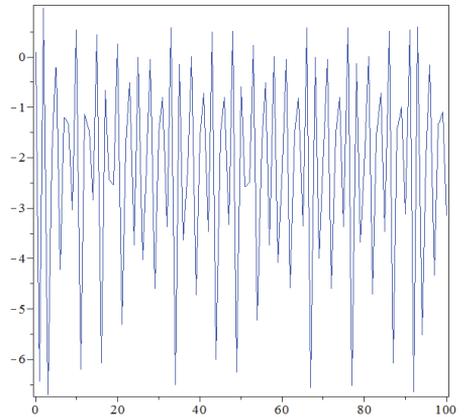
Fig.4.57 *Cell state z vs time where the vertical axis represents the output voltage of cell z and on the horizontal axis is time*

4.4 Dynamic electrical impedance of a tooth

In this work a detailed mathematical and physical model for calculating the bioimpedance of a tooth is developed based on a parallel R-C equivalent circuit [66] and a balanced Wien bridge oscillator. With the use of the appropriate computational software, namely Maxima [45] and Maple [46, 67], the relevant equations of the models can be solved analytically.

Tooth consists out of the following parts [68], see Fig.4.58:

a) Enamel, which is the hardest part. It covers and protects the exposed part of the tooth. b) Dentin, which is supports the enamel. It has microscopic channels the dentinal tubules. c) The Pulp is a soft tissue in the centre of the tooth. It contains lymph vessels and nerves. d) Cementum is the part, which covers most of the root of the tooth.
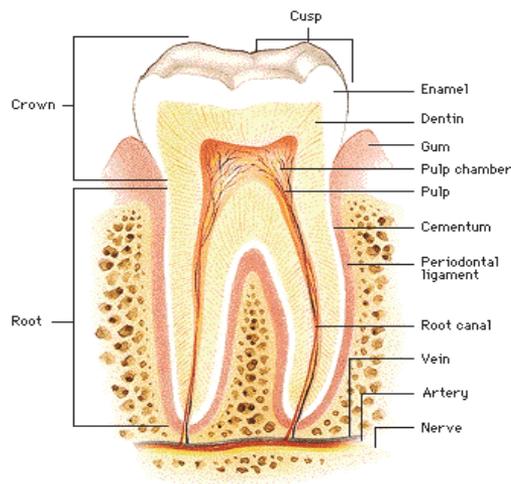
Fig.4.58 Structure of a tooth [68]

Different types of teeth have different impedances. Tooth decay occurs when bacteria produce acids as a result of exposure to the sugars that we consume thus affecting the tooth's impedance. These acids dissolve the minerals in the enamel and demineralization begins. Subsequently the decay reaches the dentin and then the pulp. In that stage the root canal must be cleaned form the diseased pulp and root filling must be applied.

We assume that the electrical equivalent of a tooth is a parallel RC circuit [66, 69, 70] (Fig.4.59). In order to measure the electrical impedance of the tooth [66], we are going to use a Wien bridge oscillator [71] showing in the following figure (Fig.4.60).
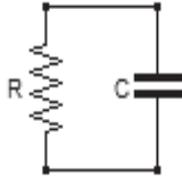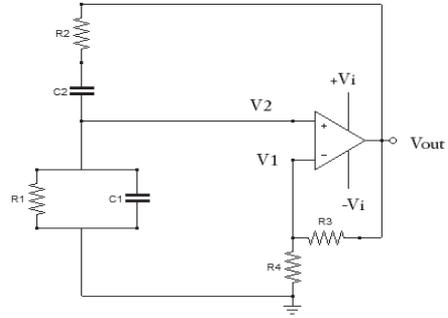
Fig.4.59 RC circuit   Fig.4.60 Wien bridge oscillator

By analyzing [44] the above circuit (Fig.4.61 and Fig.4.62), we get the equation
(4.81) and other mathematical derivatives following on the next page.
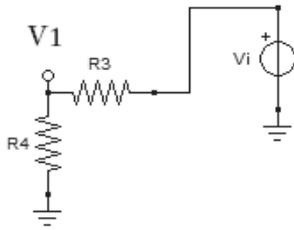
Fig.4.61 Determining the transfer function   Fig.4.62 Determining the transfer function
of the Wien bridge oscillator (resistive   of the Wien bridge oscillator (complex
shoulder)   impedance shoulder)

$$v_1(s) = \frac{V_i R_4}{R_4 + R_3}, \tag{4.81}$$

$$v_2(s) = \frac{V_i C_2 R_1 s}{1 + (C_1 R_1 + C_2 R_2 + C_2 R_1)s + C_2 C_1 R_1 R_2 s^2}, \tag{4.82}$$

$$V_{out}(s) = A(v_2(s) - v_1(s)), \tag{4.83}$$

where A is the voltage gain.

From eq. (4.81), eq. (4.82) and eq. (4.83) we get

$$V_{out}(s) = A\left(\frac{V_i(s)C_2R_1s}{1+(C_1R_1+C_2R_2+C_2R_1)s+C_2C_1R_1R_2s^2} - \frac{V_i(s)R_4}{R_4+R_3}\right) \qquad (4.84)$$

or

$$\frac{V_{out}(s)}{V_i(s)} = \frac{AC_2R_1s}{1+sC_1R_1+sC_2R_2+sC_2R_1+C_2C_1R_1R_2s^2} - \frac{AR_4}{R_4+R_3}. \qquad (4.85)$$

Considering that for the bridge to balance, it must be $R_1 = R_2$ and $C_1 = C_2$ then eq. (4.85) becomes

$$\frac{V_{out}(s)}{V_i(s)} = \frac{AC_2R_2s}{1+3sC_2R_2+C_2^2R_2^2s^2} - \frac{AR_4}{R_4+R_3}. \qquad (4.86)$$

If $R_2 = R$ and $C_2 = C$, then the eq. (4.86) becomes

$$\frac{V_{out}(s)}{V_i(s)} = \frac{ACRs}{1+3sCR+C^2R^2s^2} - \frac{AR_4}{R_4+R_3}. \qquad (4.87)$$

Taking into consideration the oscillation condition which is the above equation to be equal with 1 (loop gain of 1 causes sustained constant output), then we get

$$\frac{ACRs}{1+3sCR+C^2R^2s^2} - \frac{AR_4}{R_4+R_3} = 1. \qquad (4.88)$$

Substituting $s = j\omega$, we get

$$\frac{ACRj\omega}{1+3j\omega CR - C^2R^2\omega^2} - \frac{AR_4}{R_4+R_3} = 1 \qquad (4.89)$$

or

$$\frac{A\left(-2j\omega CRR_4 + j\omega CRR_3 - R_4 + R_4C^2R^2\omega^2\right)}{\left(-1-3j\omega CR+C^2R^2\omega^2\right)\left(R_4+R_3\right)} = 1. \qquad (4.90)$$

Assuming R>0, C>0, R_3>0, R_4>0, A>0 and ω>0 and bridge is balanced (the phase shift is 0), then the imaginary part of eq. (4.90) should be equal to zero:

$$-\frac{A\left(-1+C^2R^2\omega^2\right)\omega CR}{1+7C^2R^2\omega^2+C^4R^4\omega^4} = 0. \qquad (4.91)$$

Solving eq. (4.91) we get $\omega = \dfrac{1}{RC}$, $\qquad (4.92)$

And eq. (4.92) calculates the resonant radian frequency and the real part of eq. (4.90) should be equal to 1:

$$-\frac{A\left(R_4 + 4R_4C^2R^2\omega^2 + R_4C^4R^4\omega^4 - 3C^2R^2\omega^2R_3\right)}{\left(R_4 + R_3\right)\left(1 + 7C^2R^2\omega^2 + C^4R^4\omega^4\right)} = 1. \tag{4.93}$$

Considering eq. (4.92), eq. (4.93) becomes

$$\frac{1}{9}\frac{A\left(6R_4 - 3R_3\right)}{R_4 + R_3} = 1. \tag{4.94}$$

By solving eq. (4.94) for R$_3$ we get

$$R_3 = \frac{2R_4A - 3R_4}{3 + A}. \tag{4.95}$$

Considering that A is very big in op amps then eq. (4.95) gives that

$$R_3 = 2R_4. \tag{4.96}$$

With the help of an oscilloscope we can find the resonant frequency, then from the equation $\omega = 2\pi f$ we can calculate ω. Knowing the value of the R, we can calculate, solving eq. (4.92), the value of $C = 1/\omega R$ (or knowing the value of C we can calculate the value of R in the same way).
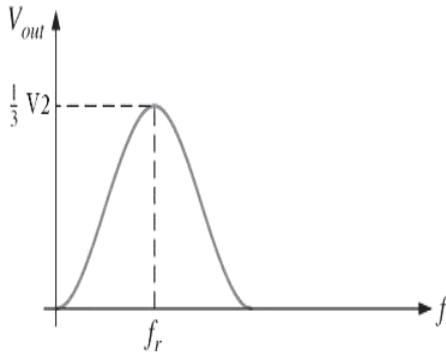
Fig.4.63 Resposce curve
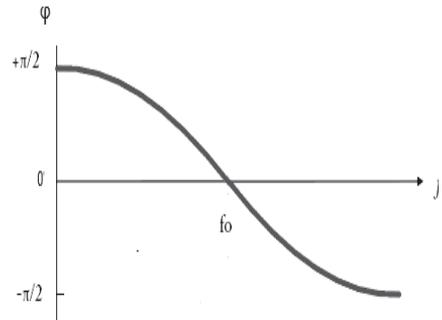
Fig.4.64 Phase vs frequency

Having balanced the bridge, we get in the output of the bridge a sine wave oscillation $V(t) = A\sin(\omega t)$.

Next step is to connect the tooth to the bridge (Fig.4.65). The output signal $V_{out}(t)$ from the oscillator will drive a known resistor R$_5$ which is connected in series with the electrodes to the tooth. The R$_5$ and the R$_6$ of the tooth will create a voltage divider.
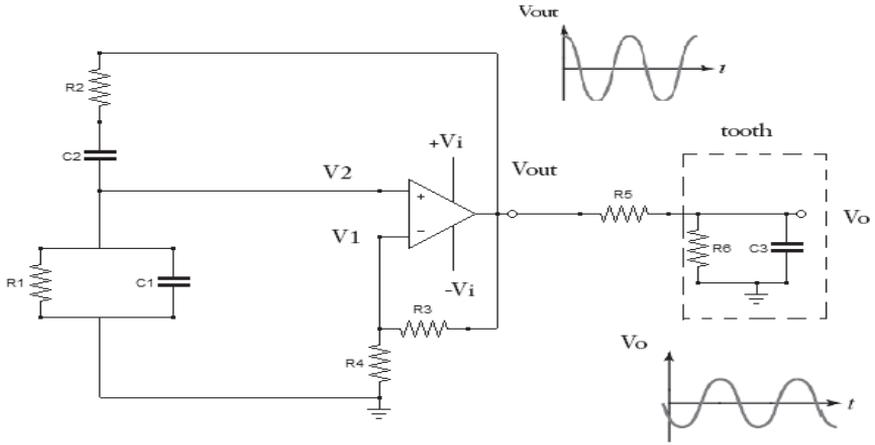
Fig.4.65 The tooth connected to the Wien bridge oscillator

Solving the equivalent circuit for the tooth, we get

$$V_o(s) = \frac{V_i(s)R_6}{R_6 + R_5 + C_3R_5R_6s} \qquad (4.97)$$

where $V_o(s)$ is the output of the parallel $R_6 C_3$ circuit and $V_i(s)$ is the input voltage in the R_5, which is the output voltage of the Wien bridge oscillator.

So, the input voltage on the R_5 is a sine wave:

$$V_i(t) = A\sin(\omega t). \qquad (4.98)$$

The Laplace transformation for the eq. (4.98) is

$$V_i(s) = \frac{A\omega}{s^2 + \omega^2}. \qquad (4.99)$$

Eq. (4.97) becomes

$$V_o(s) = \frac{A\omega R_6}{\left(s^2 + \omega^2\right)\left(R_6 + R_5 + C_3R_5R_6s\right)}. \qquad (4.100)$$

The inverse Laplace transform is

$$V_o(t) = \frac{\left(A\left(C_3\omega R_5 R_6^2\left(-\cos(\omega t) + e^{-\frac{(R_6 + R_5)t}{C_3R_5R_6}} \right) + \sin(\omega t)R_6(R_6 + R_5) \right) \right)}{R_6^2 + 2R_6R_5 + R_5^2 + \omega^2 C_3^2 R_5^2 R_6^2}. \qquad (4.101)$$

Theoretically, when $t \to \infty$ ($t = 5C_3R_5R_6/(R_6+R_5)$), the exponential becomes:

$$e^{-\frac{(R_6 + R_5)t}{C_3R_5R_6}} = 0. \qquad (4.102)$$

91

Eq. (4.101) gives

$$V_o(t) = \frac{A\left(-C_3\omega R_5 R_6^2 \cos(\omega t) + \sin(\omega t) R_6(R_6 + R_5)\right)}{R_6^2 + 2R_6 R_5 + R_5^2 + \omega^2 C_3^2 R_5^2 R_6^2}.$$
(4.103)

Using an oscilloscope attached to the tooth (where V_0 is shown in the figure 4.65) we can find the amplitude (A_1) of the waveform and the phase shift ($\Delta\varphi$) comparing it to the phase of the wave form we took in the output of the Wien bridge oscillator (V_{out} is shown in the figure 4.65).

Knowing the new amplitude A_1 and the phase shift, then we solve the following equations. According to trigonometric function

$$a.\cos(\vartheta) + b.\sin(\vartheta) = \sqrt{a^2 + b^2}\,\sin(\vartheta + \arctan(\frac{a}{b})),$$
(4.104)

eq. (4.103) becomes

$$V_0(t) = \frac{A}{R_6^2 + 2R_6 R_5 + R_5^2 + \omega^2 C_3^2 R_5^2 R_6^2} \sqrt{C_3^2 \omega^2 R_5^2 R_6^4 + R_6^2(R_6 + R_5)^2}\,\sin(\omega t + \arctan(\frac{C_3 \omega R_5 R_6}{R_6 + R_5})).$$
(4.105)

which is equivalent to the equation $V_0(t) = A_1 \sin\left(\omega t + \Delta\varphi\right).$ (4.106)

From eq. (4.105) and eq. (4.106) we get

$$A_1 = \frac{A}{R_6^2 + 2R_6 R_5 + R_5^2 + w^2 C_3^2 R_5^2 R_6^2} \sqrt{C_3^2 w^2 R_5^2 R_6^4 + R_6^2(R_6 + R_5)^2}$$
(4.107)

More compactly,

$$A_1 = \frac{AR_6}{\sqrt{(R_6 + R_5)^2 + w^2 C_3^2 R_5^2 R_6^2}}$$
(4.108)

and

$$\Delta\varphi = \arctan\left(\frac{C_3 \omega R_5 R_6}{R_6 + R_5}\right).$$
(4.109)

Solving eq. (4.108) and eq. (4.109), we can obtain the values for R_6 and C_3 of the tooth. Additionally we can calculate the resistivity ρ, the conductivity σ and the relative permittivity ε_r of the tooth. Having calculated the values of R_6 and C_3 of the tooth and measuring the surface area S of the electrodes and the distance L between them, then the following equations can be used:

$$R_6 = \rho\frac{L}{S} \text{ or } \rho = \frac{R_6 S}{L} \text{ or } \sigma = \frac{1}{\rho}$$
(4.110)

and

$$C_3 = \varepsilon_r \varepsilon_0 \frac{S}{L} \text{ or } \varepsilon_r = \frac{C_3 L}{\varepsilon_0 S}.$$
(4.111)

The model can predict the values of the resistance and the capacitance of any type of tooth. Numerical calculation of the electrical impedance of the tooth can also be useful for evaluation of the root canal length of a tooth [72]. In addition, measurements can be made in order to study how the temperature variations of an extracted tooth can influence the electrical impedance of the tooth [66].

4.5 Summary

The goal of this chapter was to develop a number of models to simulate dynamic electrical bioimpedance, fluidic bioimpedance and interaction between T-cells and B-cells using the concept of impedance. The first model, which is based on an RLC circuit in series, represents a neuron. By solving the respective differential equation and taking into account several different parameters, we are able to estimate the values for the electrical impedance of a healthy neuron and one affected by Parkinson's disease. The second model, which simulates the dynamic fluidic impedance of an artery, can be used to calculate the electrical bioimpedance of a healthy artery and one with atherosclerosis [73]. It is based on an RLC, RL and operational amplifier circuits. The third model, based on artificial neural networks, simulates the interactions between T-cells and B-cells considering that the bioimpedance of the artificial neuronal network state variable is represented by the transfer functions from antigens to immune response. The final model is a simulation of the dynamic electrical impedance of a tooth and is based on a parallel RC circuit using a Wien bridge oscillator.

It is hoped that these models will contribute to the further understanding of the electrical bioimpedance of neurons, fluidic bioimpedance of arteries and electrical bioimpedance of teeth as well as interactions between T-cells and B-cells applying the unified impedance concept for characterisation of dynamic physiological processes in different biological systems.

CONCLUSIONS

The thesis focuses on the unified mathematical and physical modelling of dynamic electrical bioimpedance, fluidic bioimpedance and interaction between T-cells and B-cells using the impedance concept. Different models are developed which deepen the understanding of the electrical and fluidic impedance of biological tissues and help to implement the electrical bioimpedance based sensing principles in medical practice. In particular, the following results can be highlighted.

1. A model which uses electrical impedance circuits with operational amplifiers, resistors, inductors and capacitors for modelling the fluidic impedance of a healthy artery and for an artery with atherosclerosis is developed. For both the former and the latter we can calculate and compare the values of the electrical equivalent components which are involved in the above model (Papers 2 and 4).

2. Both the electrical bioimpedance of a healthy neuron and a defective one are studied in detail through the use of a mathematical and physical model. Simulations were obtained by solving the differential equation for the RLC circuit. The model predicts the values of resistance of a healthy neuron and for a neuron which is affected by Parkinson's disease (Papers 1 and 3). According to the model, the latter of these neurons undergoes a loss of resistance which can, hypothetically, create a dysfunctional neuron.

3. The dynamic behaviour of the T-cells and B-cells of the immune system is studied in detail through the use of a mathematical and physical model. Simulations were obtained by solving the equation for the appropriate neuron models, in particular a three cell module. By calculating the equilibrium point of the system and taking into account the bioimpedance of the linearized model, we can determine whether the system is stable or not and whether a self immune disease is developing (Papers 8 and 10).

4. The electrical bioimpedance of a tooth is studied in detail through the use of a mathematical and physical model. Simulations were obtained by solving the equation for the appropriate parallel RC circuit. The model can predict the values of the resistance and the capacitance of a tooth (Papers 7 and 11) thus helping in the diagnosis and treatment of the diseased tooth.

It is expected that this work will encourage future research concerning Parkinson's disease, atherosclerosis and autoimmune disease, and could give

rise to innovations in dentistry. The aforementioned models could be further developed to expand our understanding in some other particular cases in biology and medicine, for example those which are to be solved within the framework of the following projects.

The results are already partly in use in the new research project "Analysis of the dynamic response of the vascular system: determination of arterial stiffness and dynamic fullness by the aid of non-invasive bioimpedance measurements (2016-2019)" signed between the East-Tallinn Central Hospital, Competence Centre ELIKO and Tallinn University of Technology in December 2015. The final goal is to develop a non-invasive method for the continuous monitoring of the central aortic blood pressure (CAP) curve through the measurement of bioimpedance of the radial artery in the wrist. Also in the Horizon 2020 – WIDESPREAD – 2014 – 2 – 668995 - ERA Chair project "Cognitive Electronics (2015-2019)" the use of the results of the thesis work is anticipated. Bioimpedance based sensing for the monitoring of cardiovascular and respiratory systems is the ultimate goal of this demanding project. Moreover, the results also support the new proposals for Horizon 2020 FLAG-ERA JTC project "Convergence (2016-2019)" and COST project "EuropeToBe (2016-2019)" submitted in April 2016.

.

REFERENCES

[1] S. Grimnes and O. G. Martinsen, Bioimpedance and Bioelectricity Basics, (3rd edition). Academic Press, 2015, London, UK.

[2] K. Moens, D. Houttekier, L. Van den Block, R. Harding, L. Morin, S. Marchetti, A. Csikos, M. Loucka, W. Naylor, D. Wilson, J. Teno, M. Cardenas-Turanzas, Y. Rhee, F. J. Garcia-Leon, L. Deliens and J. Cohen, Place of death of people living with Parkinson's disease: a population-level study in 11 countries. BMC Palliative Care, May 2015, 9pp, BioMedCentral, DOI: 10.1186/s12904-015-0021-3.

[3] R. Beaglehole, International trends in coronary heart disease mortality and incidence rates. Journal of Cardiovascular Risk. 1999; 6(2):63–68.

[4]http://www.fortressbiotech.com/research-development/immune-autoimmune.cfm, 10/12/2012.

[5] https://www.nlm.nih.gov/medlineplus/parkinsonsdisease.html, 18/01/2012.

[6] https://ghr.nlm.nih.gov/condition/parkinson-disease, 18/01/2012.

[7] http://www.webmd.com/heart-disease/what-is-atherosclerosis, 18/01/2012.

[8] http://www.fortressbiotech.com/research-development/immune-autoimmune.cfm, 10/12/2012.

[9] A. R. Von Hippel, Dielectric Materials and Applications. 1995, Boston: Artech House.

[10] R. A. Levy, Principles of Solid State Physics, 1968, Academic Press.

[11] P. Debye, Polar molecules, (1929) Chemical Cataloque Company, reprinted in New York by Dover Publications.

[12] J. P. Runt and J. J. Fitzgerald, Dielectric Spectroscopy of Polymeric Materials, Fundamentals and Applications, 1997.

[13] R. R. Cole and K. S. Cole, Dispersion and Absorption in Dielectrics I. Alternating Current Characteristics,1941, J Chem Phys , 9, 341.

[14] D. W. Davidson and R. H. Cole , Dielectric relaxation of glycerine, 1950, J. Chem Phys., 18, 1417

[15] S. Navriliak and S. J. Havriliak, Dielectric and Mechanical Relaxation in Materials – Analysis, Interpretation and Application to Polymers, 1997, Munich, Hanser.

[16] N. E. Hill, W. E. Vaughan, A. H. Price, and M. Davis, Dielectric Properties and Molecular Behaviour, Van Nostrand,1969, London.

[17] C. F. Boettcher and P. Bordewijk, Theory of Electric Polarisation, Vol. 2, 2nd ed., Elsevier Science B.V., 1992, Amsterdam.

[18] S. Havriliak and S. Negami, 1966, J. Pol. Sci.: Part C 14, 99.

[19] P.Hedvig, Dielectric Spectroscopy of Polymers, 1977, A. Hilger LTD Bristol.

[20] T. Blythe and D. Bloor, Electrical Properties of Polymers, 2nd Ed., 2005, Cambridge University Press.

[21] http://www.tf.uni-kiel.de/matwis/amat/admat_en/index.html, 15/02/2012.

[22] https://cnx.org/contents/VtjKSKsR@4/Capacitors-and-Dielectrics, 15/02/2012.

[23] P. Frubing, Dielectric spectroscopy University of Potsdam, Institute of Physics, 2001.

[24] H. Froehlich, Theory of Dielectrics. Dielectric Constant and Dielectric Loss, 2nd ed., 1958, Clarendon Press, Oxford.

[25] E. Barsoukov and J. R. Macdonald, Impedance Spectroscopy Theory, Experiment, and Applications, second edition,2005, John Wiley and Sons, Inc.

[26] C. J. F. Boettcher, Theory of Electric Polarization, Vol. 1, 2nd ed., 1993, Elsevier Science B.V., Amsterdam.

[27] http://www.medfriendly.com/cell.html, 15/02/2012.

[28] A. Rabbat, Tissue Resistivity, Cap.2, Electrical Impedance Tomography, J.G. Webter ed., Adam Hilger,1988, Bristol & New York.

[29]https://mville.digication.com/neeta_yousaf/Chemical_Composition_of_Cell_Membrane, 15/02/2012.

[30] K. S. Cole, Membranes, Ions and Impulses, University of California Press, Berkeley, 1972.

[31] H. P. Schwan, Electrical properties of tissue and cell suspensions, 1957, Adv Biol Med Phys, (5): 147–209.

[32] J. R. Bourne, J. P. Morucci, M. E. Valentinuzzi, B. Rigaud, C. J. Felice, N. Chaveau, and P. M. Marsili, 1996, Bioelectrical impedance techniques in medicine, Critical Reviews in Biomedical Engineering, 24(4-6).

[33] A. Ivorra, Bioimpedance monitoring for physicians: an overview, Review, 2003, Centre Nacional de Microelectronica, Biomedical Applications Group.

[34] I. D. Raistrick, D. R. Franceschetti, and J. R. Macdonald. Chapter 2: Theory, page 37, in Impedance Spectroscopy: Theory, Experiment and Applications, edited by E. Barsoukov and J. R. Maconald, 2005, John Wiley & Sons, Inc., Hoboken, New Jersey.

[35] J. G. Webster, Medical Instrumentation: Application & Design, 3rd ed, 1998, John Wiley.

[36] G. Cybulski, Ambulatory Impedance Cardiography - The Systems and Their Applications, 2011, Springer-Verlag Berlin Heidelberg.

[37] A. O. Raghed, L. A. Geddes, J. D. Bourland, W. A. Tacker, Tetrapolar electrode system for measuring physiological events by impedance, 1992, Med. Biol. Eng. Comput., 30, 115-117.

[38] S. Yatano, A. Fukasawa, Y. Takizawa, A Novel Neural Network Model Upon Biological and Electrical Perceptions, the 10th WSEAS International Conference on Mathematical Methods, Computational Techniques and Intelligent Systems (MAMECTIS '08), Oct. 26-28, 2008, Corfu, Greece.

[39] I. Lampl, M. Segal, N. Ulanovsky, Introduction to Neuroscience: From Neuron to Synapse, 2009, Weizmann Institute of Science.

[40] http://animatlab.com/Help/Documentation/Neural-Network-Editor/Neural-Simulation-Plug-ins/Firing-Rate-Neural-Plug-in/Neuron-Basics, 10/12/2012.

[41] http://rskbrain.weebly.com/table-of-contents.html, 15/02/2012.

[42] https://www.pinterest.com/pin/80079699599480779/, 15/02/2012.

[43] J. Huguenard and D. McCormick, Electrophysiology of the neuron, Oxford University Press, 1994, New York

[44] A. Argawal and J. Lang, Foundations of Analog and Digital Electronic Circuits, 2005, Elsevier.

[45] P. Souza, R. Fateman, J. Moses, C. Yapp, 2003, The Maxima Book.

[46] J. Carlson, J. Johnson, Multivariable Mathematics with Maple, Linear Algebra, Vector Calculus and Differential Equations, 1996, Prentice-Hall.

[47] M. Monagan, K. Geddes, K. Heal, G. Labahn, S. Vorkoetter, J. McCarron, P. DeMarco, Maple Introductory Programming Guide, 2005, Maplesoft a division of Waterloo Maple Inc.

[48] M. Adam, A. Baraboi, C. Pancu, S. Pispiris, The analysis of circuit breakers kinematics characteristics using the artificial neural netrworks, 2009, issue 2, volume 8, WSEAS TRANSACTIONS on CIRCUITS and SYSTEMS,.

[49] C. Aissi, D. Kazakos, An Improved Realization of the Chua's Circuit Using RC-OP Amps, 2004, issue 2, volume 3, WSEAS TRANSACTIONS on CIRCUITS and SYSTEMS.

[50] K. Roebenack, N. Dingeldey, Observer Based Current Estimation for Coupled Neurons, 2012, issue 7, volume 11, WSEAS TRANSACTIONS on SYSTEMS.

[51] G. Watson, A treatise on the theory of Bessel functions, 1995, Cambridge at the University Press.

[52] http://en.wikipedia.org/wiki/Atherosclerosis, 15/02/2012.

[53] http://www.teachpe.com/anatomy/arteries.php, 15/02/2012.

[54] http://apocketmerlin.tumblr.com/post/18660545870/the-hitchhikers-guide-to-the-circulatory-system, 15/02/2012.

[55] https://medicalmyths.wordpress.com/atherosclerosis/, 15/02/2012.

[56] http://www.vasal.net/athero/atherosclerotic_plaque.htm, 15/02/2012.

[57] M. Olusfen and A. Nadim, 2004, On Deriving Lumped Models for Blood Flow and Pressure in the Systematic Arteries, Journal of Mathematical Biosciences and Engineering, 2004, 1, 61-88.

[58] H. Bruus, Theoretical Microfluidics, 2008, Oxford University Press.

[59] S. Haykin, Neural Networks: A Comprehensive Foundation, 1998, 2nd ed., Prentice Hall.

[60] S. Lynch, Dynamical Systems with Applications using Maple, 2nd ed., 2009, Birkhäuser Publishing.

[61] L. Sompayrac, How the Immune System Works, 2nd ed., 2002, Blacwell Publishing.

[62] J. Pachero and J. F. Costa, The Abstract Immune Systems Algorithm, LNCS 4618, 2007, Springer, pp 199-214.

[63] P. Qiao, T. Wang and J. Su, An immunity-based model for dynamic distributed intrusion detection, Proceedings of SPIE, 2008, Volume 6973.

[64] P. Qiao, T. Wang and J. Su, An improved clone selection immune algorithm, Proceedings of SPIE, 2008, Volume 6973.

[65] http://www.zmescience.com/medicine/genetic/discarded-thymus-glands-offer-new-hope-people-autoimmune-disease/, 10/12/2012.

[66] M. Huysmans, C. Longbottom, A. Christie, P. Bruce and R. Shellis, Temperature Dependence of the Electrical Resistance of Sound and Carious Teeth, Journal of Dental Research, 2000, vol. 79 no. 7, pp. 1464-1468.

[67] M. Monagan, K. Geddes, K. Heal, G. Labahn, S. Vorkoetter, J. McCarron and P. DeMarco, Maple Introductory Programming Guide, 2005, Maplesoft a division of Waterloo Maple Inc.

[68] Human tooth, http://en.wikipedia.org/wiki/Human_tooth, 20/01/2014.

[69] T. Marjanovic, I. Lackovic and Z. Stare, Evaluation of Electrical Equivalent Circuits of a Tooth: Comparison of Circuits with Resistors and Capacitors and the Circuit with a Constant Phase Element, IFMBE Proceedings, 5th European Conference of the International Federation for Medical and Biological Engineering 14-18 September 2011 Budapest ,Hungary, Springer pp. 1261 – 1264.

[70] T. Marjanovic, Z. Stare and I. Lackovic., Verification of physical models used for root canal measurement by impedance comparison, IFMBE Proceedings, 13th International Conference on Electrical Bioimpedance and 8th

Conference on Electrical Impedance Tomography 2007, Aug. 29th – Sept. 2nd 2007, Graz, Austria, Springer pp. 715 – 718.

[71] R. Mancini and R. Palmer, Sine-Wave Oscillator, Application Report, 2001, Texas Instruments.

[72] D. Krizaj, J. Jan and V. Valencic, Numerical computation of impedances of a human tooth fro estimation of the root canal length, Biomedical Engineering, IEEE Transactions, 2002, vol. 49, issue 7, pp. 746-748.

[73] A. Sharma, A. Gupta, P. K. Kumar, J. Rajan, L. Saba, I. Nobutaka, J. R. Laird, A. Nicolades and J. S. Suri, A Review on Carotid Ultrasound Atherosclerotic Tissue Characterization and Stroke Risk Stratification in Machine Learning Framework. JS. Curr Atherosclerosis Rep., 2015, 17:55. DOI 10.1007/s11883-015-0529-2

[74]Agilent Technologies Impedance Measurement Handbook, Second Edition, 2000, Agilent Technologies.

[75] N.K. Ouzounoglou, Introduction to the microwaves, 2nd ed., 1994, Papasotiriou, Athens.

[76] HP 4284A Precision LCR Meter Operation Manual, HP Part No. 04284-90020, 1996, Hewlett Packard Company, Japan.

[77] AAMI, AAMI Electrical Safety Manual, 2008, A Comprehensive Guide to Electrical Safety Standards for Healthcare Facilities, 2008, Arlington, VA: Association for the Advancement of Medical Instrumentation.

[78] http://www.electrical-installation.org/enwiki/Electric_shock, 19/12/2012.

[79] BS 5724 Part 1: 1989/IEC601-1:1988 - British Standard - Medical electrical equipment - Part 1. General requirements for safety.

[80] IEC 60601-1 Third edition: 2005 - International standard - Medical electrical equipment - Part 1: General requirements for basic safety and essential performance.

[81] IEE Code of Practice for In-service Inspection and Testing of Electrical Equipment (ISBN 0-85296-776-4).

[82] Health Equipment Information Number 95 (HEI95) August 1981: Code of practice for acceptance testing of medical electrical equipment (withdrawn Dec 1999).

[83] http://www.ebme.co.uk/articles/electrical-safety/335-electrical-safety-tests, 19/12/2012.

[84] MDA Device Bulletin DB9801 Supplement 1: December 1999 - Checks and tests for newly delivered medical devices (replaced November 2006).

[85] G. Cronshaw, Earthing: Your questions answered, 2005, IEE Wiring Matters.

[86] M. Gerin, Electrical Installation Guide, 2008, chap E: Low Voltage distribution: Earthing scheme.

[87]http://www.electricalinstallation.org/enwiki/Measures_of_protection_again st_direct_or_indirect_contact_without_automatic_disconnection_of_supply, 19/12/2012.

ACKNOWLEDGEMENTS

ABSTRACT

In recent years electrical impedance has been growingly used in a variety of scientific fields to characterise different objects, but especially in the technology of medical diagnosing. Electrical impedance Z is the complex ratio of the voltage to an alternative current flowing through the subject. The impedance depends on the frequency of current. The complex impedance can be expressed through its real and imaginary parts or by magnitude and phase. The magnitude is the ratio of the amplitude of applied voltage to the amplitude of response current and the phase is the phase shift between the current and voltage, which is caused by capacitive and inductive components in the subject.

Electrical bioimpedance describes how a living organism responds to an externally applied low level electrical current. It can be defined as the impedance of biological specimens like organs, tissues, cells, bio-molecules. It is an opposing measure of the subject to the flow of electrical current.

The thesis analytically describes also the properties of the dielectric materials (non-conductive or poorly conductive ones) and the dependence of their dielectric permittivity on frequency. Different methods of impedance and bioimpedance measurement as well as safety standards for the measurement are presented.

In the most important part of the thesis different mathematical and physical models of dynamic electrical bioimpedance are developed. More specifically, mathematical and physical modelling of the dynamic electrical impedance of a neuron which uses electrical circuits with operational amplifiers, resistors, inductors and capacitors is analysed. Also the dynamic fluidic (hydraulic) impedance of arteries using electrical impedance equivalents RLC and operational amplifiers circuits is studied. Furthermore, a model is developed using artificial neural networks to describe the dynamic behaviour of the T-cells and B-cells of the immune system and its diseases in terms of the alterations of the dynamic electrical impedance of thymus and bone marrow. Finally the dynamic electrical impedance of a tooth is studied using a RC circuit and a Wien bridge oscillator.

KOKKUVÕTE

Viimastel aastatel on elektrilise impedantsi kasutamine erinevate objektide iseloomustamiseks saanud kasvava tähenduse mitmetes teadussuundades, kuid eriti just meditsiinilise diagnostika jaoks loodavas tehnikas. Elektriline impedants Z on kompleksarvudes väljenduv suhe elektrilise vahelduvvoolu pinge ja objekti läbiva voolu vahel, mis avaldub kas reaal- ja imaginaarosa või mooduli ja faasi kaudu. Elektriline impedants sõltub teda läbiva elektrivoolu sagedusest. Impedantsi moodul on suhe rakendatud elektripinge amplituudi ning selle tulemusena tekkiva voolu amplituudi vahel, kusjuures faas kajastab faasinihet pinge ja voolu vahel põhjustatuna mahtuvuslike ja induktiivsete komponentide olemasolust objektis.

Elektriline bioimpedants kirjeldab seda, kuidas elusorganism reageerib väljastpoolt rakendatud nõrgale elektrivoolule. Seda võib määratleda kui bioloogiliste olluste ehk substantside (organ, kude, rakk, biomolekul) elektrilist impedantsi. See on füüsikaline mõõde, mis iseloomustab kuivõrd on raskendatud elektrivoolu tee läbi bioloogiliste kudede. Doktoritöö kirjeldab analüütiliselt ka elektrit mittejuhtivate või halvasti juhtivate dielektriliste materjalide omadusi nende dielektrilise läbitavuse sagedussõltuvuse kaudu. Esitatud on erinevad meetodid elektrilise impedantsi mõõtmiseks, samuti on käsitletud rangelt reguleeritud ohutusnõudeid bioimpedantsi mõõtmise juures.

Kõige olulisem osa käsitleb dünaamilise elektrilise bioimpedantsi modelleerimist erinevate matemaatiliste ja füüsikaliste meetodite abil kasutades operatsioonvõimenditest, resistoridest, induktiivsustest ja mahtuvustest koosnevaid elektrilisi ekvivalent-lülitusi. Välja arendatud on impedantsi kontseptsioonil põhinevad matemaatilis-füüsikalised mudelid neuroni ning sidestuses oleva neuronkogumi käitumise kohta, leitud on mudelid vedeliku (vere) voolule avalduva arteri mehaanilise (hüdraulilise) impedantsi kohta ekvivalentsete elektrilist impedantsi kirjeldavate matemaatiliste mudelite kaudu. Analüüsitud on organismi immuunsüsteemi haiguslikke muutusi harknäärme ning luuüdi käitumises dünaamilise impedantsi mudelite abil. Rakendatud on Wieni sillal põhinevaid elektrilise impedantsi mudeleid hamba seisundi määramiseks.

Käesolev uurimistöö tugines institutsionaalsele uurimistööle IUT19-11: "Impedants-spektroskoopia põhine objektide identifitseerimine ja juhtimine: signaalid, algoritmid, energiasäästlikud lahendused (2014-2019)" ning osaliselt ka Horisont 2020 Euroopa teadusruumi projektile (ERA Chair): "Kognitiivelektroonika (2015-2019)", mis on suunatud teadustöö kõrgtaseme saavutamisele ja levitamisele Euroopas sensoorika ja kognitiivtehnoloogia vallas. Tulemusi kasutati ka Horizon 2020 projekti taotluse FLAG-ERA JTC 2016: "Energia-efektiivsed kantavad seadmed tervishoiu ja elustiili rakendustes (2016-2019)" konsortsiumi poolt kardiovaskulaar-süsteemi pidevjälgimise vahendite loomisele suunatud tegevuste põhjendamiseks.

APPENDIX

A-I.

COPIES OF THE SELECTED PAPERS
(Listed on pages 11-12)

I.1 Paper I: Mathematical and physical modelling of the dynamic fluidic impedance of arteries using electrical impedance equivalents.

I.2 Paper II: Using Neural Networks to model self-immune disease in terms of the alterations of the dynamic electrical impedance.

I.3 Paper III: Mathematical and Physical Modelling of the Dynamic Electrical Impedance of a Neuron.

I.4 Paper IV: Mathematical modelling of the dynamic electrical impedance of a parallel RC circuit using a Wien bridge oscillator.

I.1

Paper I

Georgios Giannoukos, Mart Min, "Mathematical and physical modelling of the dynamic fluidic impedance of arteries using electrical impedance equivalents" Mathematical Methods in Applied Science, Volume 37, Issue 5, pp. 711-717, 2014, John Wiley and Sons, Ltd, Chichester, UK

This paper is cited in a comprehensive analysis 'A Review on Carotid Ultrasound Atherosclerotic Tissue Characterization and Stroke Risk Stratification in Machine Learning Framework' by Sharma AM1, Gupta A, Kumar PK, Rajan J, Saba L, Nobutaka I, Laird JR, Nicolades A, Suri JS in the Springer journal 'Current Atherosclerosis Reports' (Curr Atheroscler Rep 2015). DOI: http://dx.doi.org/10.1007/s11883-015-0529-2

Mathematical and physical modelling of the dynamic fluidic impedance of arteries using electrical impedance equivalents

Georgios Giannoukos*† and Mart Min

Communicated by A. Kirsch

In this work, a detailed mathematical and physical model for calculating the fluidic impedance of an artery is developed. Initially, the model calculates the impedance of a healthy artery, and then, it compares this with the alteration in the impedance of an artery with atherosclerosis. Copyright © 2013 John Wiley & Sons, Ltd.

1. Introduction

Electrical bioimpedance is a method of measuring how the body impedes electrical current [1]. It can be carried out by applying a small electrical current using electrodes and collecting the results with other electrodes. In this paper, we do not use a direct measurement of bioimpedance, but we calculate the impedance of electrical circuit (electrophysical model), which is an equivalent of the arteries for determining their fluidic impedance. A detailed mathematical and physical model is presented to calculate the fluidic impedance of both a healthy artery and an artery affected by atherosclerosis [2]. These models allow us to compare the reaction of a healthy artery with that of a defective one by changing the values of resistance.

2. The problem

Arteries are elastic blood vessels that carry oxygenated blood away from the heart, except the pulmonary artery that carries deoxygenated blood [3]. The structure of an artery wall consists of three layers (Figure 1):

   a. Tunica adventitia – this is the outer covering of the walls of the arteries. It is very strong, and it is composed of connective tissues, collagen and also elastic fibres that can stretch to stop overexpansion because of the pressure of the blood.
   b. Tunica media – this is the middle layer of the walls of the arteries. It consists of smooth muscle and elastic fibres.
   c. Tunica intima – this is the inner layer of the walls of arteries. It consists of an elastic membrane and smooth endothelial cells. The blood flows in the lumen that is the hollow centre of this layer.

   Atherosclerosis occurs when the artery wall becomes thicker and hardens because of fatty material (such as cholesterol) build-up on the artery wall. These hard formations are called atheromatous plaques (Figure 2). Atheromatous plaques consist of the atheroma that is a soft yellow material at the centre of the plaque, cholesterol crystals and calcium deposition. The result is that the artery hardens and narrows that limits the normal flow of the blood (Figure 3).

3. Methods

The developed electrical models were based on RLC and RL components (where R is a resistor, L is an inductor and C is a capacitor) and operational amplifier circuits [4]. By changing the values of the components, we can calculate both the electrical impedance of the

Department of Electronics, Tallinn University of Technology, Tallinn 19086, Estonia
*Correspondence to: Georgios Giannoukos, Department of Electronics, Tallinn University of Technology, Tallinn 19086, Estonia.
†E-mail: g.giannoukos@gmail.com
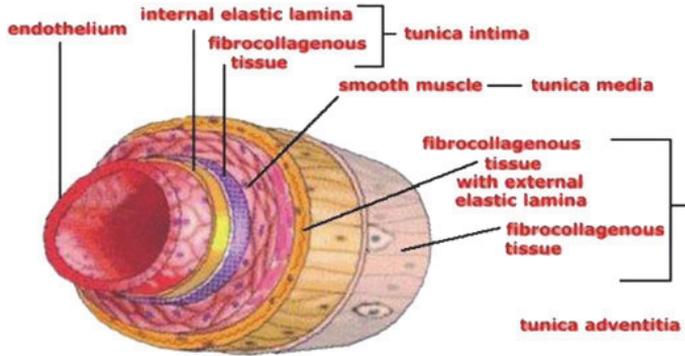
Figure 1. The structure of an artery.
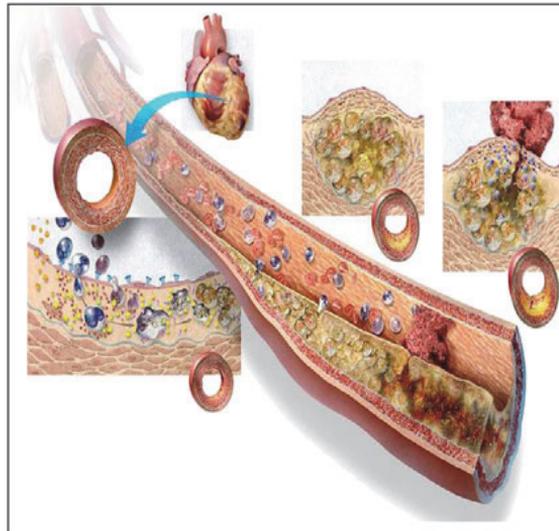
Figure 2. Atheromatous plaques.

equivalent circuit (from the electrical model) and the fluidic impedance of a healthy artery or one affected by atherosclerosis. With the use of the appropriate computational software, namely Maxima [5] and Maple [6], the relevant equations of the models can be solved analytically. The next step is to use electronic simulation software in order to evaluate the performance of the models.

The Navier–Stokes equation for the incompressible flow of Newtonian fluids is

$$\rho \left(\frac{\partial \upsilon}{\partial t} + \upsilon . \nabla \upsilon \right) = -\nabla p + \eta \nabla^2 \upsilon + F \tag{1}$$

where υ is the flow velocity, ρ is the fluid density, p is the pressure, F are the forces (such as gravity or centrifugal force) per unit volume, η is the dynamic viscosity, $\tilde{N}$ is the del operator and $\tilde{N}^2$ is the vector Laplacian. The $\partial \upsilon / \partial t$ is the unsteady acceleration, the $\upsilon \nabla \upsilon$ is the convective acceleration, the $-\nabla p$ is the pressure gradient and the $\eta \nabla^2 \upsilon$ is the viscosity. The parameters η dynamic viscosity and ρ fluid density are space and time independent.

Considering that an artery is cylindrical, we can study the Poiseuille flow in the artery [7]. Because of the cylindrical symmetry of the artery and assuming that the blood flow is axisymmetric in one dimension through a rigid artery that means the pressure inside the artery will be assumed to be independent of the radial coordinate, then the Navier–Stokes equation becomes

$$\rho \partial_t \upsilon_x(r,t) - \eta \left[\partial_r^2 + \frac{1}{r} \partial_r \right] \upsilon_x(r,t) = -\partial_r p(r,t) \tag{2}$$

Figure 3. Narrowing of an artery.
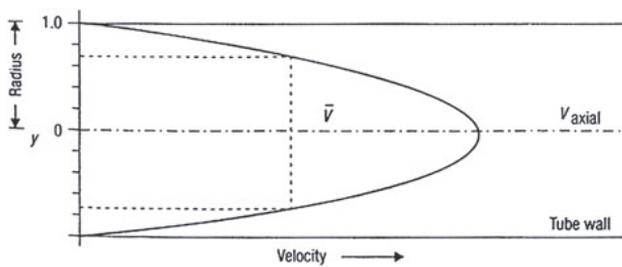
Figure 4. Blood flow in an artery.

The boundary and initial conditions for $\upsilon_\chi(r, t)$ are

$$v_x(a, t) = 0, \quad \partial_x v_x(0, t) = 0, \quad v_x(r, 0) = \frac{\Delta p}{4\eta\ell}\left(a^2 - r^2\right), \quad v_x(r, \infty) = 0 \tag{3}$$

where Δp is the change in pressure between the inlet and the outlet of the artery, and ℓ is the length of the artery taking into account that the blood stops flowing in the end (Figure 4).

The no-slip condition $v_x(a, t) = 0$ refers to the assumption that concerns the fluid–solid interface or blood vessel wall interface. No-slip boundary condition refers to the condition when the flow velocity at the tube wall is the same as the wall velocity, such that there is no 'jump' or a step change in velocity to cause discontinuity. The general assumption is that the fluid in contact with the wall does not move at all.

In the event that a Poiseuille flow starts in a circular channel, the Navier–Stokes equation becomes an inhomogenous, linear PDE.

In this case, the pressure gradient is

$$-\partial_r p(r, t) = \frac{p(0, t) - p(\ell, t)}{\ell} = \frac{\Delta p}{\ell} \tag{4}$$

where $p(0, t)$ and $p(\ell, t)$ are the pressure at the inlet and the outlet of the artery, respectively.

Therefore, Equation (2) becomes

$$\rho \partial_t v_x(r, t) - \eta\left[\partial_r^2 + \frac{1}{r}\partial_r\right]v_x(r, t) = \frac{\Delta p}{\ell} \tag{5}$$

Math. Meth. Appl. Sci. **2014**, 37 711–717

713

The equation that gives the final result for the velocity field $v_\chi(r,t)$ of a stopping Poiseuille flow in the form of a Fourier–Bessel eigenfunction expansion is the following [8]:

$$v_x(r,t) = \frac{a^2 \Delta p}{4\eta \ell} \sum_{n=1}^{\infty} \frac{8}{\gamma_n^3 J_1(\gamma_n)} J_0\left(\gamma_n \frac{r}{a}\right) \exp\left(-\gamma_n^2 \frac{v}{a^2} t\right) \tag{6}$$

where γ_n are the roots of the Bessel function.

4. Results

Considering that the dynamic viscosity of blood (in $37°$ C) is approximately $\eta = 3.10^{-3}$ Pa.s and the density of the blood is approximately $\rho = 1060$ kg/m^3, we can calculate the kinematic viscosity of the blood. So, $v = \eta/\rho = 2.83 10^{-6}$ m^2/s.

The time scale can be calculated with the following equation [8]:

$$t_{acc} = \frac{1}{\gamma_1^2} \frac{a^2}{v} = \frac{1}{\gamma_1^2} T_0 \tag{7}$$

where t_{acc} is the time scale, α is the radius of the artery, v is the kinematic viscosity of the blood and T_0 is the momentum diffusion time.

Taking into account that the smallest Bessel function root is $\gamma_1 = 2.405$, according to Equation (7), the time scale of blood in an artery with radius $\alpha = 1$ cm $= 10^{-2}$ m is calculated to be $t_{acc} = 6.1$ s and for an artery with atherosclerosis with radius $\alpha = 1$ mm $= 10^{-3}$ m is calculated to be $t_{acc} = 0.061$ s.

With the initial conditions

$$v_x(a,t) = 0, \partial_x v_x(0,t) = 0, \quad v_x(r,0) = 0, \quad v_x(r,\infty) = v_\infty \tag{8}$$

Equation (6) becomes

$$v_x(r,t) = \frac{a^2 \Delta p}{4\eta \ell}\left[1 - \frac{r^2}{a^2} - \sum_{n=1}^{\infty} \frac{8}{\gamma_n^3 J_1(\gamma_n)} J_0\left(\gamma_n \frac{r}{a}\right) \exp\left(-\gamma_n^2 \frac{v}{a^2} t\right)\right] \tag{9}$$

The volumetric flow rate Q for the elliptic channel (when an artery takes on an elliptic shape) can be calculated with the following equation [8]:

$$Q = \int_C dy dz v_x(y,z) = ab \int_0^{2\pi} d\varphi \int_0^1 d\rho \rho v_x(\rho,\varphi) = \frac{\pi}{4} \frac{1}{\eta \ell} \frac{a^3 b^3}{a^2 + b^2} \Delta p \tag{10}$$

In the case of a circular channel using $\alpha = b$, Equation (10) becomes

$$Q = \frac{\pi a^4}{8\eta \ell} \Delta p \tag{11}$$

To calculate the volumetric flow rate Q for a randomly deformed artery, the following equation can be applied:

$$Q = \frac{1}{\gamma} \frac{\Delta p}{2\eta \ell} \frac{A^3}{P^2} \tag{12}$$

where A is the cross-sectional area and P is the perimeter.

When $A = \pi a^2$ and $P = 2\pi a$, Equation (12) is reduced to Equation (11).

If $\bar{q}(s)$ is the Laplace transform of $Q(t)$ and $\bar{p}(s)$ is the Laplace transform of $p(t)$, then

$$\bar{q}(s) = \frac{\pi \bar{p}(s)}{s}\left(1 - \frac{2J_1\left(i\sqrt{s}\right)}{i\sqrt{s} J_0\left(i\sqrt{s}\right)}\right) \tag{13}$$

where

$$\bar{q}(s) = \bar{p}(s)K(s), \quad K(s) = \frac{\pi}{s}\left(1 - \frac{2J_1\left(i\sqrt{s}\right)}{i\sqrt{s} J_0\left(i\sqrt{s}\right)}\right) \tag{14}$$

and where $K(s)$ is the hydrodynamic admittance and J_0 and J_1 are the Bessel functions of orders 0 and 1, respectively.

714

Copyright © 2013 John Wiley & Sons, Ltd.

Math. Meth. Appl. Sci. **2014**, 37 711–717
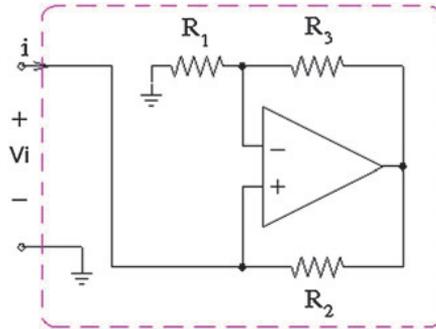
Figure 5. Operational amplifier with negative R_{eff}.

Given that the Bessel function can be expressed as a series of gamma functions, then Equation (14) can be expressed as follows:

$$
\begin{aligned}
K(s) &= \frac{\pi}{s}\left(1 - \frac{2J_1\left(i\sqrt{s}\right)}{i\sqrt{s}J_0\left(i\sqrt{s}\right)}\right) \\
&= \frac{\pi}{s}\left(1 - \left[1 + \frac{\left(i\sqrt{s}\right)^2}{8} + \frac{\left(i\sqrt{s}\right)^4}{48} + \frac{11\left(i\sqrt{s}\right)^6}{3072} + \cdots\right]\right) \\
&= \frac{\pi}{s}\left(\frac{s}{8} + \frac{s^2}{48} - \frac{11s^3}{3072} + O\left(s^4\right)\right) \\
&= \frac{\pi}{8} - \frac{\pi s}{48} + \frac{11\pi s^2}{3072} + O\left(s^3\right)
\end{aligned}
\tag{15}
$$

so the result is

$$
K(s) = \frac{\pi}{8} - \frac{\pi s}{48} + \frac{11\pi s^2}{3072} \tag{16}
$$

Considering that the impedance is

$$
H(s) = \frac{1}{K(s)} \tag{17}
$$

Equation (17) with the help of Equation (16) becomes

$$
H(s) = \frac{1}{\frac{\pi}{8} - \frac{\pi s}{48} + \frac{11\pi s^2}{3072}} \tag{18}
$$

If we compare the aforementioned impedance with the impedance of an RLC circuit in series

$$
H(s) = \frac{1}{Ls^2 + Rs + \frac{1}{C}} \tag{19}
$$

where L is the inductance, R is the resistor and C is the capacitance, we obtain the following values:

$$
L = \frac{11\pi}{3072}H, \quad C = \frac{8}{\pi}F \text{ and } R = -\frac{\pi}{48}\Omega
$$

Taking into account the negative resistance we calculated earlier, we need to replace the R in the RLC circuit in series with the following operational amplifier (Figure 5) [4]

$$
\text{which has } R_{eff} = -\frac{R_2 R_1}{R_3} \tag{20}
$$

The new circuit is illustrated in Figure 6.

Figure 6 shows an equivalent circuit model of an artery with an arbitrary pressure gradient (pressure gradient with any temporal variation).
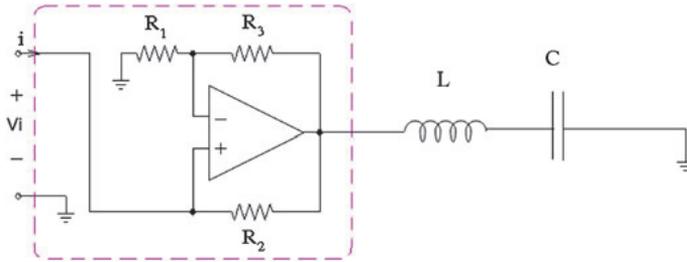
Figure 6. Equivalent circuit model of an artery.
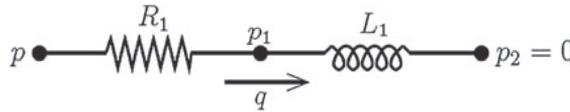
Figure 7. Equivalent circuit model of an artery at a fixed pressure gradient.

The following equation [8] derives from Equation (14)

$$Q(t) = \frac{\pi}{8}p(t) - 4\pi \sum_{n=1}^{\infty} \frac{1}{\gamma_n^4} \int_0^t e^{-\gamma_n^2(t-\tilde{t})} p'(\tilde{t}) \, d\tilde{t} \tag{21}$$

The terms in the summation are decreasing exponentials (21), so when the time tends to infinity, then only the first term contributes to the sum. So, Equation (21) becomes to Equation (22) as follows:

$$t_{acc} \frac{dq}{dt} + q = \frac{\pi a^4}{8\eta\ell} p \tag{22}$$

Equation (22) is similar to an equation of an RL circuit in series. The following circuit is equivalent to an artery in the case where the pressure gradient is fixed (constant pressure gradient) (Figure 7), and it represents a normal operation of the artery.

The differential equation for the aforementioned circuit is

$$\frac{L_1}{R_1} \frac{dq}{dt} + q = \frac{1}{R_1} p \tag{23}$$

Comparing Equations (22) and (23), we obtain

$$R_1 = \frac{8\eta\ell}{\pi\alpha^4} \text{ and } L_1 = t_{acc} \frac{8\eta\ell}{\pi\alpha^4} = \frac{8\eta\ell}{\gamma_1^2 \nu \pi \alpha^2} \tag{24}$$

5. Conclusions

With the aforementioned model, we can use electric impedance circuits with operational amplifiers, resistors, inductors and capacitors for modelling the fluidic impedance of a healthy artery and for an artery with atherosclerosis. For both the former and the latter, we can calculate and compare the values of the electrical equivalent components that are involved in the aforementioned model.

Acknowledgements

References

1. Min M, Parve T, Ronk A, Annus P, Paavle T. A synchronous sampling and demodulation in an instrument for multifrequency biompedance measurement. *IEEE Transactions on Instrumentation and Measurement* 2007; **56**:1365–72.
2. Atherosclerosis, http://en.wikipedia.org/wiki/Atherosclerosis [Accessed on 7 January 2012].

3. Artery, http://www.teachpe.com/anatomy/arteries.php.
4. Argawal A, Lang J. *Foundations of Analog and Digital Electronic Circuits*. Elsevier: San Francisco, 2005.
5. Souza P, Fateman R, Moses J, Yapp C. *The Maxima Book*, 2003. http://maxima.sourceforge.net/docs/maximabook/maximabook-19-Sept-2004.pdf.
6. Carlson J, Johnson J. *Multivariable Mathematics with Maple, Linear Algebra, Vector Calculus and Differential Equations*. Prentice-Hall: New Jersey, 1996.
7. Olusfen M, Nadim A. On deriving lumped models for blood flow and pressure in the systematic arteries. *Mathematical Biosciences and Engineering* 2004; **1**(1):61–80.
8. Bruus H. *Theoretical Microfluidics*. Oxford University Press: Oxford, 2008.

I.2

Paper II

Using Neural Networks to Model Self-immune Disease in Terms of the Alterations of the Dynamic Electrical Impedance

Georgios Giannoukos and Mart Min

Department of Electronics,
Tallinn University of Technology
Tallinn 19086
Estonia
Email: g.giannoukos@gmail.com

Abstract. In this paper a detailed mathematical and physical model is presented in order to simulate the immune system using neural networks and non-linear circuits. This model allows us to understand the interaction between T-cells and B-cells which are produced in bone marrow and mature in thymus. Immune diseases affect the bioimpedance of the immune system and cause changes in the interaction between the cells.

Keywords: bioimpedance, immune system, thymus, bone marrow, non-linear circuit, T-cell, B-cell, Computer Algebra, neural network.
PACS: 84.35.+i, 87.18.Sn, 87.19.ll, 02.70.Wz .

INTRODUCTION

The neural networks [2,3] are very important tools in the field of artificial intelligence. Recently the analogies between the brain and the immune system [1] were exploited to build artificial immune systems and immune algorithms [6,7,8] with applications in computer science. In this work a detailed mathematical and physical model for simulating the immune system is developed. The model uses neural networks of three neuron module to simulate the interaction between T-cells and B-cells taking into account that the biompedance is represented by the transference functions from antigens to immune responses. Also this model compares the dynamical behaviour of the cells of the immune system, particularly the immune memories and the bifurcations from normal behaviour to abnormal behaviour.

THE PROBLEM

Lymphocyte is a type of white blood cell. The most abundant lymphocytes are the B lymphocytes (B-cells) and the T lymphocytes (T-cells). The B-cells are produced in bone marrow which is a tissue inside the bones. Also the precursors of T-cells produced in the bone marrow and after they mature in the thymus.

The thymus is a glad of the immune system. It is located in the chest, between the breast bone and the heart. It has two lobes, the left and the right. Each lobe is composed of a number of lobules. Each lobule consists of the outer cortex and the inner medulla. The cortex has a very large number of developing T-cells and a smaller number of associated epithelial cells. T-cells migrate to the medulla in order to mature and to learn how to recognize like-cells from foreign-cells so that inappropriate immune responses are prevented.

Immune diseases are caused by different factors such as a lack of the production of enough T-cells because of the improper development of the thymus gland or an excessive immune response or even an autoimmune attack.

Methods

The developed model is based on a neural network of three neuron module which can be simulated using non linear circuits. By changing the values of the synaptic weights and the activation functions, we can simulate the dynamical behavior of the cells when the immune system is functioning normally and when it is affected by a

disease. With the use of the appropriate computational software, namely Maxima [4] and Maple [5], the relevant equations of the models can be solved analytically.

The next figure represents a T-cell or a B-cell either of which can be simulated using a non linear component [3].
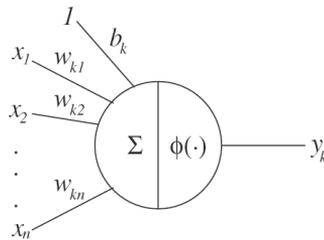
FIGURE 1. T-cell or B-cell

Where x_1, x_2, …x_n is the input signal, y_k is the output signal, w_{k1}, w_{k2},…w_{kn} is the synaptic weight between the cells, φ is the activation function and bk is the bias.

In electrical terms x_1, x_2, …x_n is the input voltage, y_k is the output voltage, w_{k1}, w_{k2},…w_{kn} is the mutual inductances, φ is the threshold of a nonlinear component and bk is the noise margin.

The activation potential and the output are given by the following equations respectively [3]:

$$v_k = \mathbf{w}_k \mathbf{x} + b_k, \quad y_k = \phi\left(v_k\right) \tag{1}$$

Figure (2) show a three neuron module. It also shows the interaction between the cells which can be an activation or inhibition interaction.
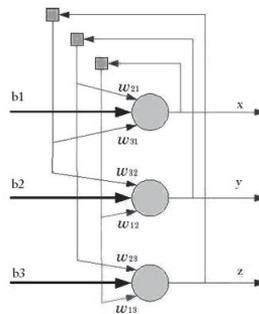
FIGURE 2. Three neuron network

Results

For a three cell module, taking into account that the state at time n+1 is determined by the state at time n, in which case we must use difference equations, then the dynamic equations are:

$$x_{n+1} = b_1 + \frac{w_{1,1}}{1 + e^{-x_n}} + \frac{w_{1,2}}{1 + e^{-y_n}} + \frac{w_{1,3}}{1 + e^{-z_n}} \tag{2}$$

$$y_{n+1} = b_2 + \frac{w_{2,1}}{1 + e^{-x_n}} + \frac{w_{2,2}}{1 + e^{-y_n}} + \frac{w_{2,3}}{1 + e^{-z_n}} \tag{3}$$

$$z_{n+1} = b_3 + \frac{w_{3,1}}{1 + e^{-x_n}} + \frac{w_{3,2}}{1 + e^{-y_n}} + \frac{w_{3,3}}{1 + e^{-z_n}} \tag{4}$$

where x's, y's, z's are the output voltages (in mV), b's are the external voltages (in mV) and w's are inductances and mutual inductances (in mH) of the cells.

Given that:

$$b_1 = -2, b_2 = 3, b_3 = 1, w_{1,1} = -20, w_{1,2} = 6, w_{1,3} = 5, w_{2,1} = -6, w_{2,2} = 0, w_{2,3} = 0, w_{3,1} = 0, w_{3,2} = 0, w_{3,3} = -10 \tag{5}$$

And when $x_{n+1} = x_n$, $y_{n+1} = y_n$ and $z_{n+1} = z_n$ (equilibrium point) then equations (2), (3) and (4) written as a vector with the right hand sides become:

$$\left[-2 - \frac{20}{1 + e^{-x}} + \frac{6}{1 + e^{-y}} + \frac{5}{1 + e^{-z}}, 3 - \frac{6}{1 + e^{-x}}, 1 - \frac{10}{1 + e^{-z}} \right] \tag{6}$$

The solution is:

$$x = -1.077049108, y = 1.475610890, z = -1.241591258 \tag{7}$$

The Jacobian of equation (6) is:

$$A = \begin{vmatrix} -\dfrac{20\,e^{-x}}{\left(1 + e^{-x}\right)^2} & \dfrac{6\,e^{-y}}{\left(1 + e^{-y}\right)^2} & \dfrac{5\,e^{-z}}{\left(1 + e^{-z}\right)^2} \\[3mm] -\dfrac{6\,e^{-x}}{\left(1 + e^{-x}\right)^2} & 0 & 0 \\[3mm] 0 & 0 & -\dfrac{10\,e^{-z}}{\left(1 + e^{-z}\right)^2} \end{vmatrix} \tag{8}$$

If we take into account equation (6) then equation (7) becomes:

$$B = \begin{vmatrix} -\dfrac{20\,e^{1.077049108}}{\left(1 + e^{1.077049108}\right)^2} & \dfrac{6\,e^{-1.475610890}}{\left(1 + e^{-1.475610890}\right)^2} & \dfrac{5\,e^{1.241591258}}{\left(1 + e^{1.241591258}\right)^2} \\[3mm] -\dfrac{6\,e^{1.077049108}}{\left(1 + e^{1.077049108}\right)^2} & 0 & 0 \\[3mm] 0 & 0 & -\dfrac{10\,e^{1.241591258}}{\left(1 + e^{1.241591258}\right)^2} \end{vmatrix} \tag{9}$$

In the case of a mosfet (non-linear component) the derivative of the voltage (output) with respect to the current (input) is the equivalent electrical impedance. Then in this case (9) is the equivalent impedance for the linearized model.

The eigenvalues (in sec^{-1}) of the impedance matrix (9) are:

$$\left[-3.494618911, -0.2956991448, -1.739118121 \right] \tag{10}$$

Because of at least one of the absolute values in equation (10) being greater than 1, according to the stability theorem for discrete systems represented by difference equations, the system is unstable.

The figure (4) represents a stable immune memory and a normal immune system. The immune system keeps the memory of the self-antigens and the immune system does not attack the body.
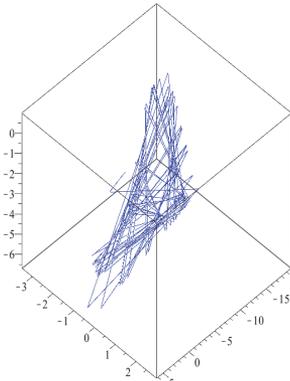
FIGURE 3. Chaotic attractor
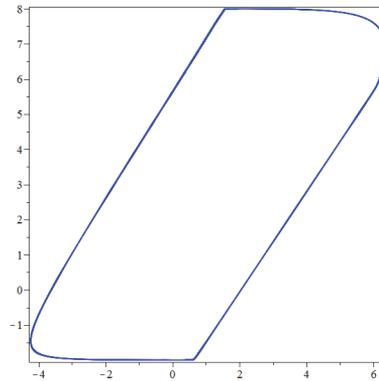
FIGURE 4. System of two normal cells

CONCLUSIONS

In this work the dynamical behavior of T-cells and B-cells of the immune system is studied in detail through the use of a mathematical and physical model. Simulations were obtained by solving the equation for the appropriate neuron models and especially a three cell module. Calculating the equilibrium point of the system and taking into account the bioimpedance of the linearized model we can find out if the system is stable or not and if a self immune disease is developing or not.

ACKNOWLEDGMENTS

REFERENCES

1. Sompayrac L. How the Immune System Works, 2nd ed., *Blacwell Publishing*. 2002
2. Haykin S. Neural Networks: A Comprehensive Foundation , 2nd ed., *Prentice Hall*. 1998.
3. Lynch S. Dynamical Systems with Applications using Mapple, 2nd ed., *Birkhäuser Publishing*. 2009.
4. Souza P., Fateman R., Moses J. and Yapp C. The Maxima Book. 2003.
5. Carlson J. and Johnson J. Multivariable Mathematics with Maple, Linear Algebra, Vector Calculus and Differential Equations, *Prentice-Hall*. 1996.
6. Pachero J. and Costa J.F. The Abstract Immune Systems Algorithm, LNCS 4618, *Springer*, 2007, pp 199-214.
7. Qiao P., Wang T. and Su J. An immunity-based model for dynamic distributed intrusion detection, *Proceedings of SPIE*, 2008,Volume **6973**.
8. Qiao P., Wang T. and Su J. An improved clone selection immune algorithm, *Proceedings of SPIE*, 2008,Volume **6973**.

I.3

Paper III

Georgios Giannoukos, Mart Min, "Mathematical and Physical Modelling of the Dynamic Electrical Impedance of a Neuron" International Journal of Circuits, Systems and Signal Processing, Volume 6, Issue 5, 2012, pp. 359-366, ISSN: 1998-4464, North Atlantic University Union, (NAUN), Salem, Oregon, USA.

URL:http://www.naun.org/multimedia/NAUN/circuitssystemssignal/16-587.pdf

Mathematical and Physical modelling of the dynamic electrical impedance of a neuron

Georgios Giannoukos, Mart Min

Abstract— In this work a mathematical and a physical model of a neuron is put forward using an RLC circuit or operational amplifier circuits. The model can calculate the resistance of a healthy neuron and then by decreasing the value of the resistance we can predict how the neuron will react.

Keywords— Biompedance, neuron, Parkinson's disease, resistance, RLC circuit

I. INTRODUCTION

Bioimpedance is a method of measuring how the body impedes electrical current [1]. It can be done by applying a small electrical current using electrodes and collecting the results with other electrodes. It can be applied to the skin or to the tissues, the heart, the neurons, blood volume, calculating lean body mass, fat body mass and many other components in the body [1]. In this work a detailed mathematical and physical model for calculating the bioimpedance of an adrenergic neuron is developed. Initially the model calculates the biompedance of a healthy adrenergic neuron at different frequencies of a current and then it compares that with the alteration in the bioimpedance of an adrenergic neuron with Parkinson's disease [2]. Also this model compares the differences in the bioimpedance between the affected adrenergic neuron before and after medical treatment.

II. PROBLEM FORMULATION

The basic structural and functional unit of the nervous system is the nerve cell or neuron [3,4]. The nerve cells produce electrical signals transmitted from one part of the cell to another, while generating biochemical substances (acetylcholine - Ach) in order to communicate with other cells. A neuron consists of the cell body, the axon and the dendrites (see Figure 1).

The neurons exchange information through a synapse (see Figure 2).

Fig.1: The structure of a neuron

Fig.2: Synapse between two neurons

Georgios Giannoukos is with the Electronics Department, Tallinn University of Technology, Ehitajate tee 5, 19086, Estonia (email: g.giannoukos@gmail.com).
Mart Min is with the Electronics Department, Tallinn University of Technology, Ehitajate tee 5, 19086, Estonia (email: min@elin.ttu.ee).
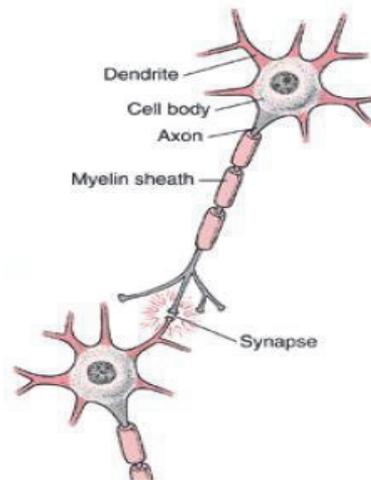
One of the functions of synapses is to determine the conduction of electrical impulses in one direction only. Therefore we can say that the synapses function as a transistor that allows the passage of electrical current in one direction [3].
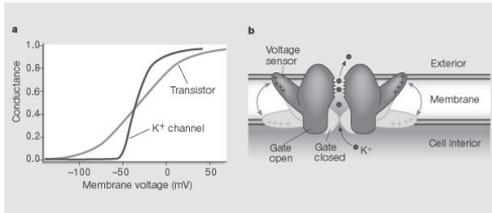
Fig.3: Comparison between a transistor's and a neuron's Conductance vs Membrane Voltage diagram

Along the surface of each neuron, potential electrical difference is due to the presence of excess negative charges on the inside and excess positive charges on the outer membrane which is why the neuron is polarized. The interior of the cell is typically 60-90mV more negative than the outside. This potential difference is called the resting potential of the neuron. When the neuron is stimulated an immediate change in the resting potential occurs. The change in the potential difference is called action potential and is transmitted along the axis.
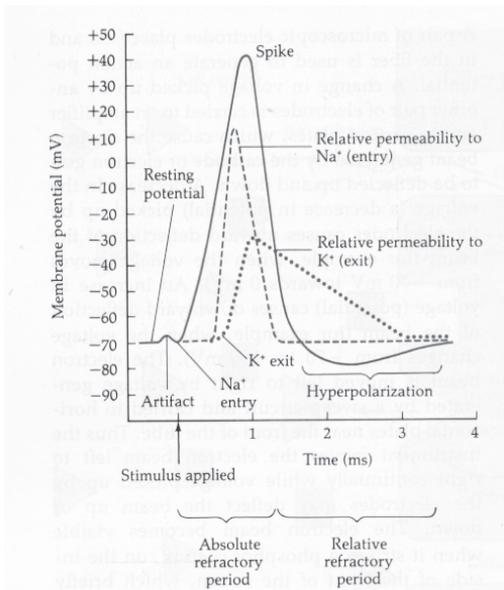
Fig.4: Membrane potential vs time

III. METHODS

The developed models were based on RLC and Operational Amplifier circuits [5]. By changing the values of the components, we can calculate the bioimpedance of a healthy neuron or one affected by Parkinson's disease. With the use of the appropriate computational software, namely Maxima [6] and Maple [7,8], the relevant equations of the models can be solved analytically. The next step is to use electronic simulation software in order to evaluate the performance of the models. Lastly, we check the biompedance of neurons which have undergone medical treatment, using the above models.

We assume the following RLC circuit:
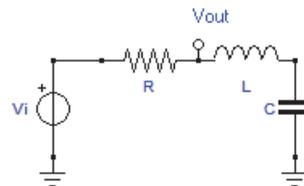
Fig.5: RLC circuit

The differential equation in terms of the charge for the RLC circuit is the following [9]:

$$L \left(\frac{\mathrm{d}^2}{\mathrm{d}t^2} q(t) \right) + R \left(\frac{\mathrm{d}}{\mathrm{d}t} q(t) \right) + \frac{q(t)}{C} = 0$$

(1)

We assume that we have an RLC circuit with resistance R which is decreasing exponentially with time, so the differential equation is:

$$L \left(\frac{\mathrm{d}^2}{\mathrm{d}t^2} q(t) \right) + R(t) \left(\frac{\mathrm{d}}{\mathrm{d}t} q(t) \right) + \frac{q(t)}{C} = 0$$

(2)

If $R(t)=R.e-t/\tau$ equation 2 becomes:

$$L \left(\frac{\mathrm{d}^2}{\mathrm{d}t^2} q(t) \right) + R\, \mathrm{e}^{-\frac{t}{\tau}} \left(\frac{\mathrm{d}}{\mathrm{d}t} q(t) \right) + \frac{q(t)}{C} = 0$$

(3)

The transfer function of the circuit is

$$V_{out} = \frac{V_i \left(1 + CLs^2\right)}{1 + (CR)s + (CL)s^2}$$

(4)

with damping factor

$$a = \frac{R}{2L}$$

(5)

resonance frequency

$$\omega_0 = \frac{1}{\sqrt{LC}}$$

(6)

and quality factor

$$Q = \frac{\omega_0}{2a}$$

(7)

or

$$Q = \frac{1}{R}\sqrt{\frac{L}{C}}$$

(8)
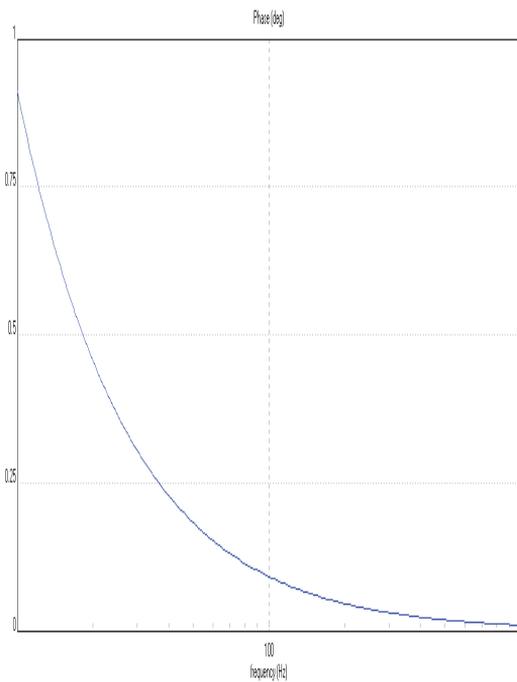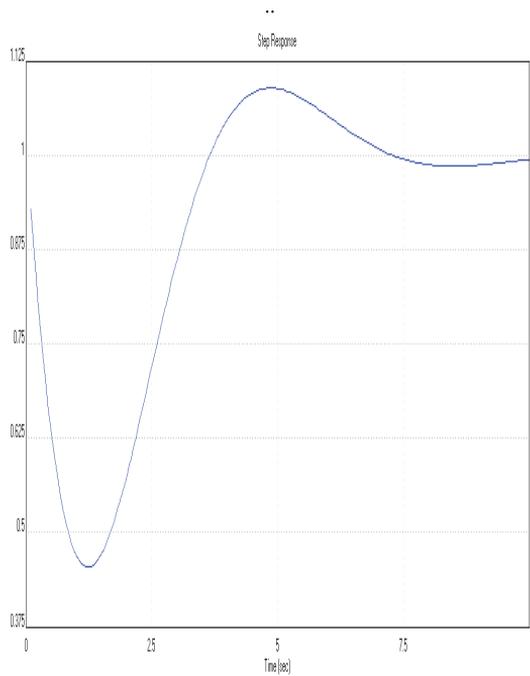
Fig.7: Step response of the RLC circuit

Instead of a typical RLC circuit we can use the following circuits [5] which behave in a manner very similar to an RLC circuit taking into account that bio inductors do not exist so in this case L in a similar differential equation is replaced with a combination of resistances and capacitors [10].
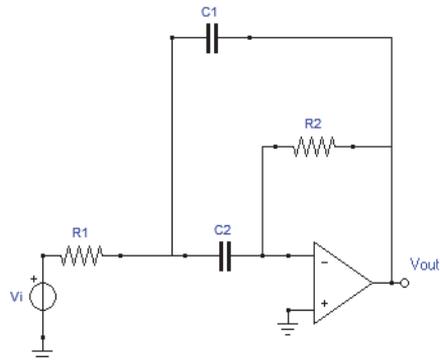
Fig.8: Circuit which behave similar to an RLC circuit

Fig.6: Phase vs frequency of the RLC circuit

The impedance model of the above circuit is shown in the next figure
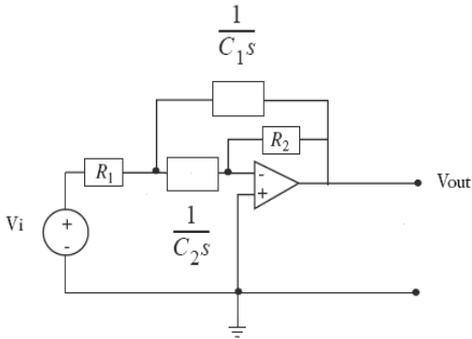
Fig.9: Impedance model of the circuit in fig.8

The transfer function of this circuit is

$$V_{out} = \frac{-V_i C_2 R_2 s}{1 + (C_1 R_1 + C_2 R_1)s + (C_1 C_2 R_1 R_2)s^2}$$

(9)

with damping factor

$$a = \frac{C_1 + C_2}{2C_1 C_2 R_2}$$

(10)

resonance frequency

$$\omega_0 = \frac{1}{\sqrt{C_1 C_2 R_1 R_2}}$$

(11)

and quality factor

$$Q = \frac{\sqrt{C_1 C_2 R_1 R_2}}{C_1 R_1 + C_2 R_1}$$

(12)
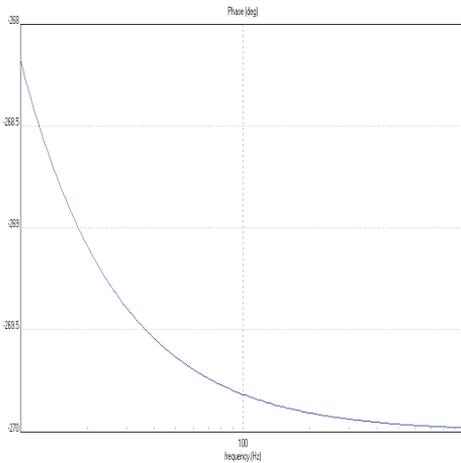
Fig.10: Phase vs frequency of the circuit in fig.8
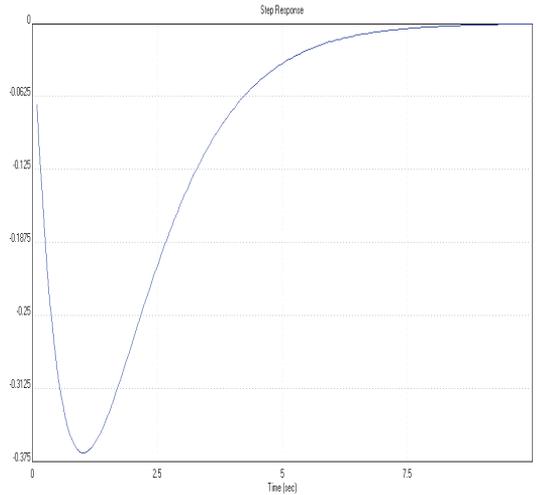
Fig.11: Step response of the circuit in fig. 8

Another similar circuit is the following
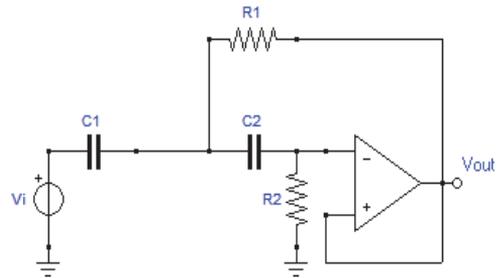
Fig.12: Circuit which behave similar to an RLC circuit

The impedance model of the above circuit is shown in the next figure
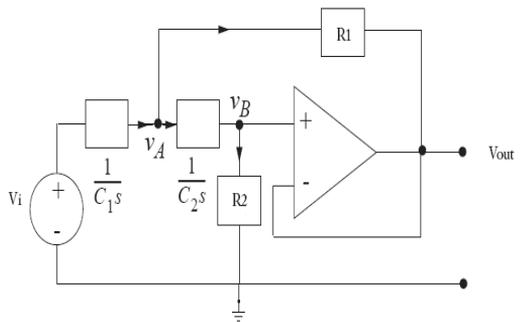
Fig.13: Impedance model of the circuit in fig, 12

The transfer function of this circuit is:

$$V_{out} = \frac{V_i C_1 C_2 R_1 R_2 s^2}{1 + (C_1 R_1 + C_2 R_1)s + (C_1 C_2 R_1 R_2)s^2}$$

(13)

with damping factor

$$a = \frac{C_1 + C_2}{2 C_1 C_2 R_2}$$

(14)

resonance frequency

$$\omega_0 = \frac{1}{\sqrt{C_1 C_2 R_1 R_2}}$$

(15)

and quality factor

$$Q = \frac{\sqrt{C_1 C_2 R_1 R_2}}{C_1 R_1 + C_2 R_1}$$

(16)
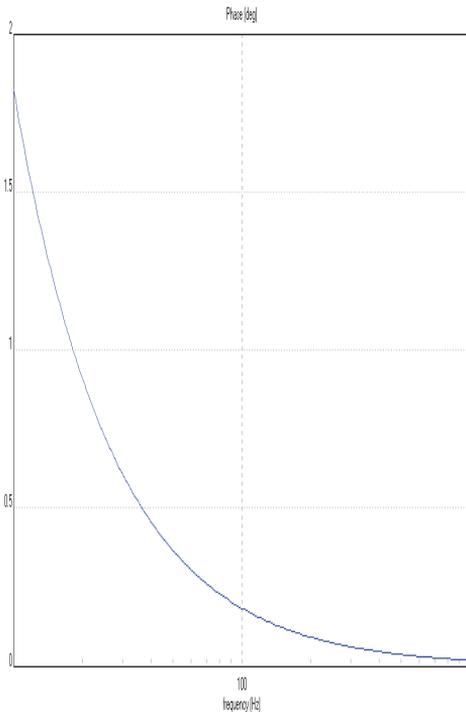
Fig.14: Phase vs frequency of the circuit in fig.6
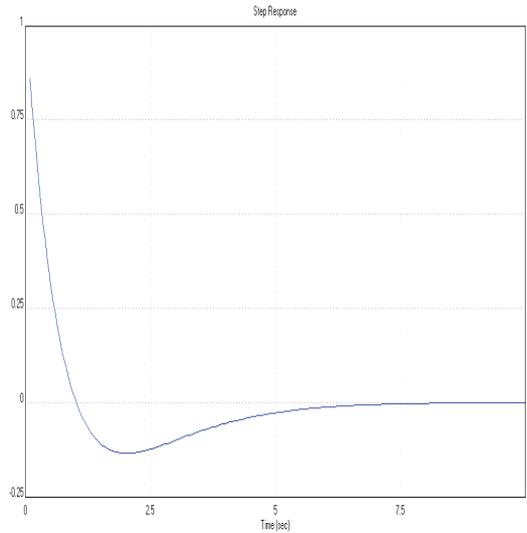
Fig.15: Step response of the circuit in fig. 6

IV. PROBLEM SOLUTION

The solution to equation (1) is:

$$q(t) = \_C1\, e^{-\frac{1}{2}\frac{\left(CR - \sqrt{C^2 R^2 - 4CL}\right)t}{CL}} + \_C2\, e^{-\frac{1}{2}\frac{\left(CR + \sqrt{C^2 R^2 - 4CL}\right)t}{CL}}$$

(17)

The condition for no oscillation which a healthy neuron satisfies but a defective neuron doesn't is:

$$0 \le C^2 R^2 - 4CL$$

(18)

it is to say

$$2\sqrt{\frac{L}{C}} \le R$$

(19)

For initial conditions q(0)=0 and i(0)=i0 we choose _C1=1 and _C2=-1, equation 17 is now:

$$q(t) = e^{-\frac{1}{2}\frac{\left(CR - \sqrt{C^2 R^2 - 4CL}\right)t}{CL}} - e^{-\frac{1}{2}\frac{\left(CR + \sqrt{C^2 R^2 - 4CL}\right)t}{CL}}$$

(20)

Experimental results show that a neuron's response time is 10^{-4} seconds and according to equation 17, the effective time is R/2L and according to equation 19, it is possible to find appropriate values for the parameters L and C, the above give the following values: $L=10^{-3}$H and $C=10^{-6}$F [11].

With the above values equation 20 becomes:

$$q(t) = e^{-500000000 \left(\frac{1}{1000000} R - \sqrt{\frac{1}{1000000000000} R^2 - \frac{1}{250000000}} \right) t}$$
$$- e^{-500000000 \left(\frac{1}{1000000} R + \sqrt{\frac{1}{1000000000000} R^2 - \frac{1}{250000000}} \right) t}$$

$$(21)$$

And equation 19 gives the following result:

$$63.24555320 \leq R$$

$$(22)$$

With the value R=70 Ohms equation 21 becomes:

$$q(t) = e^{-20000.00000\, t} - 1.\, e^{-50000.00000\, t}$$

$$(23)$$

According to equation 23 the following graph q=f(t), given that q is in Coulombs and t is in seconds, can be drawn
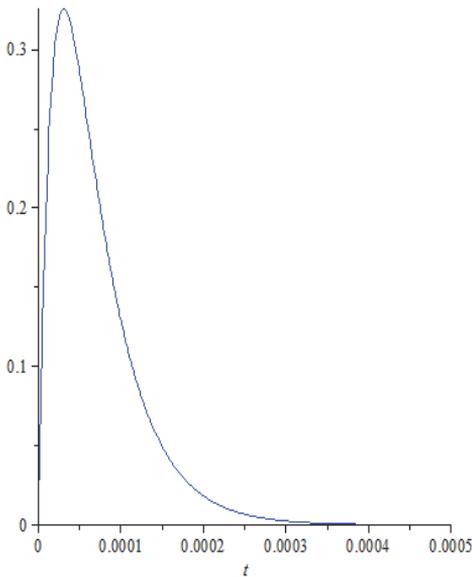
Fig.16: Charge vs time

If R is very low, close to zero then equation 21 becomes:

$$q(t) = e^{31622.77660\, I\, t} - 1.\, e^{-31622.77660\, I\, t}$$

$$(24)$$

According to equation 21 the following graph q=f(t), given that q is in Coulombs and t is in seconds, can be drawn
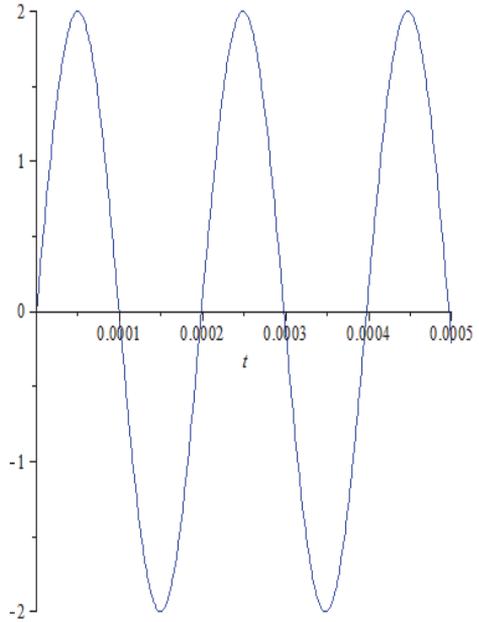
Fig.17: Charge vs time

As we can see when resistance is high (R=70 Ohms) there is no oscillation (no shaking) but when resistance is low (close to zero) there is oscillation (shaking). Thus, it appears that Parkinson's disease is caused by decreasing resistance in the neuron.

The solution to equation 3 is given in terms of Bessel functions [12]:

$$q(t) = -\Bigg(\Bigg(2\, \mathrm{BesselK}\Big(\frac{1}{2}\; \frac{-\sqrt{C}\,\sqrt{L} + 2\,I\tau}{\sqrt{C}\,\sqrt{L}},$$

$$-\frac{1}{2}\,\frac{R\tau}{L} \Big) i_0\, L^{3/2}\,\sqrt{C}\,\tau + \mathrm{BesselK}\Big(\frac{1}{2}\; \frac{-\sqrt{C}\,\sqrt{L} + 2\,I\tau}{\sqrt{C}\,\sqrt{L}},$$

$$-\frac{1}{2}\,\frac{R\tau}{L} \Big) Q_0\, R\,\sqrt{C}\,\sqrt{L}\,\tau - 2\,I\,\mathrm{BesselK}\Big(\frac{1}{2}\; \frac{\sqrt{C}\,\sqrt{L} + 2\,I\tau}{\sqrt{C}\,\sqrt{L}},$$

$$-\frac{1}{2}\,\frac{R\tau}{L} \Big) Q_0\, L\,\tau - 2\,\mathrm{BesselK}\Big(\frac{1}{2}\; \frac{\sqrt{C}\,\sqrt{L} + 2\,I\tau}{\sqrt{C}\,\sqrt{L}},$$

$$-\frac{1}{2}\,\frac{R\tau}{L} \Big) i_0\, L^{3/2}\,\sqrt{C}\,\tau + 2\,I\,\mathrm{BesselK}\Big(\frac{1}{2}\; \frac{-\sqrt{C}\,\sqrt{L} + 2\,I\tau}{\sqrt{C}\,\sqrt{L}},$$

$$-\frac{1}{2}\,\frac{R\tau}{L} \Big) Q_0\, L\,\tau$$

$$-\, Q_0\,\sqrt{C}\,\sqrt{L}\,\mathrm{BesselK}\Big(\frac{1}{2}\; \frac{3\sqrt{C}\,\sqrt{L} + 2\,I\tau}{\sqrt{C}\,\sqrt{L}},\; -\frac{1}{2}\,\frac{R\tau}{L} \Big) R\,\tau$$

$$-\, 2\,\mathrm{BesselK}\Big(\frac{1}{2}\; \frac{\sqrt{C}\,\sqrt{L} + 2\,I\tau}{\sqrt{C}\,\sqrt{L}},\; -\frac{1}{2}\,\frac{R\tau}{L} \Big) Q_0\, L^{3/2}\,\sqrt{C} \Bigg)$$

$$\mathrm{e}^{-\frac{1}{2}\,\frac{-R\tau^2\,\mathrm{e}^{-\frac{t}{\tau}} + t\,L}{\tau\,L}} \Bigg(\mathrm{BesselI}\Big(\frac{1}{2}\; \frac{-\sqrt{C}\,\sqrt{L} + 2\,I\tau}{\sqrt{C}\,\sqrt{L}},$$

$$-\frac{1}{2}\,\frac{R\tau\,\mathrm{e}^{-\frac{t}{\tau}}}{L} \Big) + \mathrm{BesselI}\Big(\frac{1}{2}\; \frac{\sqrt{C}\,\sqrt{L} + 2\,I\tau}{\sqrt{C}\,\sqrt{L}},$$

$$-\frac{1}{2}\,\frac{R\tau\,\mathrm{e}^{-\frac{t}{\tau}}}{L} \Big) \Bigg) \Bigg) \Bigg/ \Bigg(\sqrt{\mathrm{e}^{\frac{R\tau}{L}}}\,\sqrt{C}\,\sqrt{L}\Big($$

$$-R\,\tau\,\mathrm{BesselI}\Big(\frac{1}{2}\; \frac{-\sqrt{C}\,\sqrt{L} + 2\,I\tau}{\sqrt{C}\,\sqrt{L}},$$

$$-\frac{1}{2}\,\frac{R\tau}{L} \Big) \mathrm{BesselK}\Big(\frac{1}{2}\; \frac{\sqrt{C}\,\sqrt{L} + 2\,I\tau}{\sqrt{C}\,\sqrt{L}},\; -\frac{1}{2}\,\frac{R\tau}{L} \Big)$$

$$+ 2\,L\,\mathrm{BesselI}\Big(\frac{1}{2}\; \frac{\sqrt{C}\,\sqrt{L} + 2\,I\tau}{\sqrt{C}\,\sqrt{L}},$$

$$-\frac{1}{2}\,\frac{R\tau}{L} \Big) \mathrm{BesselK}\Big(\frac{1}{2}\; \frac{-\sqrt{C}\,\sqrt{L} + 2\,I\tau}{\sqrt{C}\,\sqrt{L}},\; -\frac{1}{2}\,\frac{R\tau}{L} \Big)$$

$$-\, \mathrm{BesselI}\Big(\frac{1}{2}\; \frac{3\sqrt{C}\,\sqrt{L} + 2\,I\tau}{\sqrt{C}\,\sqrt{L}},$$

$$-\frac{1}{2}\,\frac{R\tau}{L} \Big) R\,\tau\,\mathrm{BesselK}\Big(\frac{1}{2}\; \frac{-\sqrt{C}\,\sqrt{L} + 2\,I\tau}{\sqrt{C}\,\sqrt{L}},\; -\frac{1}{2}\,\frac{R\tau}{L} \Big)$$

$$+\, \mathrm{BesselI}\Big(\frac{1}{2}\; \frac{3\sqrt{C}\,\sqrt{L} + 2\,I\tau}{\sqrt{C}\,\sqrt{L}},$$

$$-\frac{1}{2}\,\frac{R\tau}{L} \Big) R\,\tau\,\mathrm{BesselK}\Big(\frac{1}{2}\; \frac{\sqrt{C}\,\sqrt{L} + 2\,I\tau}{\sqrt{C}\,\sqrt{L}},\; -\frac{1}{2}\,\frac{R\tau}{L} \Big)$$

$$-\, R\,\tau\,\mathrm{BesselK}\Big(\frac{1}{2}\; \frac{-\sqrt{C}\,\sqrt{L} + 2\,I\tau}{\sqrt{C}\,\sqrt{L}},$$

$$-\frac{1}{2}\,\frac{R\tau}{L} \Big) \mathrm{BesselI}\Big(\frac{1}{2}\; \frac{\sqrt{C}\,\sqrt{L} + 2\,I\tau}{\sqrt{C}\,\sqrt{L}},\; -\frac{1}{2}\,\frac{R\tau}{L} \Big)$$

$$+\, \mathrm{BesselK}\Big(\frac{1}{2}\; \frac{3\sqrt{C}\,\sqrt{L} + 2\,I\tau}{\sqrt{C}\,\sqrt{L}},$$

$$-\frac{1}{2}\,\frac{R\tau}{L} \Big) R\,\tau\,\mathrm{BesselI}\Big(\frac{1}{2}\; \frac{-\sqrt{C}\,\sqrt{L} + 2\,I\tau}{\sqrt{C}\,\sqrt{L}},\; -\frac{1}{2}\,\frac{R\tau}{L} \Big)$$

$$+\, \mathrm{BesselK}\Big(\frac{1}{2}\; \frac{3\sqrt{C}\,\sqrt{L} + 2\,I\tau}{\sqrt{C}\,\sqrt{L}},$$

$$-\frac{1}{2}\,\frac{R\tau}{L} \Big) R\,\tau\,\mathrm{BesselI}\Big(\frac{1}{2}\; \frac{\sqrt{C}\,\sqrt{L} + 2\,I\tau}{\sqrt{C}\,\sqrt{L}},\; -\frac{1}{2}\,\frac{R\tau}{L} \Big)$$

$$+\, 2\,L\,\mathrm{BesselK}\Big(\frac{1}{2}\; \frac{\sqrt{C}\,\sqrt{L} + 2\,I\tau}{\sqrt{C}\,\sqrt{L}},$$

$$-\frac{1}{2}\,\frac{R\tau}{L} \Big) \mathrm{BesselI}\Big(\frac{1}{2}\; \frac{-\sqrt{C}\,\sqrt{L} + 2\,I\tau}{\sqrt{C}\,\sqrt{L}},\; -\frac{1}{2}\,\frac{R\tau}{L} \Big) \Bigg) \Bigg)$$

$$(25)$$

Assume a neuron affected by Parkinson's disease, considering that the disease takes approximately 5 years (60 months) to develop and taking into account that the effective time is R/2L according to equation 20, it is possible to find appropriate values for the parameters L and C. The above give the following values: L=10H and C=20F. Also as we calculated before, values for R for the affected neuron should be under 63 Ohms approximately. We can choose any value below that, so we choose R=10 Ohms (any value in R under 63 Ohms will give similar results). The fact that the disease causes total degeneration within 10 years (120 months) after its first appearance and the life span of a person affected by Parkinson's disease after that is approximately 15 years (180 months) should be taken into account. Considering all the above as well as the fact that the time required for the neuron to loose its resistance is approximately 15 months, τ=15 months, so now equation 3 becomes:

$$10\left(\frac{\mathrm{d}^2}{\mathrm{d}t^2}\, q(t) \right) + 10\, \mathrm{e}^{-\frac{1}{15}t}\left(\frac{\mathrm{d}}{\mathrm{d}t}\, q(t) \right) + \frac{1}{20}\, q(t) = 0$$

$$(26)$$

According to equation 26 the following graphs q=f(t) (Fig.18) and i=f(q) (Fig.19) can be drawn, given that q is in Coulombs, i is in Amperes and t is in months
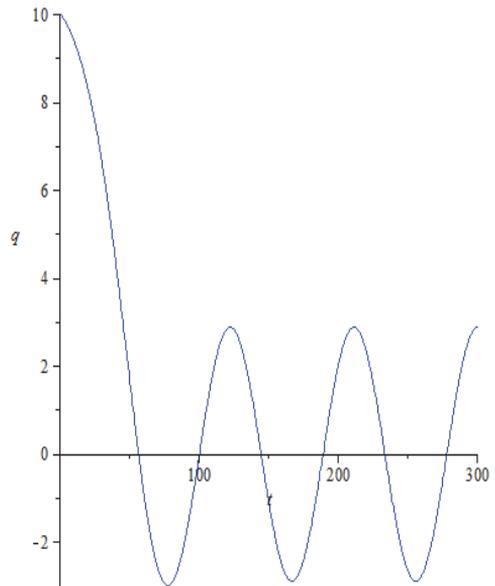
Fig.18: Charge vs time
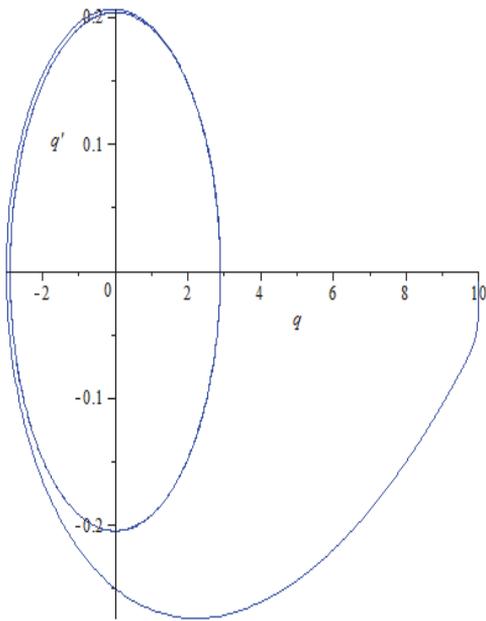
Fig.19: Current vs time

V. CONCLUSIONS

In this work biompedance both of a healthy neuron and a defective one is studied in detail through the use of a mathematical and physical model. Simulations were obtained by solving the differential equation for the RLC circuit. The model predicts the values of resistance of a healthy neuron and for a neuron which is affected by Parkinson's disease. The medication which a person affected by this disease takes aims to increase the neuron's resistance.

ACKNOWLEDGMENT

The authors thank Professor Toomas Rang and Dr. Toomas Parve for support and collaboration.

REFERENCES

[1]   .   M. Min, T. Parve, A. Ronk, P. Annus and T. Paavle, A Synchronous Sampling and Demodulation in an Instrument for Multifrequency Biompedance Measurement, IEEE Trans. Inst. Meas. 56 1365-72 (2007).
[2]   A. Dip, B. Ramaswamy, C. Ferguson, C. Jones, C. Tugwell, C. Taggart, F. Lindop, K. Durrant, K. Green, K. Hyland, S. Barter, S. Gay, The Professional's Guide to Parkinson's Disease, 2007, Parkinson's Disease Society.
[3]   S. Yatano, A. Fukasawa, Y. Takizawa, A Novel Neural Network Model Upon Biological and Elecrrical Perceptions, the 10th WSEAS International Conference on Mathematical Methods, Computational Techniques and Intelligent Systems (MAMECTIS '08), Corfu, Greece, Oct. 26-28, 2008.
[4]   I. Lampl, M. Segal, N. Ulanovsky, Introduction to Neuroscience: From Neuron to Synapse, 2009, Weizmann Institute of Science.
[5]   A. Argawal and J. Lang, Foundations of Analog and Digital Electronic Circuits, 2005, Elsevier.
[6]   P. Souza, R. Fateman, J. Moses, C. Yapp, The Maxima Book, 2003.
[7]   J. Carlson, J. Johnson, Multivariable Mathematics with Maple, Linear Algebra, Vector Calculus and Differential Equations, 1996, Prentice-Hall.
[8]   M. Monagan, K. Geddes, K. Heal, G. Labahn, S. Vorkoetter, J. McCarron, P. DeMarco, Maple Introductory Programming Guide, 2005, Maplesoft a division of Waterloo Maple Inc.
[9]   M. Adam, A. Baraboi, C. Pancu, S. Pispiris, The analysis of circuit breakers kinematics characteristics using the artificial neural netrworks,2009, issue 2, volume 8, WSEAS TRANSACTIONS on CIRCUITS and SYSTEMS,.
[10] C. Aissi, D. Kazakos, An Improved Realization of the Chua's Circuit Using RC-OP Amps, 2004, issue 2, volume 3, WSEAS TRANSACTIONS on CIRCUITS and SYSTEMS.
[11] K. Roebenack, N. Dingeldey, Observer Based Current Estimation for Coupled Neurons, 2012, issue 7, volume 11, WSEAS TRANSACTIONS on SYSTEMS.
[12] G. Watson, A treatise on the theory of Bessel functions, 1995, Cambridge at the University Press.

I.4

Paper IV

Mathematical modelling of the dynamic electrical impedance of a parallel RC circuit using a Wien bridge oscillator[1]

Georgios Giannoukos* and Mart Min

Thomas Johann Seebeck Department of Electronics, Tallinn University of Technology, Tallinn, Estonia

Abstract. In this paper a detailed mathematical model is presented in order to calculate the dynamic electrical impedance of a parallel RC circuit. The proposed model is based in an op-amp balanced Wien bridge oscillator and a voltage divider. From the amplitude of the signal and the phase shift we can calculate the resistance and the capacitance of a parallel RC circuit which can be used as an electrical equivalent of a tooth or a neuron.

Keywords: Biompedance, tooth, resistance, capacitor, Wien bridge oscillator, voltage divider, Operational Amplifier

1. Introduction

In this work a detailed mathematical model for calculating the impedance of a parallel RC circuit with the use of a Wien bridge oscillator is developed. The parallel RC circuit can be used as an electrical equivalent of a tooth or a neuron which in that case is possible the equivalent bioimpedance to be calculated. Bioimpedance is a method of measuring how the body impedes electrical current [1]. It can be done by applying a small electrical current using electrodes and collecting the results with other electrodes. It can be applied to the skin or to the tissues, the heart, the neurons, blood volume, calculating lean body mass, fat and many other components in the body [1].

With the use of the appropriate computational software, namely Maxima [2] and Maple [3,4], the relevant equations of the models can be solved analytically.

2. Problem

We assume a parallel R-C circuit which can represent an electrical equivalent of a tooth or a neuron etc.

In order to measure the electrical impedance we are going to use a Wien bridge oscillator [7] shown in the following figure.

---

[1] A preliminary version of this paper was presented at the 12th International Conference of Numerical Analysis and Applied Mathematics (ICNAAM 2014), 22–28 September 2014, Rhodes, Greece.

*Corresponding author: Georgios Giannoukos, Thomas Johann Seebeck Department of Electronics, Tallinn University of Technology, Tallinn 19086, Estonia. E-mail: g.giannoukos@gmail.com.
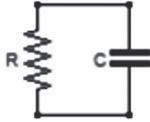
Fig. 1. R-C circuit.
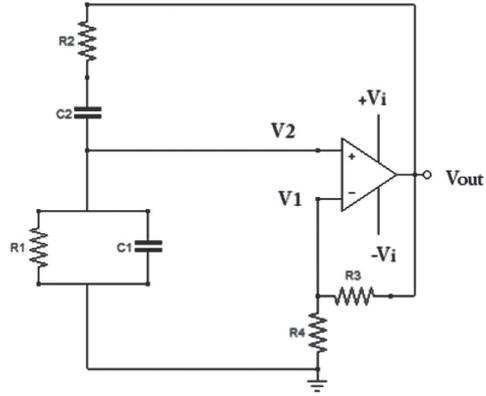
Fig. 2. Wien bridge oscillator.

By analyzing [8] the above circuit we get the following equations

$$v_1(s) = \frac{V_i R_4}{R_4 + R_3} \tag{1}$$

$$v_2(s) = \frac{V_i C_2 R_1 s}{1 + (C_1 R_1 + C_2 R_2 + C_2 R_1)s + C_2 C_1 R_1 R_2 s^2} \tag{2}$$

$$V_{out}(s) = A(v_2(s) - v_1(s)) \tag{3}$$

Where A is the voltage gain
From Eqs (1), (2) and (3) we get:

$$V_{out}(s) = A \left(\frac{V_i C_2 R_1 s}{1 + (C_1 R_1 + C_2 R_2 + C_2 R_1)s + C_2 C_1 R_1 R_2 s^2} - \frac{V_i R_4}{R_4 + R_3} \right) \tag{4}$$

or

$$\frac{V_{out}(s)}{V_i} = \frac{A C_2 R_1 s}{1 + s C_1 R_1 + s C_2 R_2 + s C_2 R_1 + C_2 C_1 R_1 R_2 s^2} - \frac{A R_4}{R_4 + R_3} \tag{5}$$

Considering that for the bridge to balance R_1 must be equal to R_2 and C_1 equal to C_2 then Eq. (5) becomes

$$\frac{V_{out}(s)}{V_i} = \frac{A C_2 R_2 s}{1 + 3s C_2 R_2 + C_2^2 R_2^2 s^2} - \frac{A R_4}{R_4 + R_3} \tag{6}$$

If $R_2 = R$ and $C_2 = C$ then Eq. (6) becomes

$$\frac{V_{out}(s)}{V_i} = \frac{A C R s}{1 + 3s C R + C^2 R^2 s^2} - \frac{A R_4}{R_4 + R_3} \tag{7}$$

Taking into consideration the oscillation condition which is the above equation when it is equal to 1 (loop gain of 1 causes sustained constant output) then we get

$$\frac{A C R s}{1 + 3s C R + C^2 R^2 s^2} - \frac{A R_4}{R_4 + R_3} = 1 \tag{8}$$
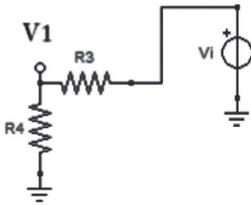
Fig. 3. Part of the Wien bridge oscillator.
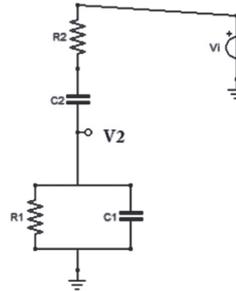
Fig. 4. Part of the Wien bridge oscillator.

If we substitute s with $s = j.\omega$, then we get

$$\frac{ACRj\omega}{1 + 3j\omega CR - C^2 R^2 \omega^2} - \frac{AR_4}{R_4 + R_3} = 1 \tag{9}$$

or

$$\frac{A\left(-2j\omega CRR_4 + j\omega CRR_3 - R_4 + R_4 C^2 R^2 \omega^2\right)}{\left(-1 - 3j\omega CR + C^2 R^2 \omega^2\right)\left(R_4 + R_3\right)} = 1 \tag{10}$$

Assuming $R > 0$, $C > 0$, $R_3 > 0$, $R_4 > 0$, $A > 0$ and $\omega > 0$ and because the bridge is balanced, the phase shift is 0 and the imaginary part of Eq. (10) should be equal to zero:

$$-\frac{A\left(-1 + C^2 R^2 \omega^2\right)\omega CR}{1 + 7C^2 R^2 \omega^2 + C^4 R^4 \omega^4} = 0 \tag{11}$$

Solving Eq. (11) we get

$$\omega = \frac{1}{RC} \tag{12}$$

Equation (12) calculates the resonant radian frequency and the real part of Eq. (10) should be equal to 1:

$$-\frac{A\left(R_4 + 4R_4 C^2 R^2 \omega^2 + R_4 C^4 R^4 \omega^4 - 3C^2 R^2 \omega^2 R_3\right)}{\left(R_4 + R_3\right)\left(1 + 7C^2 R^2 \omega^2 + C^4 R^4 \omega^4\right)} = 1 \tag{13}$$

From Eqs (12) and (13) we get

$$\frac{1}{9}\frac{A\left(6R_4 - 3R_3\right)}{R_4 + R_3} = 1 \tag{14}$$

by solving Eq. (14) for R3 we get:

$$R_3 = \frac{2R_4 A - 3R_4}{3 + A} \tag{15}$$

Given that that A is very big in op amps, then Eq. (15) gives

$$R3 = 2R_4 \tag{16}$$

With the help of an oscilloscope we can find the resonant frequency and then from the equation $\omega = 2\pi f$ we can calculate ω. Knowing the value of R we can calculate the value of C by solving Eq. (12) $C = 1/\omega R$ (or by knowing the value of C we can calculate the value of R in the same way).

Having balanced the bridge, we get an oscillation in the output of the bridge which is

$$V(t) = A\sin(\omega t). \tag{17}$$
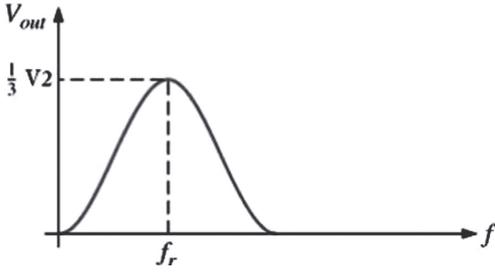
Fig. 5. Responce curve.
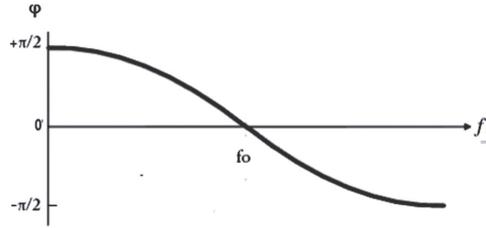
Fig. 6. Phase vs frequency.
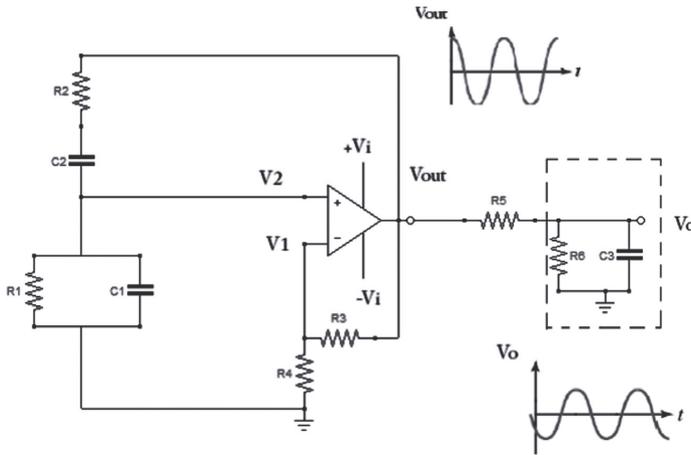
Fig. 7. The parallel R6–C3 circuit connected to the Wien bridge oscillator.

3. Results

The next step is to connect the parallel R_6–C_3 circuit to the bridge. The output signal (out(t)) from the oscillator will drive a known resistor R_5 which is connected to the parallel R_6–C_3 circuit in series with electrodes. The R_5 and the R_6 of the parallel R_6–C_3 circuit will create a voltage divider.

Solving the equivalent circuit for the parallel R_6–C_3 circuit we get

$$V_o(s) = \frac{V_i(s)R_6}{R_6 + R_5 + C_3 R_5 R_6 s} \tag{18}$$

Where $V_o(s)$ is the output of the parallel R_6–C_3 circuit and $V_i(s)$ is the input voltage in R5 which is the output voltage of the Wien bridge oscillator.

So, the input voltage in R_5 is

$$V_i(t) = A\sin(\omega t) \tag{19}$$

The Laplace transformation for Eq. (19) is

$$V_i(s) = \frac{A\omega}{s^2 + \omega^2}$$ (20)

Equation (18) becomes

$$V_o(s) = \frac{A\omega R_6}{(s^2 + \omega^2)(R_6 + R_5 + C_3 R_5 R_6 s)}$$ (21)

The inverse Laplace transform is

$$V_o(t) = \frac{\left(A\left(C_3\omega R_5 R_6^2\left(-\cos(\omega t) + e^{-\frac{(R_6+R_5)t}{C_3 R_5 R_6}}\right) + \sin(\omega t)R_6(R_6 + R_5)\right)\right)}{R_6^2 + 2R_6 R_5 + R_5^2 + \omega^2 C_3^2 R_5^2 R_6^2}$$ (22)

Theoretically when $t \to \infty$ but practically when $t = 5C_3 R_5 R_6/(R_6 + R_5)$ the exponential becomes

$$e^{-\frac{(R_6+R_5)t}{C_3 R_5 R_6}} = 0$$ (23)

Equation (22) gives

$$V_o(t) = \frac{A\left(-C_3\omega R_5 R_6^2 \cos(\omega t) + \sin(\omega t)R_6(R_6 + R_5)\right)}{R_6^2 + 2R_6 R_5 + R_5^2 + \omega^2 C_3^2 R_5^2 R_6^2}$$ (24)

Using an oscilloscope attached to the parallel R_6–C_3 circuit (where V_0 is shown in figure (7)) we can find the amplitude (A_1) of the wave form and the phase shift ($\Delta\varphi$) by comparing it to the phase of the wave form we took in the output of the Wien bridge oscillator (V_{out} is shown in figure (7)).

By knowing the new amplitude A_1 and the phase shift we can solve the following equations.

According to trigonometric function:

$$a.\cos(\vartheta) + b.\sin(\vartheta) = \sqrt{a^2 + b^2}\sin\left(\vartheta + \arctan\left(\frac{a}{b}\right)\right)$$ (25)

Equation (24) becomes

$$V_0(t) = \frac{A}{R_6^2 + 2R_6 R_5 + R_5^2 + \omega^2 C_3^2 R_5^2 R_6^2}\sqrt{C_3^2\omega^2 R_5^2 R_6^4 + R_6^2(R_6^+ R_5)^2}$$
$$\sin\left(\omega t + \arctan\left(\frac{C_3\omega R_5 R_6}{R_6 + R_5}\right)\right)$$ (26)

which is equivalent to the equation

$$V_0(t) = A_1\sin(\omega t + \Delta\varphi)$$ (27)

From Eqs (26) and (27) we get

$$A_1 = \frac{A}{R_6^2 + 2R_6 R_5 + R_5^2 + w^2 C_3^2 R_5^2 R_6^2}\sqrt{C_3^2 w^2 R_5^2 R_6^4 + R_6^2(R_6^+ R_5)^2}$$ (28)

or

$$A_1 = \frac{A R_6}{\sqrt{(R_6^+ R_5)^2 + w^2 C_3^2 R_5^2 R_6^2}}$$ (29)

and

$$\Delta\phi = \arctan\left(\frac{C_3\omega R_5 R_6}{R_6 + R_5}\right) \tag{30}$$

By solving Eqs (29) and (30) we can obtain the values R_6 and C_3 of the parallel RC circuit.

If we use the parallel R_6–C_3 circuit as an electrical equivalent of a tooth [5,6] then additionally we can calculate the resistivity ρ, the conductivity σ and the relative permittivity ε_r of the tooth. Having calculated the values of R_6 and C_3 of the tooth and measuring the surface area S of the electrodes and the distance L between them then the following equations can be used.

$$R_6 = \rho\frac{L}{S} \tag{31}$$

or

$$\rho = \frac{R_6 S}{L} \text{ or } \sigma = \frac{1}{\rho} \tag{32}$$

And

$$C_3 = \varepsilon_r\varepsilon_0\frac{S}{L} \tag{33}$$

or

$$\varepsilon_r = \frac{C_3 L}{\varepsilon_0 S} \tag{34}$$

4. Conclusions

In this work the impedance of a parallel RC circuit is studied in detail with the help of a Wien bridge oscillator and through the use of a mathematical and physical model. Simulations were obtained by solving the equation for the appropriate circuit. The model can predict the values of the resistance and the capacitance of any parallel RC circuit which can be used as an electrical equivalent of a tooth or a neuron.

Acknowledgments

References

[1]   M. Min, T. Parve, A. Ronk, P. Annus and T. Paavle, A synchronous sampling and demodulation in an instrument for multifrequency bioimpedance measurement, *IEEE Trans. Inst. Meas* **56** (2007), 1365–1372.
[2]   P. Souza, R. Fateman, J. Moses and C. Yapp, The Maxima Book, 2003.

[3]   J. Carlson and J. Johnson, Multivariable Mathematics with Maple, Linear Algebra, Vector Calculus and Differential Equations, 1996, Prentice-Hall.

[4]   M. Monagan, K. Geddes, K. Heal, G. Labahn, S. Vorkoetter, J. McCarron and P. DeMarco, Maple Introductory Programming Guide, 2005, Maplesoft a division of Waterloo Maple Inc.

[5]   T. Marjanovic, I. Lackovic and Z. Stare, Evaluation of Electrical Equivalent Circuits of a Tooth: Comparison of Circuits with Resistors and Capacitors and the Circuit with a Constant Phase Element, IFMBE Proceedings, 5th European Conference of the International Federation for Medical and Biological Engineering 14–18 September 2011 Budapest, Hungary, Springer, pp. 1261–1264.

[6]   T. Marjanovic, Z. Stare and I. Lackovic, Verification of physical models used for root canal measurement by impedance comparison, IFMBE Proceedings, 13th International Conference on Electrical Bioimpedance and 8th Conference on Electrical Impedance Tomography 2007, Aug. 29th–Sept. 2nd 2007, Graz, Austria, Springer, pp. 715–718.

[7]   R. Mancini and R. Palmer, Sine-Wave Oscillator, Application Report, Texas Instruments, 2001

[8]   A. Argawal and J. Lang, Foundations of Analog and Digital Electronic Circuits, ELSEVIER, 2005.

A-II.

PROGRAMMING CODES

Program 1: Chaotic attractor for a minimal chaotic neuromodule
```
x:=array(0..100000):y:=array(0..100000):
b1:=-2:b2:=3:w11:=-20:w21:=-6:w12:=6:imax:=10000:
x[0]:=1:y[0]:=0.2:
for i from 0 to imax do
x[i+1]:=evalf(b1+w11/(1+exp(-x[i]))+w12/(1+exp(-y[i]))):
y[i+1]:=evalf(b2+w21/(1+exp(-x[i]))):
end do:
with(plots):
points:=[[x[n],y[n]]$n=50..imax]:
pointplot(points,style=point,symbol=point,color=blue,axes=BOXED,
font=[TIMES,ROMAN,15]);
```

Program 2: Bifurcation diagram for a bi-stable neuron module which displays quasiperiodic and bi-stable behaviours
```
start:=7:Max:=7:b2:=3:b1:=2:w12:=-4:w21:=5:
halfN:=9999:N1:=1+halfN:itermax:=2*halfN+1:
x[0]:=-3:y[0]:=-2:
for n from 0 to halfN do
w11:=start-n*Max/halfN:
x[n+1]:=evalf(b1+w11*tanh(x[n])+w12*tanh(0.3*y[n])):
y[n+1]:=evalf(b2+w21*tanh(x[n])):
end do:
with(plots):
points:=[[start-j*Max/N1,x[j]]$j=0..halfN] :
P1 :=pointplot(points,style=point,symbol=point,color=blue,axes=BOXED,
font=[TIMES,ROMAN,15]);
for n from N1 to itermax do
w11:=(n-N1)*Max/halfN:
x[n+1]:=evalf(b1+w11*tanh(x[n])+w12*tanh(0.3*y[n])):
y[n+1]:=evalf(b2+w21*tanh(x[n])):
end do:
points:=[[start+(j-N1)*Max/N1,x[N1+j]]$j=0..halfN] :
P2 :=pointplot(points,style=point,symbol=point,color=blue,axes=BOXED,
font=[TIMES,ROMAN,15]);
display({P1,P2},labels=['w11','x[n]']);
```

Program 3: System of two normal cells
```
restart:
x:=array(0..100000):y:=array(0..100000):
imax:=15000:
x[0]:=1:y[0]:=0.2:
for i from 0 to imax do
x[i+1]:=evalf(2+3.5*tanh(x[i])-4*tanh(0.3*y[i])):
y[i+1]:=evalf(3+5*tanh(x[i])):end do:
with(plots):
points:=[[x[n],y[n]]$n=50..imax]:
pointplot(points,style=point,symbol=point,color=blue,axes=BOXED,
font=[TIMES,ROMAN,15]);
```

Program 4: Chaotic attractor, Cell state x vs time, Cell state y vs time, Cell state z vs time
```
x:=array(0..100000):y:=array(0..100000):z:=array(0..100000):
b[1]:=-2:b[2]:=3:b[3]:=1:w[1,1]:=-20:w[1,2]:=6:w[2,1]:=
6:w[2,2]:=0:w[1,3]:=5:w[2,3]:=-4:w[3,3]:=-10:w[3,1]:=-3:w[3,2]:=0:
imax:=100: [0]:=1:y[0]:=0.2: z[0]:=0.1:
for i from 0 to imax do
x[i+1]:=evalf(b[1]+w[1,1]/(1+exp(x[i]))+w[1,2]/(1+exp(y[i]))+w[1,3]/(1+exp(-
z[i]))):
y[i+1]:=evalf(b[2]+w[2,1]/(1+exp(x[i]))+w[2,2]/(1+exp(y[i]))+w[2,3]/(1+exp(-
z[i]))):
z[i+1]:=evalf(b[3]+w[3,1]/(1+exp(-x[i]))+w[3,2]/(1+exp(y[i]))+w[3,3]/(1+exp(-
z[i]))):
end do:with(plots):
points:=[[x[n],y[n],z[n]]$n=0..imax]:
points1:=[[n,x[n]]$n=0..imax]:
points2:=[[n,y[n]]$n=0..imax]:
points3:=[[n,z[n]]$n=0..imax]:
pointplot3d(points,connect=true,style=line,symbol=point,color=blue,axes=BOXED,f
ont=[TIMES,ROMAN,15]);
pointplot(points1,connect=true,style=line,symbol=point,color=blue,axes=BOXED,fo
nt=[TIMES,ROMAN,15]);
pointplot(points2,connect=true,style=line,symbol=point,color=blue,axes=BOXED,fo
nt=[TIMES,ROMAN,15]);
pointplot(points3,connect=true,style=line,symbol=point,color=blue,axes=BOXED,fo
nt=[TIMES,ROMAN,15]);
```

A-III.

MATHEMATICAL CALCULATIONS

Solution of the differential equation (4.3) of neuron (page 54) on the basis of equivalent circuit (Fig. 4.7, page 55) derived through Bessel functions:

$$
q(t) = - \Bigg(\Bigg(\bigg(2\,\text{BesselK}\Big(\tfrac{1}{2}\, \tfrac{-\sqrt{C}\,\sqrt{L} + 2\,I\,\tau}{\sqrt{C}\,\sqrt{L}},
$$

$$
-\tfrac{1}{2}\,\tfrac{R\,\tau}{L} \bigg)\, i_0\, L^{3/2}\,\sqrt{C}\,\tau + \text{BesselK}\Big(\tfrac{1}{2}\, \tfrac{-\sqrt{C}\,\sqrt{L} + 2\,I\,\tau}{\sqrt{C}\,\sqrt{L}},
$$

$$
-\tfrac{1}{2}\,\tfrac{R\,\tau}{L} \bigg)\, Q_0\, R\,\sqrt{C}\,\sqrt{L}\,\tau - 2\,I\,\text{BesselK}\Big(\tfrac{1}{2}\, \tfrac{\sqrt{C}\,\sqrt{L} + 2\,I\,\tau}{\sqrt{C}\,\sqrt{L}},
$$

$$
-\tfrac{1}{2}\,\tfrac{R\,\tau}{L} \bigg)\, Q_0\, L\,\tau - 2\,\text{BesselK}\Big(\tfrac{1}{2}\, \tfrac{\sqrt{C}\,\sqrt{L} + 2\,I\,\tau}{\sqrt{C}\,\sqrt{L}},
$$

$$
-\tfrac{1}{2}\,\tfrac{R\,\tau}{L} \bigg)\, i_0\, L^{3/2}\,\sqrt{C}\,\tau + 2\,I\,\text{BesselK}\Big(\tfrac{1}{2}\, \tfrac{-\sqrt{C}\,\sqrt{L} + 2\,I\,\tau}{\sqrt{C}\,\sqrt{L}},
$$

$$
-\tfrac{1}{2}\,\tfrac{R\,\tau}{L} \bigg)\, Q_0\, L\,\tau
$$

$$
- Q_0\,\sqrt{C}\,\sqrt{L}\,\text{BesselK}\Big(\tfrac{1}{2}\, \tfrac{3\sqrt{C}\,\sqrt{L} + 2\,I\,\tau}{\sqrt{C}\,\sqrt{L}}, -\tfrac{1}{2}\,\tfrac{R\,\tau}{L} \Big)\, R\,\tau
$$

$$
- 2\,\text{BesselK}\Big(\tfrac{1}{2}\, \tfrac{\sqrt{C}\,\sqrt{L} + 2\,I\,\tau}{\sqrt{C}\,\sqrt{L}}, -\tfrac{1}{2}\,\tfrac{R\,\tau}{L} \Big)\, Q_0\, L^{3/2}\,\sqrt{C} \Big)
$$

$$
e^{-\tfrac{1}{2}\,\tfrac{-R\,\tau^2\,e^{-\tfrac{t}{\tau}} + t\,L}{\tau\,L}} \Big(\text{BesselI}\Big(\tfrac{1}{2}\, \tfrac{-\sqrt{C}\,\sqrt{L} + 2\,I\,\tau}{\sqrt{C}\,\sqrt{L}},
$$

$$
-\tfrac{1}{2}\,\tfrac{R\,\tau\,e^{-\tfrac{t}{\tau}}}{L} \Big) + \text{BesselI}\Big(\tfrac{1}{2}\, \tfrac{\sqrt{C}\,\sqrt{L} + 2\,I\,\tau}{\sqrt{C}\,\sqrt{L}},
$$

$$
-\tfrac{1}{2}\,\tfrac{R\,\tau\,e^{-\tfrac{t}{\tau}}}{L} \Big) \Big) \Bigg) \Bigg/ \Bigg(\sqrt{e^{\tfrac{R\,\tau}{L}}}\,\sqrt{C}\,\sqrt{L} \Big(
$$

$$
-R\,\tau\,\text{BesselI}\Big(\tfrac{1}{2}\, \tfrac{-\sqrt{C}\,\sqrt{L} + 2\,I\,\tau}{\sqrt{C}\,\sqrt{L}},
$$

$$
-\tfrac{1}{2}\,\tfrac{R\,\tau}{L} \Big)\, \text{BesselK}\Big(\tfrac{1}{2}\, \tfrac{\sqrt{C}\,\sqrt{L} + 2\,I\,\tau}{\sqrt{C}\,\sqrt{L}}, -\tfrac{1}{2}\,\tfrac{R\,\tau}{L} \Big)
$$

$$
+ 2\,L\,\text{BesselI}\Big(\tfrac{1}{2}\, \tfrac{\sqrt{C}\,\sqrt{L} + 2\,I\,\tau}{\sqrt{C}\,\sqrt{L}},
$$

$$
-\tfrac{1}{2}\,\tfrac{R\,\tau}{L} \Big)\, \text{BesselK}\Big(\tfrac{1}{2}\, \tfrac{-\sqrt{C}\,\sqrt{L} + 2\,I\,\tau}{\sqrt{C}\,\sqrt{L}}, -\tfrac{1}{2}\,\tfrac{R\,\tau}{L} \Big)
$$

$$
- \text{BesselI}\Big(\tfrac{1}{2}\, \tfrac{3\sqrt{C}\,\sqrt{L} + 2\,I\,\tau}{\sqrt{C}\,\sqrt{L}},
$$

$$
-\tfrac{1}{2}\,\tfrac{R\,\tau}{L} \Big)\, R\,\tau\,\text{BesselK}\Big(\tfrac{1}{2}\, \tfrac{-\sqrt{C}\,\sqrt{L} + 2\,I\,\tau}{\sqrt{C}\,\sqrt{L}}, -\tfrac{1}{2}\,\tfrac{R\,\tau}{L} \Big)
$$

$$
+ \text{BesselI}\Big(\tfrac{1}{2}\, \tfrac{3\sqrt{C}\,\sqrt{L} + 2\,I\,\tau}{\sqrt{C}\,\sqrt{L}},
$$

$$
-\tfrac{1}{2}\,\tfrac{R\,\tau}{L} \Big)\, R\,\tau\,\text{BesselK}\Big(\tfrac{1}{2}\, \tfrac{\sqrt{C}\,\sqrt{L} + 2\,I\,\tau}{\sqrt{C}\,\sqrt{L}}, -\tfrac{1}{2}\,\tfrac{R\,\tau}{L} \Big)
$$

$$
- R\,\tau\,\text{BesselK}\Big(\tfrac{1}{2}\, \tfrac{-\sqrt{C}\,\sqrt{L} + 2\,I\,\tau}{\sqrt{C}\,\sqrt{L}},
$$

$$
-\tfrac{1}{2}\,\tfrac{R\,\tau}{L} \Big)\, \text{BesselI}\Big(\tfrac{1}{2}\, \tfrac{\sqrt{C}\,\sqrt{L} + 2\,I\,\tau}{\sqrt{C}\,\sqrt{L}}, -\tfrac{1}{2}\,\tfrac{R\,\tau}{L} \Big)
$$

$$
+ \text{BesselK}\Big(\tfrac{1}{2}\, \tfrac{3\sqrt{C}\,\sqrt{L} + 2\,I\,\tau}{\sqrt{C}\,\sqrt{L}},
$$

$$
-\tfrac{1}{2}\,\tfrac{R\,\tau}{L} \Big)\, R\,\tau\,\text{BesselI}\Big(\tfrac{1}{2}\, \tfrac{-\sqrt{C}\,\sqrt{L} + 2\,I\,\tau}{\sqrt{C}\,\sqrt{L}}, -\tfrac{1}{2}\,\tfrac{R\,\tau}{L} \Big)
$$

$$
+ \text{BesselK}\Big(\tfrac{1}{2}\, \tfrac{3\sqrt{C}\,\sqrt{L} + 2\,I\,\tau}{\sqrt{C}\,\sqrt{L}},
$$

$$
-\tfrac{1}{2}\,\tfrac{R\,\tau}{L} \Big)\, R\,\tau\,\text{BesselI}\Big(\tfrac{1}{2}\, \tfrac{\sqrt{C}\,\sqrt{L} + 2\,I\,\tau}{\sqrt{C}\,\sqrt{L}}, -\tfrac{1}{2}\,\tfrac{R\,\tau}{L} \Big)
$$

$$
+ 2\,L\,\text{BesselK}\Big(\tfrac{1}{2}\, \tfrac{\sqrt{C}\,\sqrt{L} + 2\,I\,\tau}{\sqrt{C}\,\sqrt{L}},
$$

$$
-\tfrac{1}{2}\,\tfrac{R\,\tau}{L} \Big)\, \text{BesselI}\Big(\tfrac{1}{2}\, \tfrac{-\sqrt{C}\,\sqrt{L} + 2\,I\,\tau}{\sqrt{C}\,\sqrt{L}}, -\tfrac{1}{2}\,\tfrac{R\,\tau}{L} \Big) \Big) \Bigg)
$$

153

Solution of the equation (4.61) on page 81
given as III-1 below:

$$x = -2 - \frac{20}{1+e^{-x}} + \frac{6}{1+e^{-y}}, \; y = 3 - \frac{6}{1+e^{-x}}. \tag{III-1}$$

The solution of eq. (III-1) is

$$x = -1.28037, \; y=1.69508 \tag{III-2}$$

If eq. (III-1) is written as a vector with the right hand sides, then it becomes

$$\left[-2 - \frac{20}{1+e^{-x}} + \frac{6}{1+e^{-y}}, 3 - \frac{6}{1+e^{-x}} \right] \tag{III-3}$$

The Jacobian of eq. (III-3) is

$$A = \begin{bmatrix} -\dfrac{20e^{-x}}{\left(1+e^{-x}\right)^2} & \dfrac{6e^{-y}}{\left(1+e^{-y}\right)^2} \\ -\dfrac{6e^{-x}}{\left(1+e^{-x}\right)^2} & 0 \end{bmatrix} \tag{III-4}$$

Taking into account eq. (III-2), then the eq. (III-4) becomes to eq. (III-5):

$$B = \begin{bmatrix} -\dfrac{20e^{1.28037}}{\left(1+e^{1.28037}\right)^2} & \dfrac{6e^{-1.69508}}{\left(1+e^{-1.69508}\right)^2} \\ -\dfrac{6e^{1.28037}}{\left(1+e^{1.28037}\right)^2} & 0 \end{bmatrix} \tag{III-5}$$

The eigenvalues (in sec^{-1}) of the impedance matrix of eq. (III-5) are:

$$[-3.14872, \; -0.25499]. \tag{III-6}$$

Solution of the eq. (4.66) on page 82
given as eq. (III-7) below:

$$\left[x_{n+2} = -2 - \frac{20}{1+e^{-x_{n+1}}} + \frac{6}{1+e^{-y_{n+1}}}, y_{n+2} = 3 - \frac{6}{1+e^{-x_{n+1}}} \right]$$
(III-7)

The solution of eq. (III-7) is following:

$$x = -1.28037, \ y=1.69508$$
(III-8)

The Jacobian of eq. (III-7) is

$$B = \begin{bmatrix} -\dfrac{20e^{14.18518916}}{\left(1+e^{14.18518}\right)^2} & \dfrac{6e^{2.37301}}{\left(1+e^{2.37301}\right)^2} & \dfrac{5e^{-0.98117}}{\left(1+e^{-0.98117}\right)^2} \\[20pt] -\dfrac{6e^{14.18518}}{\left(1+e^{14.18518}\right)^2} & 0 & 0 \\[20pt] 0 & 0 & -\dfrac{10e^{-0.98117}}{\left(1+e^{-0.98117}\right)^2} \end{bmatrix}$$
(III-9)

The eigenvalues (in sec⁻¹) of the impedance matrix of eq. (III-9) are

$$[-3.14872, \ -0.25499] \quad .$$
(III-10)

The solution of eq. (4.74) on page 85
given as III-11 below:

$$x = -2 - \frac{20}{1+e^{-x}} + \frac{6}{1+e^{-y}} + \frac{5}{1+e^{-z}},$$
$$y = 3 - \frac{6}{1+e^{-x}}, z = 1 - \frac{10}{1+e^{-z}}$$
(III-11)

The solution of eq. (136), here of (III-11), is:

$$x = -1.07704, y = 1.47561, z = -1.24159 .$$
(III-12)

155

If eq. (III-11) is written as a vector with the right hand sides, then it becomes

$$\left[-2 - \frac{20}{1+e^{-x}} + \frac{6}{1+e^{-y}} + \frac{5}{1+e^{-z}}, 3 - \frac{6}{1+e^{-x}}, 1 - \frac{10}{1+e^{-z}} \right] \tag{III-13}$$

The Jacobian of eq. (III-13) is

$$A = \begin{bmatrix} -\dfrac{20e^{-x}}{\left(1+e^{-x}\right)^2} & \dfrac{6e^{-y}}{\left(1+e^{-y}\right)^2} & \dfrac{5e^{-z}}{\left(1+e^{-z}\right)^2} \\ -\dfrac{6e^{-x}}{\left(1+e^{-x}\right)^2} & 0 & 0 \\ 0 & 0 & -\dfrac{10e^{-z}}{\left(1+e^{-z}\right)^2} \end{bmatrix} \tag{III-14}$$

If we taking into account eq. (III-12), then eq. (III-14) becomes

$$B = \begin{bmatrix} -\dfrac{20e^{1.07704}}{\left(1+e^{1.07704}\right)^2} & \dfrac{6e^{-1.47561}}{\left(1+e^{-1.47561}\right)^2} & \dfrac{5e^{1.24159}}{\left(1+e^{1.24159}\right)^2} \\ -\dfrac{6e^{1.07704}}{\left(1+e^{1.07704}\right)^2} & 0 & 0 \\ 0 & 0 & -\dfrac{10e^{1.24159}}{\left(1+e^{1.24159}\right)^2} \end{bmatrix} \tag{III-15}$$

The eigenvalues (in sec^{-1}) of the impedance matrix of the eq. (III-15) are:

$$[-3.49461, \ -0.29569, \ -1.73911]. \tag{III-16}$$

Solution of the eq. (4.78) on page 85
given as eq. III-19 below:

$$\left[x_{n+2} = -2 - \frac{20}{1+e^{-x_{n+1}}} + \frac{6}{1+e^{-y_{n+1}}} + \frac{5}{1+e^{-z_{n+1}}} , y_{n+2} = 3 - \frac{6}{1+e^{-x_{n+1}}} , z_{n+2} = 1 - \frac{10}{1+e^{-z_{n+1}}} \right] \quad \text{(III-17)}$$

The solution of eq. (III-17) is following:

$$x = -14.18518, \ y = -2.37301, \ z = 0.98117 . \quad \text{(III-18)}$$

The Jacobian of eq. (III-17) expresses as given below:

$$B = \begin{bmatrix} -\dfrac{20e^{14.18518}}{\left(1+e^{14.18518}\right)^2} & \dfrac{6e^{2.37301}}{\left(1+e^{2.37301}\right)^2} & \dfrac{5e^{-0.98117}}{\left(1+e^{-0.98117}\right)^2} \\[4mm] -\dfrac{6e^{14.18518}}{\left(1+e^{14.18518}\right)^2} & 0 & 0 \\[4mm] 0 & 0 & -\dfrac{10e^{-0.98117}}{\left(1+e^{-0.98117}\right)^2} \end{bmatrix} \quad \text{(III-19)}$$

The eigenvalues (in sec⁻¹) of the impedance matrix of the eq. (III-23) are as follows below, eq. (III-24):

$[-0.000006+0.001392\,\text{j}, \ -0.000006\text{-}0.001392\,\text{j}, \ -1.983156]. \quad \text{(III-24)}$

A-IV.

METHODS OF IMPEDANCE MEASUREMENT

Appendix IV gives a short overview of the various methods of impedance measurement. The measurement of dielectric properties of a material, according to the prior analysis, determines the size of an equivalent circuit, thus the impedance of a device. In practice the impedance measurements performed depend on the type and form of the device being measured (device under test, DUT), the frequency range of measurement and the desired accuracy of the results, always in combination with the cost and usability of the equipment [74].

IV.1 Bridge method

When there is no current flow through the detector D (Fig. IV-1), which means the bridge is balanced, the value of the unknown impedance Z_x can be calculated from the equation:

$$Z_x = \frac{Z_1 Z_3}{Z_2}.$$

(IV-1)
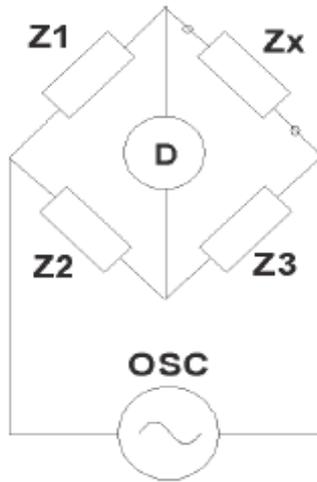
Fig.IV-1 Bridge method [74]

IV.2 Resonant method

The resonance of the circuit (Fig. IV-2) is achieved setting the value of the variable capacitor C. Then the unknown parameters R_x and L_x are calculated from the value of C, the resonant frequency and the quality factor Q the latter of which is directly measured with a voltmeter connected to the variable capacitor. Considering the low loss of the circuit, it is possible to measure very large values of Q up to 300.
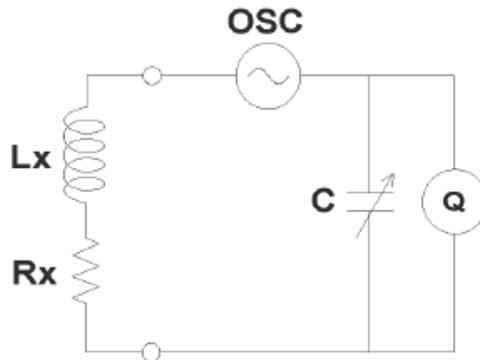
Fig.IV-2 Resonant method [74]

IV.3 Current-to-Voltage I-V method

The unknown impedance Z_x can be calculated from measured values of current and voltage (Fig. IV-3). The current is calculated by measuring the voltage drop across a resistor R, whose value is precisely known and is relatively small. In practice instead of R a low loss transformer is often used, but this introduces a lower limit to the frequency range of the method. The following equation applies:

$$Z_x = \frac{V_1}{I} = \frac{V_1}{V_2} R \ .$$
(IV-2)
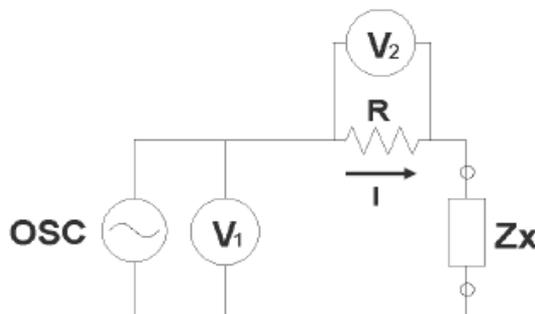
Fig.IV-3 I-V method [74]

IV.4 Radio frequency (RF) current-to-voltage (I-V) method

The RF I-V method is based on the same principle as the simple I-V method, but it uses a matched measuring circuit (50 Ω) and a coaxial accuracy test connector for operation at higher frequencies. There are two configurations suitable for low and high impedance values. The equation below applies for low frequencies (Fig. IV-4):

$$Z_x = \frac{V}{I} = \frac{2R}{\frac{V_2}{V_1} - 1} \Rightarrow Z_x = \frac{2RV_1}{V_2 - V_1} \quad . \tag{IV-3}$$
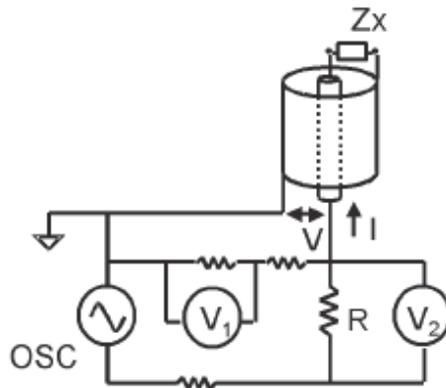
Fig.IV-4 RF I-V method for low frequencies (Low impedance type) [74]

For high frequencies (Fig. IV-5) the impedance is expressed as

$$Z_x = \frac{V}{I} = \frac{R}{2}\left(\frac{V_1}{V_2} - 1\right) \Rightarrow Z_x = \frac{R(V_1 - V_2)}{2V_2} \quad . \tag{IV-4}$$
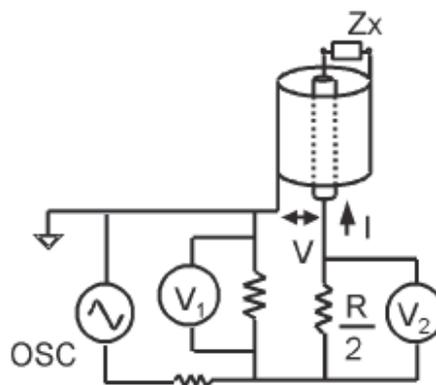
Fig.IV-5 RF I-V method for high frequencies (High impedance type) [74]

IV.5 Network analysis method

This method is suitable for high frequencies, especially microwave. It obtains the reflection coefficient as the ratio of the reflected to the incident signal. The impedance is determined by the reflection coefficient according to the microwave theory [75]. A Network Analyzer is used for the production and measurement of signals and a directional coupler or bridge to detect the reflected signal (Fig. IV-6).
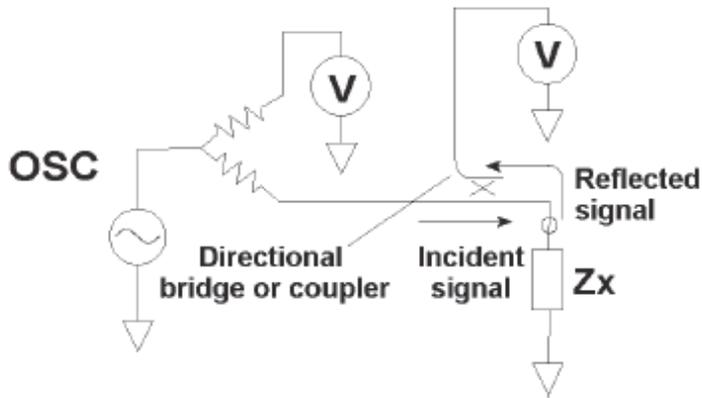
Fig.IV-6 Network analysis method: a circuit diagram [74]

IV.6 Auto-balanced bridge method

With the operation of the I-V converter, the current which flows through the unknown impedance Z_x and the current which flows through the resistance R_r will be in balance. Point L is maintained at potential zero potential and is called as a virtual ground. The impedance Z_x is estimated by measuring the potential at point H and the potential difference at the ends of R (Fig. IV-7).
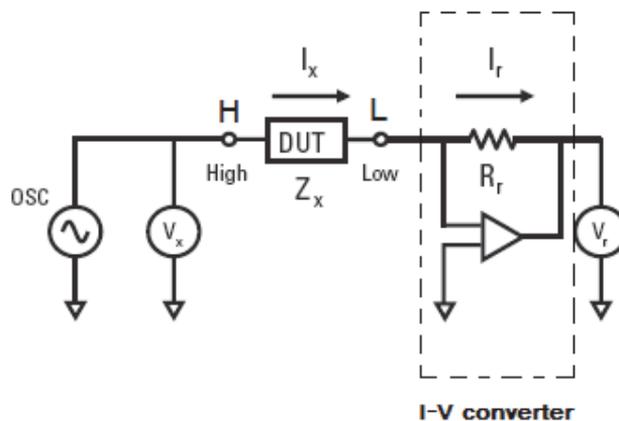
Fig.IV-7 Auto-balanced bridge method [74]

The following equation applies:

$$I_x = \frac{V_x}{Z_x} \Rightarrow Z_x = \frac{V_x}{I_x} \qquad \text{(IV-5)}$$

Knowing that $I_r = \frac{V_r}{R_r}$, $\qquad$ (IV-6)

and considering that $I_x = I_r \Rightarrow I_x = \frac{V_r}{R_r}$. $\qquad$ (IV-7)

From eq. (IV-5) and eq. (IV-7) we get $Z_x = \frac{V_x}{I_x} = R_r \frac{V_x}{V_r}$. $\qquad$ (IV-8)

The advantage of this method is the wide frequency range and the precision for a wide range of impedances. It is the primary method used for measurements at low and medium frequencies.

At higher frequencies, the accuracy of results is reduced because of performance limits of the operational amplifier. The wideband LCR bridges and impedance analyzers use a sophisticated null detector, phase detector, loop filter and a vector modulator to increase the available frequency range above 1 MHz, with a maximum of 110 MHz.

The following Fig. IV-8 shows a simplified diagram of the Agilent impedance analyser [76].
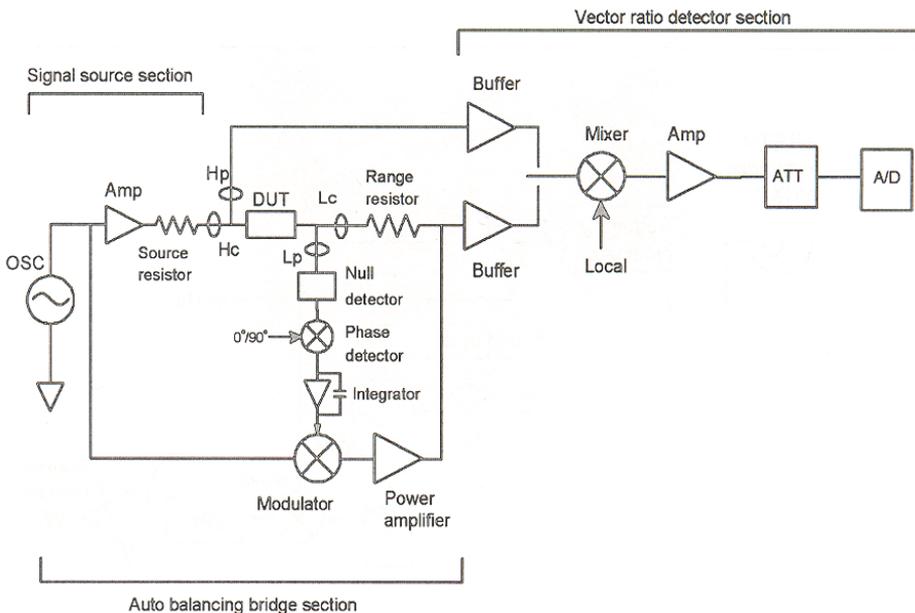
Fig.IV-8 Simplified diagram of the Agilent impedance analyser [74]

As seen from the figure IV-8, the analog part of the device consists of the signal source section, the auto balancing bridge section, and the vector ratio detector section. There is also the digital part, which controls the operation of the analog section, converts the measured data to digital with an A/D converter, processes and stores measurement data and communicates with the user through a connection to a computer.

IV.7 Summary

In this sub-section of the Appendix we analysed the different methods of measuring impedance. The most common methods were used for these measurements, those being the bridge method, the resonant method, the I-V method, the RF I-V method, the network analysis method and the auto-balanced bridge method. The equivalent circuits for each of these are given. It is expected that this analysis will help in choosing the right method and device of measurement for the particular task at hand in order to obtain the most credible results.

A-V.

MEASUREMENT SAFETY

Measurement safety, more specifically, possible dangers when using medical equipment is discussed as well as the impact of electric shock on the human body. Additionally, the different classifications and types of medical equipment as well as the standards and the medical equipment nomenclature are presented. Then a description is given of the measurement of leakage currents, namely the enclosure leakage current, the patient leakage current, the earth leakage current and the capacity leakage current. Finally, the SELV-PELV system protection against electric shock is mentioned.

V.1 Hazards in use of medical devices

Medical equipment use is not always safe as technical staff and patients may be directly exposed to electrical or electronic hazards. Briefly some of the most common risks are the following.

Firstly, there are risks related to the malfunction of the device itself or the absence of required electrical safety measures such as:

- Fire or explosion.
- Improper or insufficient output terminals.
- Total shutdown or extensive electrical / mechanical failures
- Mechanical hazards.
- Electromagnetic Interference.
- Exposure to non-permitted electrical currents.

Additionally, as a result of the use of faulty equipment or faulty operation there may be serious consequences for the patients, such as:

- Cessation of cardiac function.
- Atrial fibrillation or cardiac arrhythmias.
- Injuries.
- Burns.
- Respiratory problems or even cessation of respiratory function.
- Muscle aches.
- Damage to the nervous system.

V.2 Electric shock and effects on the human body

Electrical current has the following effects on the human body [77]:

- Interference with the operation of the neuromuscular system because of a change in the resting potential of the cell membrane.
- Burns due to the conversion of electrical energy to heat.
- Mechanical injury resulting in violent muscle contractions.

The predominantly electric nature of the transmission of nerve impulses is responsible for the high sensitivity of the body to the external electric current. Electric charges which are too small to cause thermal damage can cause a change in the formation of proteins and perforation integrity of cell membranes that is threatening to normal cell function. Momentary contact with live cables can cause cellular damage (breakage and cell lysis) not related to heat release and with more prolonged contact thermal burns may occur. The blood vessels may undergo thrombosis and occlusion, resulting in tissue ischemia and necrosis. The muscle wasting can lead to acute renal failure (due to occlusion of the renal tubules, myoglobin is released). Broken bones, muscle and tendon rupture can occur during the violent muscle contractions. Studies have shown that less than 1% of people can feel an alternative electrical current of 0.3 mA and frequency 50 Hz. The usual value for which electricity is felt by men is 1.1 mA and women 0.7 mA of frequency of 50 Hz. The current is felt by the human in the form of a tingling sensation. The maximum current which is considered harmless to humans is 5 mA though the shock it causes is acutely felt. At this point we should emphasize that if a man takes hold of current carrying conductor then the muscles of the hand are stimulated and contract. Thus a person is involuntarily forced to hold tighter although he is being electrocuted. In relatively low amperage the person can control his muscles, overcoming the current and thus free himself from the current carrying conductor. These levels depend on muscle mass but when the value of electrical current is high then the danger can be life threatening. The electrical current values and the symptoms are given below.

Current (mA)	Symptoms
0.7-1.1	The threshold of perception of electricity
5	The maximum harmless value. Causes annoying shock
20	Tetanic muscle contractions
100	Ventricular fibrillation
2000	Cardiopulmonary arrest. Burns

Table V-1: AC effects in humans, f=50Hz

The main resistance of the electrical current in humans is the resistance of the skin which can vary depending on the thickness and the moisture of the contact surface.

The resistance of patients in the intensive-care unit (ICU) is sufficiently smaller than the resistance of a healthy person mainly because:

- Skin resistance is reduced in the area where the electrodes of bioelectric metering have been placed.
- The use of intravenous fluids or catheters may have the effect of bypassing the current path to the skin.
- It has been found that the skin resistance of the patient is directly related to the use of drugs and many psychological and clinical factors.

The effect of reducing the resistance of the patient is the risk he runs of electric shock from current values which are considered harmless to a healthy person. A table with various tissues and corresponding resistance features is shown below.

Tissue	Resistance
Mucosal lacerations	100 - 500 Ω/cm^2
Wet skin	500 - 1500 Ω/cm^2
Sweaty skin	1500 - 2500 Ω/cm^2
Palm, medial thigh (vascular areas)	2500 - 10000 Ω/cm^2
Dry skin	10.000 – 100.000 Ω/cm^2

Table V-2: Resistance of different tissues

The nerves, muscles and blood vessels have lower resistance. In general, the body fluids are good conductors because of significant concentrations of ions. The bones have the greatest resistance. It should be noted that children have thinner skin and a higher percentage of water in the body than adults and therefore are more vulnerable to electric shocks. So when the skin resistance is low then the electricity enters internal structures of the body, but if the resistance is greater, the electricity causes skin burns in most cases because it is turned into thermal energy. Through studies an empirical equation has been found which relates the period of time with the minimum current that is required to induce ventricular fibrillation. It is given as $I_{min} = 115/t^{1/2}$ (mA) for short-term shocks lower than the cardiac cycle (< 1 s). This is the electrical current, which will induce ventricular fibrillation and is large enough to affect the vulnerable phase of the cardiac cycle (T wave, repolarization phase of the ventricles). Shock longer than the cardiac cycle cause premature extensor contractions, which make the myocardium more vulnerable after 4 to 5 cycles. The amount of heat generated is equal to $Q = I^2 \cdot R \cdot t$. So, for a given current the greater the duration of exposure the greater thermal damage is for the tissues. Finally, we should note that when a person is subject to an electric shock, then the sweat glands are stimulated resulting in the secretion of sweat which reduces the resistance of the skin thereby increasing electrical current, as time passes.
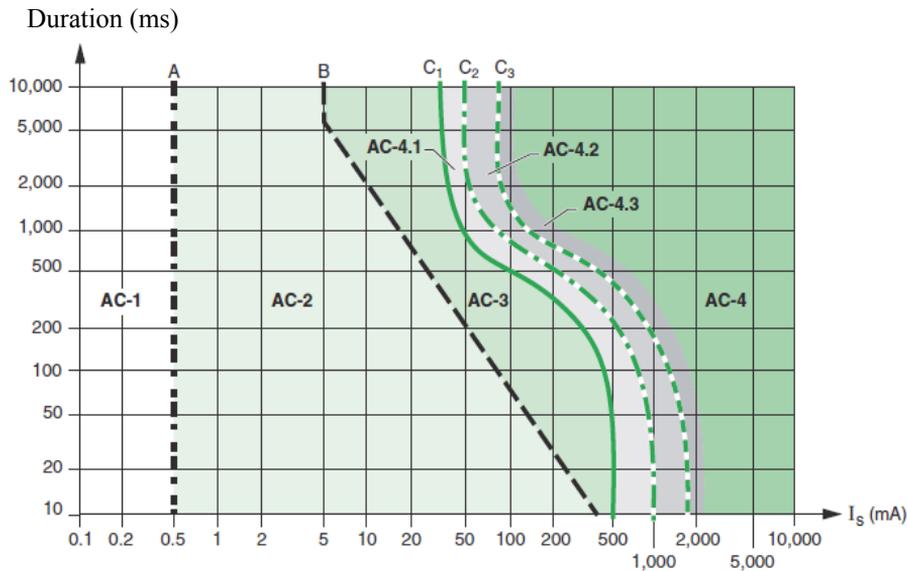
Fig.V-1 Duration curve to electrical current [78]

The explanation of each zone in Fig.V-1 is given below [78].

• Zone AC-1: Not perceived.
• Zone AC-2: Perceived.
• Zone AC-3: Reversible effect - muscle contraction.
• Zone AC-4.1: Up to 5% probability of ventricular fibrillation.
• Zone AC-4.2: Up to 50% probability of ventricular fibrillation.
• Zone AC-4.3: Over 50% probability of ventricular fibrillation.

The explanation of each curve in Fig.V-1 is given below:

• Curve A: Threshold of perception
• Curve B: The limit of muscular reactions
• Curve C1: Limit: 0% probability of ventricular fibrillation
• Curve C2: Limit: 5% probability of ventricular fibrillation
• Curve C3: Limit: 50% probability of ventricular fibrillation

V.3 Safety standards for medical equipment

The application of safety and quality checks in the use of medical devices ensures the best possible level of security is provided to both patients and medical staff [79, 80]
Checking electrical safety refers to all medical devices used in areas such as operating theaters and ICU and those used for diagnostic purposes which transfer energy to the patient or record vital signs such as ECG and patient monitor.

Safety checks are carried out in accordance with international standards, some of which are given below:

- IEC 60601-1 «Medical electrical equipment – Part 1: General requirements for safety 1»

These ensure that medical devices operate within the set safety limits.

- IEC 60601-2: «Medical electrical equipment - Part 1: General requirements for safety 2»

These include checking important devices such as diathermy, defibrillators and monitors and ensure that critical parameters such as output power, leakage currents etc are within limits and therefore the operation is safe.

Certain subcategories of the above standard are given below:

- IEC 60601-2-4: «Medical electrical equipment - Part 2: Particular requirements for the safety of cardiac defibrillators and cardiac defibrillator – monitors»
- IEC 60601-2-2: «Medical electrical equipment - Part 2: Particular requirements for the safety of high frequency surgical equipment»
- IEC 60601-2-27: «Medical electrical equipment - Part 2: Particular requirements for the safety of electrocardiographic monitoring equipment»

Also standards related to the safety of medical equipment are shown in the following table:

NFPA	NFPA 99 Standards for health care facilities 1993
AAMI/ANSI	American National Standards: Safe Current Limits for Electromedical Apparatus 1993
DIN/VDE	DIN/VDE 0751-1 Repair, modification and testing of medical electrical equipment; general requirements 1990

Table V-3: Standards related to the safety of medical equipment

V.4 Electrical safety checks for medical devices

To ensure a safe medical environment and detection - prevention of adverse effects on patients and users, electrical safety checks are probably the most important issue. By conducting a series of controlled tests the existence of leakage currents which may cause electric shock, can be detected and in most cases the electrical safety check can provide strong evidence of a failure of the device to operate as it should. The aim is the systematic checking of electrical safety of all those devices that operate either in vital medical facilities (operating rooms, intensive care units, etc.) or come in contact with the patient (defibrillators, ECG, Patient Monitor etc). For this purpose, certain control protocols-standards in accordance with international standards IEC 60601-1 are applied. With these control protocols the medical devices are checked to determine if their operation is safe and if they are within the specified safety limits so that they operate correctly for both the patient and for the user. The standard defines the requirements of the tests for protection against possible hazards including electrical grounding protection, earth leakage currents, patient leakage currents and patient auxiliary currents, which will be analysed below. Also HEI 95

and DB9801 standards are recommended for the checking of medical devices [81, 82].

The electrical devices are distinguished by the means of protection they have which is either single or double insulation. There are two categories which are given below:

a) the type of protection against electrical accident are the following: class I, whose devices have an additional means of protection with a permanent protective earth conductor connection with the metal parts of the casing, and class II, whose devices include basic insulation as well as enhanced insulation;

b) the degree of protection provided by the applied parts, including devices that provide a specific degree of security, which may have leakage currents within acceptable limits and reliability of the protective earth conductor.

For the proper checking of medical devices there are tests for the insulation to check whether there are leakage currents. These tests use AC current and test equipment at certain levels of humidity. The measuring resistance value for class I devices (Fig.V-2) should be greater than 50 MΩ, but in some rare cases may be less [83].

Applicable to:	Class I, all types
Limits:	Not less than 50 MΩ
DB9801 recommended:	Yes
HEI 95 recommended:	Yes
Notes:	Equipment containing mineral insulated heaters may give values down to 1MΩ. Check equipment is switched on.
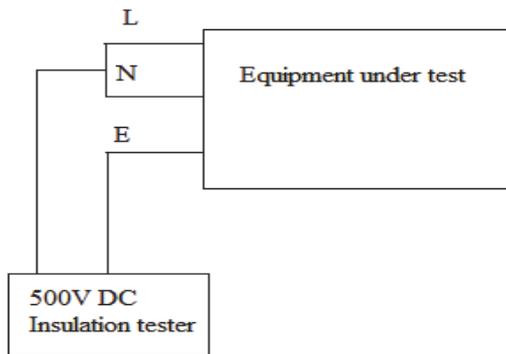
Fig.V-2 Insulation resistance measurement for Class I devices [83]

Applicable to	Class II, all types having applied parts
Limits:	Not less than 50 MΩ
DB9801 recommended:	No
HEI 95 recommended:	Yes
Notes:	Move probe to find worst case
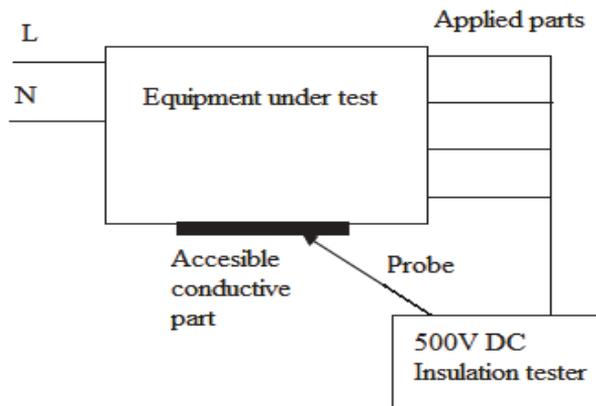
Fig.V-3 Insulation resistance measurement for Class II devices [83]

As regards the devices of Class II (Fig.V-3), the measuring value of the resistance should not be less than 50 MΩ [82, 84].

V.5 Measurement of leakage currents

Measurement circuits have been designed to simulate the average typical electrical characteristics of the human body in order to ensure a traceable simulation of current as if flowing through a human body and these circuits are known as Body Models or Measuring Devices (MD in IEC 60601-1 standard). The diagram below shows the MD (Fig.V-4).
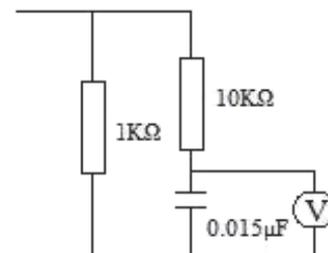
Fig.V-4 Circuit for the measuring device (MD) [83]

V.6 Enclosure Leakage Current

The current flowing from the enclosure or other accessible metal parts of the appliance to earth or to another part of the enclosure through another conductive path other than of the protective earth conductor is called Enclosure Leakage Current (Fig.V-5) [83]. Such currents are likely to flow on the housing even when the protective earth conductor presents no discontinuity through another conductive path other than that of the protective earth conductor. The schematic interpretation of the enclosure leakage current measurement is shown in the following figure.
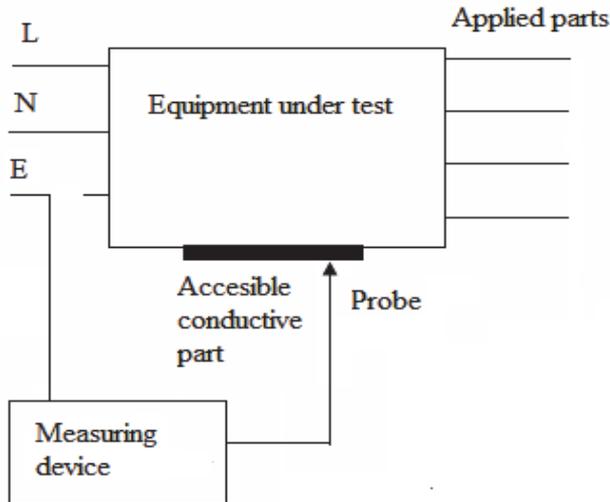
Fig.V-5 Test circuit for Enclosure Leakage Current [83]

V.7 Patient leakage current

Patient leakage current is the leakage current that flows through a patient connected to an applied part or parts. It can either flow from the applied parts via the patient to earth or from an external source of high potential via the patient and the applied parts to earth (Fig.V-6 and Fig.V-7) [83]. A patient being exposed to external voltage due to an external voltage source would result in a serious accident and although it is unlikely to occur it is advisable to safeguard against it [85, 86].
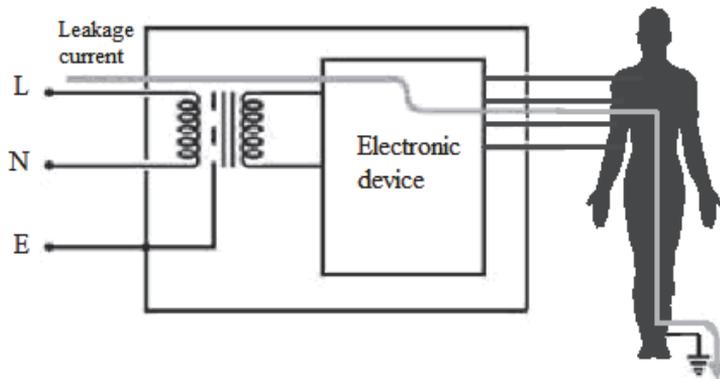
Fig.V-6 Patient leakage current from an electrical equipment [83]
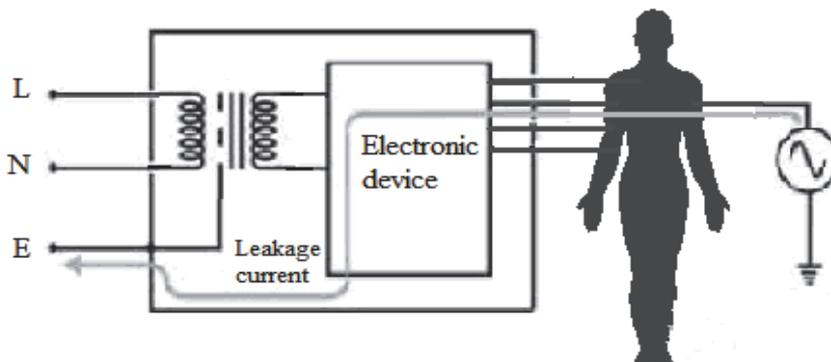
Fig.V-7 Patient leakage current to an electrical equipment [83]

Checking the patient leakage current is divided into two checks of which the first examines the current flowing through the applied parts and from the device, while the second examines the current that will flow through the parts when a potential difference appears in the patient because of the existence of an external power supply. For the first check, all electrodes are connected together and the measuring device is placed between the protective earth conductor and the connection of the electrodes. In the second check an external voltage is applied to the electrodes through the checking device and a power supply is inserted between the terminals of the measuring device and the protective earth conductor. For internally powered devices with accessible metal parts in particular, the patient leakage current is measured between the electrodes and a point on the housing and the terminals of the measuring device are placed accordingly.

The following figure (Fig.V-8) [83] shows the schematic interpretation of the patient leakage current measurement.
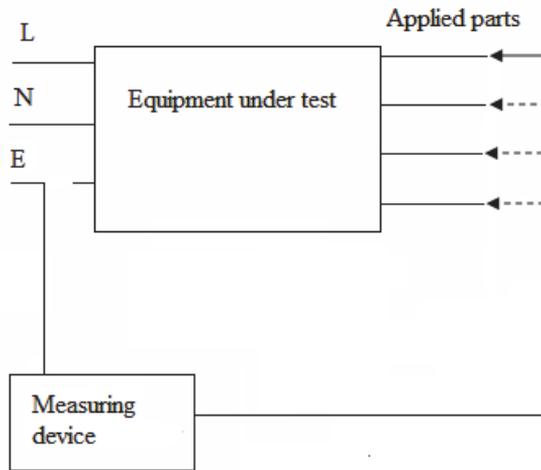
Fig.V-8 Test circuit for patient leakage current measurement [83]

V.8 Earth leakage current

Earth leakage current is the current that escapes from the device to the protective earth conductor leaking from the main parts and is due to capacitive effects (Fig.V-9) [83]. In the event of interruption of the protective earth conductor, current will flow (leak) to earth through the patient [85, 86].
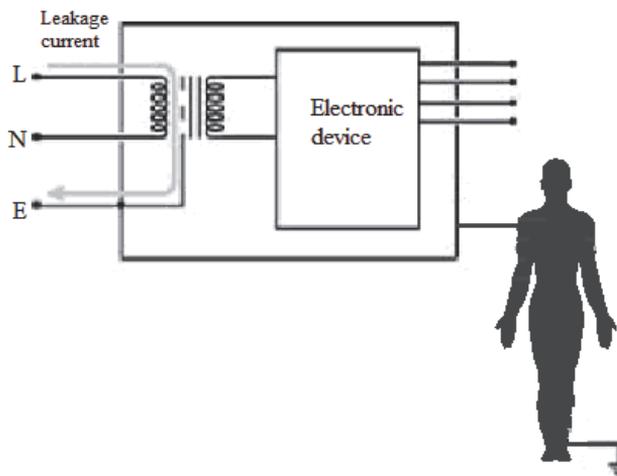
Fig.V-9 A route of the leakage current to earth [83]

The following figure (Fig.V-10) shows the schematic interpretation of the measurement of the leakage current to earth.
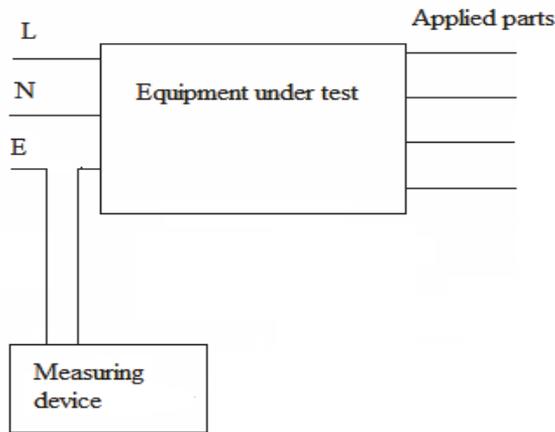
Fig.V-10 Test circuit for the measurement of leakage current to earth [83]

V.9 Patient protection using grounding system

Medical facilities are different from ordinary household and industrial premises, because they should combine smooth functioning with some increased security requirements. A typical example is the emergency electrical loads of a hospital (for instance operating theatres, blood refrigerator and intensive care unit) which, in the event of a power failure, are powered by a power generator. All buildings should have a grounding system to eliminate any risk of leaking electricity. For this reason, there should be a distribution network with three lines which are responsible for the insulation. The earth normally encountered is the operating ground and the protective earth. The difference between grounding and earthing protection function is shown below (Fig.V-11).
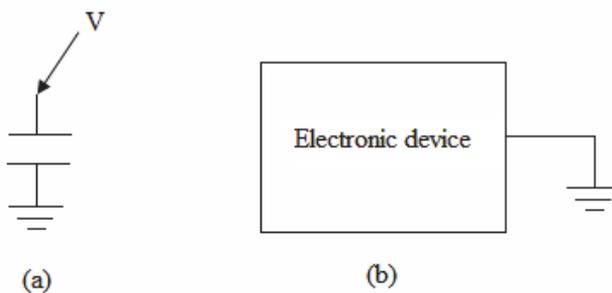
Fig.V-11: (a) Operating ground, (b) Protective earth

The grounding function is necessary for the operation of the circuit and the grounding protection is designed to protect people from the leakage current to the metal casing

of an electrical device with which they come in contact. The way in which the protective grounding works is shown below (Fig.V-12), where the resistance of the human consists of two parts: the core (about 500 Ω) and skin (1 ... 100 KΩ depending on its humidity) [85].
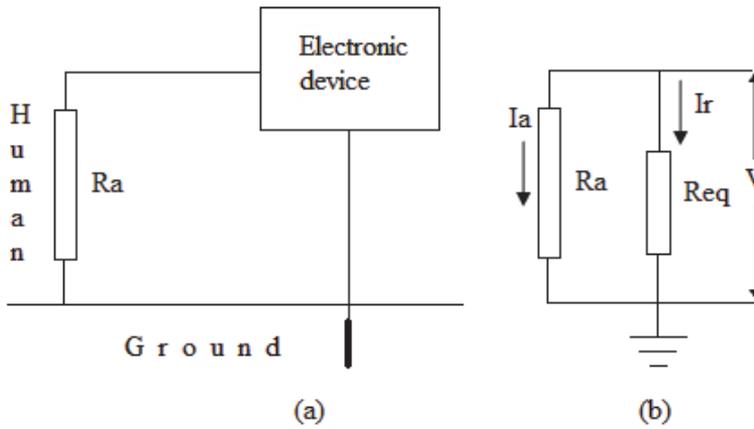
Fig.V-12 Explanation of circuit protective earth circuit [83]

The more humid the skin the smaller the resistance. When a person comes into contact with the metal housing of a shielded electrical device, in which a leakage current occurs ((a) in the above figure), then the leakage current is limited (resistance R_a), depending on the value of total resistance of the ground circuit. The equivalent circuit of the above arrangement of the leakage current is shown in (b) of the above figure. From the equivalent circuit above we see that if $R_{eq} \ll R_a$ then $I_r \gg I_a$

Therefore, for the best possible protection we should seek a grounding resistance value, which approaches the theoretical value R = 0. The total value of earth resistance is, in practice, a few Ω. According to the above, when there is no protective earth installation, or the value of the ground resistance is large (and the resistance of the human body is small) then there are risks to humans who come into contact with the metal casings of the various electrical devices [86].

V.10 Measurement of the capacitive leakage current

The leakage current is due to capacitive or magnetic coupling and damage of insulation, the most important causes of which are:

a) the capacity between the phase conductor and the grounding conductor of the power supply cable of a device;

b) the capacities of the primary winding of the transformer to earth (in almost all electrical devices there is a transformer for different voltages);

c) the capacity with respect to the external sources.
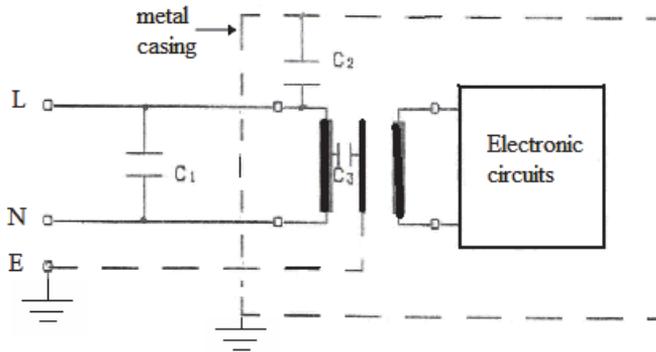
Fig.V-13 Basic root cause of leakage currents of capacitive couplings in bioelectric measurements devices [86]

The value of the current because of C_1 is a few mA (5-20 µA for 3m cable length). This value of the current penetrates the patient when the earth conductor is disconnected and the patient is in contact (e.g. by hand) with the metal housing of the device. So when other leakage currents are caused, then the total value of the leakage current can be dangerous for the patient.

The checks conducted on the measurement of the leakage current are the following [36]:

a) from the phase conductor to the metal housing of an electrical device when there is (for some reason) a grounding conductor. The maximum value of the current is 100 mA;

b) from the phase conductor to the connection terminals of the electrodes on the measuring bioelectric device. The maximum value of the leakage current is 20 µA for devices of emergency medical units and 50 µA for other units;

c) from external sources. The maximum value of the current is 20 µA.

The circuit for measuring the leakage current from external sources is given in Fig. V-14 on the next page. The value of the resistors and capacitors (R = 120 kΩ, R1 = 1 kΩ, R2 = 10 Ω and C = 0.15 µF) in Fig.V-13 apply to the network 110 V, 60 Hz (US specifications).

Tests with the circuit in Fig.V-14 (and also other circuits for the remaining measurements) are carried out in the following four cases:
• supply voltage switch in 'on position',
• supply voltage switch in 'off position',
• normal polarity,
• reverse polarity.
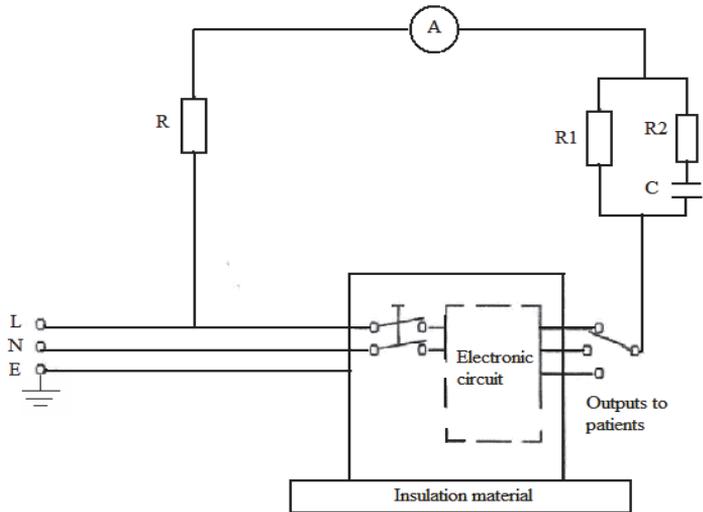
Fig.V-14 Measuring the leakage currents from capacitive coupling to external sources   (by the standards of the U.S.: R = 120 KΩ, R₁ = 1 KΩ, R₂ = 10 Ω and C = 0.15 μF) [86]

V.11 SELV-PELV system

The ultra low voltage circuits SELV, PELV (Fig.V-15) are very important protection against electric shock [87].

- SELV: Safety extra-low voltage
- PELV: Protected extra-low voltage

The nominal low voltage does not exceed 50 V (RMS) for alternating current or 120 V for DC.

V.11.1 SELV protection

The separation of the active parts of the circuit to which SELV is applied from the active parts of other circuits and from earth must be ascertained by measuring the insulation resistance. The value of resistance must comply with Table 4. Measuring the grounding resistance in SELV systems should adhered to the following:

• The measurements should be made between SELV conductors and the grounding conductor and between the active conductors of other circuits in the system and the minimum value taken by the resistance should be 0.25 MΩ.

• Any electrical appliances affecting the measurement should to be disconnected.

• The voltage of the gauge should be 250 V.

V.11.2 PELV protection

The separation of the active part of the circuit to which PELV is applied from active parts of other circuits must be ascertained by measuring the insulation resistance. The values of resistance must comply with Table V-4.

Circuit voltage (V)	DC test voltage (V)	Minimum insulation resistance (MΩ)
SELV, PELV	250	0.25
Up to 500V	500	0.5
Over 500V	1000	1

Table V-4: Minimum value of acceptable insulation resistance
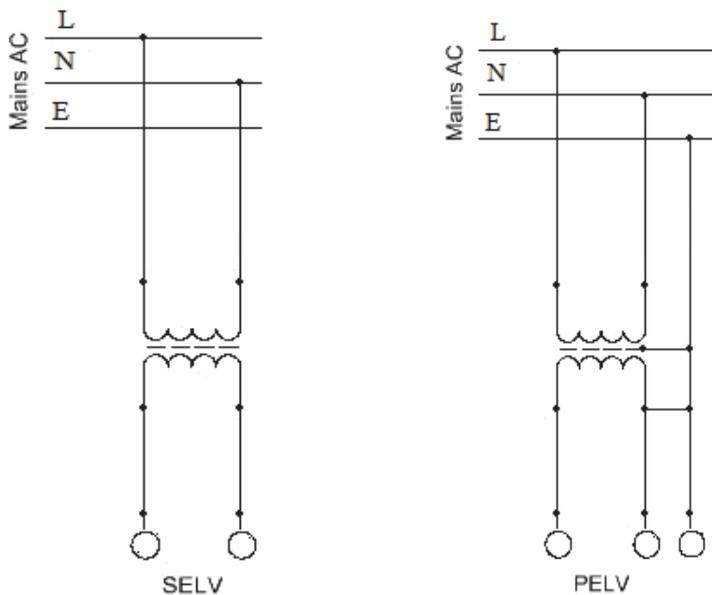
Fig.V-15 SELV –PELV systems

From tests it has been noticed that the most reliable protection is from safety extra low voltage (SELV), which is not grounded unlike PELV which is grounded.

V.12 Summary

The aim of this sub-section of the Appendix was to discuss the importance of measurement safety. We analysed the hazards involved in the use of medical equipment as well as such effects of electric shock on the human body as burns, muscle spasms and respiratory problems. For electrical safety and protection purposes, classes and types of medical equipment are then given, the former of which are categorized as Class I, II and III and the latter Type B, BF and CF. The significance of safety standards are then discussed. After that different types of leakage current are analysed, specifically the enclosure leakage current, the patient leakage current, the earth leakage current and the capacity leakage current, and then the respective test circuit is given. Finally, the SELV (safety extra-low voltage) and PELV (protected extra-low voltage) systems against electric shock are mentioned.

It is hoped that, owing to the importance of measurement safety, this work will encourage further study in this domain in order to perform human experiments properly and to design new experimental devices in full accordance with the requirements.

See also:

Georgios Giannoukos, Mart Min, "Modelling of Dynamic Electrical Bioimpedance and Measurements Safety", 2nd American Applied Sciences Research Institute (AASRI) Conference on Computational Intelligence and Bioinformatics (CIB 2013), December 27-28, 2013, Jeju Island, Korea. AASRI Procedia (ELSEVIER), volume 6, pp. 12-18, 2014, DOI: http://dx.doi.org/10.1016/j.aasri.2014.05.003

Curriculum vitae

1. Personal data

Name:	Georgios Giannoukos
Date and place of birth:	28.02.1965, Athens, Greece
E-mail address:	g.giannoukos@gmail.com

2. Education

Educational Institution	Graduation year	Education (field of study/degree)
Aristotle University of Thessaloniki - Greece	1989	BSc in Physics
Alecu Russo State University of Baltsi – Moldova	2003	MSc in Informatics
Hellenic Open University - Greece	2014	MEd in Adult Education

3. Language competence

Language	Level
Greek	Native
English	Fluent
German	Basic

4. Work and Teaching Experience:

I. 1991 - 1992: in charge of the Greek military telecommunication system in a forward-scatter military base during my military service.

II. 2004 - 2005: Laboratory Assistant at the Technological Educational Institute (TEI) of Lamia, Greece – Department of Information Technology and Department of Electrical Engineering.

III. 2002 - 2014: part-time Physics teacher in secondary state schools in Greece.

IV. September 1992 – today: Physics teacher in private schools for secondary school students in Greece.

Elulookirjeldus

1. Isikuandmed
Nimi: Georgios Giannoukos
Sünni aeg ja -koht: 28.02.1965, Ateena, Kreeka
E-maili aadress: g.giannoukos@gmail.com

2. Hariduskäik

Õppeasutus	Lõpetamise aeg	Haridus (eriala/kraad)
Aristotle University of Thessaloniki - Greece	1989	BSc in Physics
Alecu Russo State University of Baltsi – Moldova	2003	MSc in Informatics
Hellenic Open University - Greece	2014	MEd in Adult Education

3. Keelteoskus

Keel	Level
Kreeka	Emakeel
Inglise	Kõrgtase
Saksa	Põhiteadmised

4. Töö ja õpetamiskogemused:

I. 1991 - 1992: ajateenistus Kreeka armees vastutajana sõjaväe hajusa telekommunikatsiooni süsteemi eest sõjaväebaasis.

II. 2004 - 2005: laborant tehnoloogilise hariduse instituudis (Educational Institute Lamia), Kreeka - Infotehnoloogia ja elektrotehnika osakond.

III. 2002 - 2014: osalise tööajaga füüsikaõpetaja riigigümnaasiumites Kreekas.

IV. September 1992 - tänaseni: füüsikaõpetaja eragümnaasiumis Kreekas.

DISSERTATIONS DEFENDED AT
TALLINN UNIVERSITY OF TECHNOLOGY ON
INFORMATICS AND SYSTEM ENGINEERING

1. **Lea Elmik**. Informational Modelling of a Communication Office. 1992.

2. **Kalle Tammemäe**. Control Intensive Digital System Synthesis. 1997.

3. **Eerik Lossmann**. Complex Signal Classification Algorithms, Based on the Third-Order Statistical Models. 1999.

4. **Kaido Kikkas**. Using the Internet in Rehabilitation of People with Mobility Impairments – Case Studies and Views from Estonia. 1999.

5. **Nazmun Nahar**. Global Electronic Commerce Process: Business-to-Business. 1999.

6. **Jevgeni Riipulk**. Microwave Radiometry for Medical Applications. 2000.

7. **Alar Kuusik**. Compact Smart Home Systems: Design and Verification of Cost Effective Hardware Solutions. 2001.

8. **Jaan Raik**. Hierarchical Test Generation for Digital Circuits Represented by Decision Diagrams. 2001.

9. **Andri Riid**. Transparent Fuzzy Systems: Model and Control. 2002.

10. **Marina Brik**. Investigation and Development of Test Generation Methods for Control Part of Digital Systems. 2002.

11. **Raul Land**. Synchronous Approximation and Processing of Sampled Data Signals. 2002.

12. **Ants Ronk**. An Extended Block-Adaptive Fourier Analyser for Analysis and Reproduction of Periodic Components of Band-Limited Discrete-Time Signals. 2002.

13. **Toivo Paavle**. System Level Modeling of the Phase Locked Loops: Behavioral Analysis and Parameterization. 2003.

14. **Irina Astrova**. On Integration of Object-Oriented Applications with Relational Databases. 2003.

15. **Kuldar Taveter**. A Multi-Perspective Methodology for Agent-Oriented Business Modelling and Simulation. 2004.

16. **Taivo Kangilaski**. Eesti Energia käiduhaldussüsteem. 2004.

17. **Artur Jutman**. Selected Issues of Modeling, Verification and Testing of Digital Systems. 2004.

18. **Ander Tenno**. Simulation and Estimation of Electro-Chemical Processes in Maintenance-Free Batteries with Fixed Electrolyte. 2004.

19. **Oleg Korolkov**. Formation of Diffusion Welded Al Contacts to Semiconductor Silicon. 2004.

20. **Risto Vaarandi**. Tools and Techniques for Event Log Analysis. 2005.

21. **Marko Koort**. Transmitter Power Control in Wireless Communication Systems. 2005.

22. **Raul Savimaa**. Modelling Emergent Behaviour of Organizations. Time-Aware, UML and Agent Based Approach. 2005.

23. **Raido Kurel**. Investigation of Electrical Characteristics of SiC Based Complementary JBS Structures. 2005.

24. **Rainer Taniloo**. Ökonoomsete negatiivse diferentsiaaltakistusega astmete ja elementide disainimine ja optimeerimine. 2005.

25. **Pauli Lallo**. Adaptive Secure Data Transmission Method for OSI Level I. 2005.

26. **Deniss Kumlander**. Some Practical Algorithms to Solve the Maximum Clique Problem. 2005.

27. **Tarmo Veskioja**. Stable Marriage Problem and College Admission. 2005.

28. **Elena Fomina**. Low Power Finite State Machine Synthesis. 2005.

29. **Eero Ivask**. Digital Test in WEB-Based Environment 2006.

30. **Виктор Войтович**. Разработка технологий выращивания из жидкой фазы эпитаксиальных структур арсенида галлия с высоковольтным p-n переходом и изготовления диодов на их основе. 2006.

31. **Tanel Alumäe**. Methods for Estonian Large Vocabulary Speech Recognition. 2006.

32. **Erki Eessaar**. Relational and Object-Relational Database Management Systems as Platforms for Managing Softwareengineering Artefacts. 2006.

33. **Rauno Gordon**. Modelling of Cardiac Dynamics and Intracardiac Bioimpedance. 2007.

34. **Madis Listak**. A Task-Oriented Design of a Biologically Inspired Underwater Robot. 2007.

35. **Elmet Orasson**. Hybrid Built-in Self-Test. Methods and Tools for Analysis and Optimization of BIST. 2007.

36. **Eduard Petlenkov**. Neural Networks Based Identification and Control of Nonlinear Systems: ANARX Model Based Approach. 2007.

37. **Toomas Kirt**. Concept Formation in Exploratory Data Analysis: Case Studies of Linguistic and Banking Data. 2007.

38. **Juhan-Peep Ernits**. Two State Space Reduction Techniques for Explicit State Model Checking. 2007.

39. **Innar Liiv**. Pattern Discovery Using Seriation and Matrix Reordering: A Unified View, Extensions and an Application to Inventory Management. 2008.

40. **Andrei Pokatilov**. Development of National Standard for Voltage Unit Based on Solid-State References. 2008.

41. **Karin Lindroos**. Mapping Social Structures by Formal Non-Linear Information Processing Methods: Case Studies of Estonian Islands Environments. 2008.

42. **Maksim Jenihhin**. Simulation-Based Hardware Verification with High-Level Decision Diagrams. 2008.

43. **Ando Saabas**. Logics for Low-Level Code and Proof-Preserving Program Transformations. 2008.

44. **Ilja Tšahhirov**. Security Protocols Analysis in the Computational Model – Dependency Flow Graphs-Based Approach. 2008.

45. **Toomas Ruuben**. Wideband Digital Beamforming in Sonar Systems. 2009.

46. **Sergei Devadze**. Fault Simulation of Digital Systems. 2009.

47. **Andrei Krivošei**. Model Based Method for Adaptive Decomposition of the Thoracic Bio-Impedance Variations into Cardiac and Respiratory Components. 2009.

48. **Vineeth Govind**. DfT-Based External Test and Diagnosis of Mesh-like Networks on Chips. 2009.

49. **Andres Kull**. Model-Based Testing of Reactive Systems. 2009.

50. **Ants Torim**. Formal Concepts in the Theory of Monotone Systems. 2009.

51. **Erika Matsak**. Discovering Logical Constructs from Estonian Children Language. 2009.

52. **Paul Annus**. Multichannel Bioimpedance Spectroscopy: Instrumentation Methods and Design Principles. 2009.

53. **Maris Tõnso**. Computer Algebra Tools for Modelling, Analysis and Synthesis for Nonlinear Control Systems. 2010.

54. **Aivo Jürgenson**. Efficient Semantics of Parallel and Serial Models of Attack Trees. 2010.

55. **Erkki Joasoon**. The Tactile Feedback Device for Multi-Touch User Interfaces. 2010.

56. **Jürgo-Sören Preden**. Enhancing Situation – Awareness Cognition and Reasoning of Ad-Hoc Network Agents. 2010.

57. **Pavel Grigorenko**. Higher-Order Attribute Semantics of Flat Languages. 2010.

58. **Anna Rannaste**. Hierarcical Test Pattern Generation and Untestability Identification Techniques for Synchronous Sequential Circuits. 2010.

59. **Sergei Strik**. Battery Charging and Full-Featured Battery Charger Integrated Circuit for Portable Applications. 2011.

60. **Rain Ottis**. A Systematic Approach to Offensive Volunteer Cyber Militia. 2011.

61. **Natalja Sleptšuk**. Investigation of the Intermediate Layer in the Metal-Silicon Carbide Contact Obtained by Diffusion Welding. 2011.

62. **Martin Jaanus**. The Interactive Learning Environment for Mobile Laboratories. 2011.

63. **Argo Kasemaa**. Analog Front End Components for Bio-Impedance Measurement: Current Source Design and Implementation. 2011.

64. **Kenneth Geers**. Strategic Cyber Security: Evaluating Nation-State Cyber Attack Mitigation Strategies. 2011.

65. **Riina Maigre**. Composition of Web Services on Large Service Models. 2011.

66. **Helena Kruus**. Optimization of Built-in Self-Test in Digital Systems. 2011.

67. **Gunnar Piho**. Archetypes Based Techniques for Development of Domains, Requirements and Sofware. 2011.

68. **Juri Gavšin**. Intrinsic Robot Safety Through Reversibility of Actions. 2011.

69. **Dmitri Mihhailov**. Hardware Implementation of Recursive Sorting Algorithms Using Tree-like Structures and HFSM Models. 2012.

70. **Anton Tšertov**. System Modeling for Processor-Centric Test Automation. 2012.

71. **Sergei Kostin**. Self-Diagnosis in Digital Systems. 2012.

72. **Mihkel Tagel**. System-Level Design of Timing-Sensitive Network-on-Chip Based Dependable Systems. 2012.

73. **Juri Belikov**. Polynomial Methods for Nonlinear Control Systems. 2012.

74. **Kristina Vassiljeva**. Restricted Connectivity Neural Networks based Identification for Control. 2012.

75. **Tarmo Robal**. Towards Adaptive Web – Analysing and Recommending Web Users` Behaviour. 2012.

76. **Anton Karputkin**. Formal Verification and Error Correction on High-Level Decision Diagrams. 2012.

77. **Vadim Kimlaychuk**. Simulations in Multi-Agent Communication System. 2012.

78. **Taavi Viilukas**. Constraints Solving Based Hierarchical Test Generation for Synchronous Sequential Circuits. 2012.

79. **Marko Kääramees**. A Symbolic Approach to Model-based Online Testing. 2012.

80. **Enar Reilent**. Whiteboard Architecture for the Multi-agent Sensor Systems. 2012.

81. **Jaan Ojarand**. Wideband Excitation Signals for Fast Impedance Spectroscopy of Biological Objects. 2012.

82. **Igor Aleksejev**. FPGA-based Embedded Virtual Instrumentation. 2013.

83. **Juri Mihhailov**. Accurate Flexible Current Measurement Method and its Realization in Power and Battery Management Integrated Circuits for Portable Applications. 2013.

84. **Tõnis Saar**. The Piezo-Electric Impedance Spectroscopy: Solutions and Applications. 2013.

85. **Ermo Täks**. An Automated Legal Content Capture and Visualisation Method. 2013.

86. **Uljana Reinsalu**. Fault Simulation and Code Coverage Analysis of RTL Designs Using High-Level Decision Diagrams. 2013.

87. **Anton Tšepurov**. Hardware Modeling for Design Verification and Debug. 2013.

88. **Ivo Müürsepp**. Robust Detectors for Cognitive Radio. 2013.

89. **Jaas Ježov**. Pressure sensitive lateral line for underwater robot. 2013.

90. **Vadim Kaparin**. Transformation of Nonlinear State Equations into Observer Form. 2013.

92. **Reeno Reeder**. Development and Optimisation of Modelling Methods and Algorithms for Terahertz Range Radiation Sources Based on Quantum Well Heterostructures. 2014.

93. **Ants Koel**. GaAs and SiC Semiconductor Materials Based Power Structures: Static and Dynamic Behavior Analysis. 2014.

94. **Jaan Übi**. Methods for Coopetition and Retention Analysis: An Application to University Management. 2014.

95. **Innokenti Sobolev**. Hyperspectral Data Processing and Interpretation in Remote Sensing Based on Laser-Induced Fluorescence Method. 2014.

96. **Jana Toompuu**. Investigation of the Specific Deep Levels in p-, i- and n-Regions of GaAs p^+-pin-n^+ Structures. 2014.

97. **Taavi Salumäe**. Flow-Sensitive Robotic Fish: From Concept to Experiments. 2015.

98. **Yar Muhammad**. A Parametric Framework for Modelling of Bioelectrical Signals. 2015.

99. **Ago Mõlder**. Image Processing Solutions for Precise Road Profile Measurement Systems. 2015.

100. **Kairit Sirts**. Non-Parametric Bayesian Models for Computational Morphology. 2015.

101. **Alina Gavrijaševa**. Coin Validation by Electromagnetic, Acoustic and Visual Features. 2015.

102. **Emiliano Pastorelli**. Analysis and 3D Visualisation of Microstructured Materials on Custom-Built Virtual Reality Environment. 2015.

103. **Asko Ristolainen**. Phantom Organs and their Applications in Robotic Surgery and Radiology Training. 2015.

104. **Aleksei Tepljakov**. Fractional-order Modeling and Control of Dynamic Systems. 2015.

105. **Ahti Lohk**. A System of Test Patterns to Check and Validate the Semantic Hierarchies of Wordnet-type Dictionaries. 2015.

106. **Hanno Hantson**. Mutation-Based Verification and Error Correction in High-Level Designs. 2015.

107. **Lin Li**. Statistical Methods for Ultrasound Image Segmentation. 2015.

108. **Aleksandr Lenin**. Reliable and Efficient Determination of the Likelihood of Rational Attacks. 2015.

109. **Maksim Gorev**. At-Speed Testing and Test Quality Evaluation for High-Performance Pipelined Systems. 2016.

110. **Mari-Anne Meister**. Electromagnetic Environment and Propagation Factors of Short-Wave Range in Estonia. 2016.

111. **Syed Saif Abrar**. Comprehensive Abstraction of VHDL RTL Cores to ESL SystemC. 2016.

112. **Arvo Kaldmäe**. Advanced Design of Nonlinear Discrete-time and Delayed Systems. 2016.

113. **Mairo Leier**. Scalable Open Platform for Reliable Medical Sensorics. 2016.